Geochemical characterization of sulfide mineral weathering for remediation of acid producing mine wastes
by Stuart Russell Jennings

A thesis submitted in partial fulfillment of the requirements for the degree of Master of Science in Land Rehabilitation
Montana State University

Abstract:
The generation of acid mine drainage as a consequence of sulfide mineral oxidation is a widespread source of resource degradation. The objective of this investigation was to evaluate the influence of sulfide mineral weatherability on acid generation processes. In addition to acid generation by pyrite, the weathering characteristics of common sulfide minerals was investigated and correlated to detection by acid-base account (ABA) methodologies.

The influence of particle morphology, and not particle size, was found to exert the dominant control on mineral weathering processes. Massive morphology particles generated acid at a significantly greater rate than euhedral morphology samples. Acid generation was a consequence of mineral dissolution which occurred nonuniformly across the surface of minerals during oxidation. Mineral surface weathering occurred at sites of excess energy including grain edges, steps, defects, microcracks and inclusions, resulting in the formation of etch pits.

Massive morphology particles exhibited the greatest density of crystalline defect, and had the greatest rate of oxidation.

Sulfide minerals found to be acid generating, in addition to pyrite, include marcasite, pyrrhotite, arsenopyrite, chalcopyrite and sphalerite. Minerals containing sulfur in the atomic structure which were not acid producing include barite, anhydrite, gypsum, anglesite, jarosite, chalcocite and galena. Delineation of acid producing and nonacid producing sulfur forms by ABA extraction methods, a standard operating procedure used in the United States, was determined to be ineffective.

Effective mineral classification, particle morphology identification and observation of mineral weathering processes were accomplished by scanning electron microscopy. Accurate assessment of sulfur form distribution and sulfide mineral weathering characteristics are required for effective remediation of sites impacted by mining.

GEOCHEMICAL CHARACTERIZATION OF SULFIDE MINERAL WEATHERING FOR REMEDIATION OF ACID PRODUCING MINE WASTES

by

Stuart Russell Jennings

A thesis submitted in partial fulfillment
of the requirements for the degree

of

Master of Science

in

Land Rehabilitation

MONTANA STATE UNIVERSITY
Bozeman, Montana

September 1993

APPROVAL

of a thesis submitted by

Stuart Russell Jennings

This thesis has been read by each member of the thesis committee and has been found to be satisfactory regarding content, English usage, format, citations, bibliographic style, and consistency, and is ready for submission to the College of Graduate Studies.

September 7, 1993
Date

Douglas J. Dollhopf
Chairperson, Graduate Committee

Approved for the Major Department

September 13, 1993
Date

John Paterson
Head, Major Department

Approved for the College of Graduate Studies

10/19/93
Date

Graduate Dean

STATEMENT OF PERMISSION TO USE

In presenting this thesis in partial fulfillment of the requirements for a master's degree at Montana State University, I agree that the Library shall make it available to borrowers under rules of the Library.

If I have indicated my intention to copyright this thesis (paper) by including a copyright notice page, copying is allowable only for scholarly purposes, consistent with "fair use" as prescribed in the U.S. Copyright Law. Requests for permission for extended quotation from or reproduction of this thesis in whole or in parts may be granted only by the copyright holder.

Signature 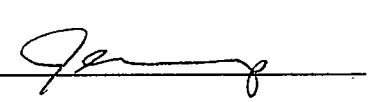

Date 9/15/93

ACKNOWLEDGEMENTS

I wish to extend my thanks to the many coal and metal mines unnamed in this report, which provided valuable insight and sample material for use in research. I thank my graduate committee, comprised of Dr. Douglas Dollhopf, Mr. Dennis Neuman, and Dr. Bill Inskeep, for their technical guidance. Special thanks are also bestowed upon Dawn Major for her tireless efforts at the computer. Appreciation is extended to current and former land rehabilitation graduate students Don Dahlgren, James Poell and Bryce Romig. Thanks are also extended to Dr. Dick Lund for his invaluable guidance on statistical methods, and to Kathrin Olson-Rutz for her assistance with computer statistical software. Computer graphic assistance was provided by Bill Moody. Electron microprobe analyses were performed by Dr. David Mogk who provided essential data and interpretation of sulfide mineral nonhomogeneity. Mineral processing and scanning electron microscopy was performed at Montana Tech under the supervision of Dr. Vern Griffith and Bill Huestis who provided conscientious guidance and steady support throughout the project.

TABLE OF CONTENTS

TABLE OF CONTENTS--Continued

TABLE OF CONTENTS--Continued

LIST OF TABLES

LIST OF TABLES--Continued

LIST OF FIGURES

LIST OF FIGURES--Continued

LIST OF FIGURES--Continued

ABSTRACT

The generation of acid mine drainage as a consequence of sulfide mineral oxidation is a widespread source of resource degradation. The objective of this investigation was to evaluate the influence of sulfide mineral weatherability on acid generation processes. In addition to acid generation by pyrite, the weathering characteristics of common sulfide minerals was investigated and correlated to detection by acid-base account (ABA) methodologies.

The influence of particle morphology, and not particle size, was found to exert the dominant control on mineral weathering processes. Massive morphology particles generated acid at a significantly greater rate than euhedral morphology samples. Acid generation was a consequence of mineral dissolution which occurred nonuniformly across the surface of minerals during oxidation. Mineral surface weathering occurred at sites of excess energy including grain edges, steps, defects, microcracks and inclusions, resulting in the formation of etch pits. Massive morphology particles exhibited the greatest density of crystalline defect, and had the greatest rate of oxidation.

Sulfide minerals found to be acid generating, in addition to pyrite, include marcasite, pyrrhotite, arsenopyrite, chalcopyrite and sphalerite. Minerals containing sulfur in the atomic structure which were not acid producing include barite, anhydrite, gypsum, anglesite, jarosite, chalcocite and galena. Delineation of acid producing and nonacid producing sulfur forms by ABA extraction methods, a standard operating procedure used in the United States, was determined to be ineffective.

Effective mineral classification, particle morphology identification and observation of mineral weathering processes were accomplished by scanning electron microscopy. Accurate assessment of sulfur form distribution and sulfide mineral weathering characteristics are required for effective remediation of sites impacted by mining.

INTRODUCTION

The generation of acid as a consequence of sulfide mineral oxidation, dominantly as pyrite, is a pervasive source of resource degradation in the United States. Acid production from mine and mill waste is the source of one of the largest hazardous waste problems in the western states. Remediation of land contaminated by acid producing minerals is based on laboratory measurement of potential acidity, though methods used to assess potential acidity in mine wastes are inadequate to predict whether acid will be produced during or following site remediation. A dilemma often results when mine waste potential acidity from sulfide minerals is great, but skepticism regarding whether the sulfides will yield acid result in project plans applying lime far short of the tens or even hundreds of tons of lime per 1000 tons of waste required to neutralize potential acidity. Reacidification of mine wastes in the future may be the legacy for our lack of knowledge today.

Minerals containing sulfur are common in coal and hardrock mining environments either as sulfides or sulfates. Pyrite is the most common sulfide mineral, and is implicated in the generation of acid upon oxidation. Though pyrite oxidation is the source of acid problems in many areas, the physical properties of pyrite which impact the rate of oxidation are unknown. Physical properties of pyrite include particle size, morphology, crystal form, electrical conductivity, presence of impurity and defect. Additionally, when sulfide minerals other than pyrite are present in mine waste material, the resulting products of their oxidation

is unknown. Therefore, the remediation of acid generating materials is dependent on the weathering characteristics of the sulfide particles present, though analytical methods to detect differences in particle weatherability are lacking. Compounding the difficulty in assessing the acid generation potential of samples from diverse geological settings is the laboratory analysis of potential acidity, the results of which are treated differently by different investigators to calculate potential acidity. The measurement of potential acidity and neutralization potential by laboratory analysis is an inadequate approach to characterization of the acid generation properties of a sample since calculation of potential acidity assumes that acid is generated only by pyrite. When nonacid forming sulfide and sulfate minerals in addition to pyrite are present and counted as pyrite in the calculation of potential acidity, remedial design error can occur. Error can also occur when acid forming minerals are considered as nonacid forming sulfur forms in the calculation of potential acidity resulting in underestimation of the net acid generation potential.

Study Objectives

To address current inadequacies in the understanding of acid generation from mine waste minerals, this investigation was performed to address the following research objectives:

- evaluate the influence of sulfide size and morphology on mineral weatherability;
- determine the acid producing characteristics of minerals other than pyrite;
- assess pyrite crystalline variability in different geochemical environments;
- determine extraction efficiency of solutions commonly used to characterize potential acidity of sulfur bearing minerals;
- demonstrate relevance of characterizing mineral size, morphology, and sulfur mineral composition for remedial planning.

These research objectives are addressed in the following thesis which is comprised of four separate experiments. The methods and associated results from each experiment are presented in independent sections. A brief introduction to each experiment is also included in each section.

LITERATURE REVIEW

Pyrite Formation, Particle Size And Morphology

The formation of pyrite commonly occurs in two distinct geological settings; during diagenesis and lithification in depositional sedimentary environments, and in association with igneous intrusive mineral assemblages during lithification. Pyrite is the most common Fe-S mineral, is widespread in occurrence, and is especially common in both coal and hardrock mine environments.

Sedimentary Pyrite Formation

In marine settings pyrite forms during shallow burial by the reaction of detrital iron minerals with H_2S produced by sulfate reducing bacteria in the presence of organic substrate. The major steps in the process of sedimentary pyrite formation include: bacterial sulfate reduction, reaction of hydrogen sulfide gas with iron minerals to form iron monosulfides, and reaction of iron monosulfides with elemental sulfur to form pyrite (Berner 1970, 1983). The euxinic conditions required for microbial sulfate reduction and subsequent pyrite formation are common in geologic environments where coal is formed. Consequently, many coal depositional sedimentary sequences contain 1-5 percent pyrite. Pyrite formed by depositional sedimentary processes is observed in many crystalline and amorphous, noncrystalline (massive) forms (Grady 1977, Williams et al. 1982, Arora et al. 1978), ranging in size from sub-micron to centimeter dimensions.

Primary FeS_2 is formed contemporaneously with deposition and diagenesis of sediments. Framboidal pyrite is a commonly observed morphological form of primary pyrite composed of spherical clusters of sub-micron size particles. Framboidal FeS_2 is typically observed in sedimentary environments where iron minerals, organic matter and sulfate reducing bacteria are present. In addition to spherical FeS_2 framboids occurring as isolated spheres, primary or massive FeS_2 is periodically observed as a secondary overgrowth on framboids.

Secondary FeS_2 is formed after diagenesis and lithification by the influence of percolating water, which supplies sulfate to organic rich, iron bearing sedimentary rock where microbial reduction occurs. Unlike primary FeS_2 which develops strong euhedral crystal faces in response to growth of a continuous crystalline lattice, massive FeS_2 is amorphous and the development of a continuous crystalline structure is weak. Massive FeS_2 is commonly observed as cleat coatings in coal, as well as in isolated patches and concretions. Massive pyrite has been observed as particles from micrometer to centimeter size, though typically massive pyrite occurs as 150-600 μm size particles.

Igneous Pyrite Formation

Pyrite is common in igneous mineral assemblages as a primary or secondary mineral. Pyrite is found either disseminated in an igneous body as isolated crystals or concentrated in sulfide veins enriched by hydrothermal fluids. The relative abundance of either morphological occurrence of pyrite, as a primary or

secondary mineral, is entirely dependent on the geologic environment and associated history of mineralization. Pyrite concentrations from 1-10 percent are not uncommon in mineralized igneous rock.

Primary pyrite occurs as euhedral crystals which formed contemporaneously with lithification of the igneous body. Primary pyrite exhibits strong euhedral crystal faces formed by slow development of a regular crystalline lattice. Euhedral pyrite can occur as sub-micron to centimeter size particles in either a disseminated or vein occurrence.

Secondary pyrite occurs as massive noncrystalline masses of FeS_2 which are deposited either during the lithification of an igneous body, or after cooling as massive veins of pyrite and other sulfides. Massive pyrite can occur as sub-micron to centimeter size particles.

Iron-Sulfur Mineral Chemistry

In the mineral kingdom there are many minerals which contain both iron and sulfur. In the Fe-S system, pyrite is the most common mineral, followed by pyrrhotite ($Fe_{1-x}S$), though many Fe_x-S_y minerals with different thermodynamic stabilities are known. The thermodynamic conditions present in the geologic environment of formation dictate which of the many Fe-S minerals will form (Kullerud and Yoder 1959, Shuey 1975, Ribbe 1975).

Though pyrite is a common mineral in many geological environments, appreciable physical property variation occurs. Physical property variation within

pyrite crystals derived from different geological settings can include stoichiometry, density, electrical conductivity (Smith 1942), crystal form (Dana 1944), presence of impurities, thin section optical anisotropism (Stanton 1957), defect density, presence of solid or fluid inclusions, semiconducting type (Shuey 1975) and reflectivity.

Pyrite is not typically considered to be nonstoichiometric, but deviation from the predicted chemical composition, $FeS_{2.00}$, has been reported (Shuey 1975, Haines 1986). Smith (1942) analyzed 10 pyrite crystals and found a trend toward sulfur deficiency. The 10 analyses ranged from $FeS_{1.94}$ - $FeS_{2.01}$. While ratios of $FeS_{1.91}$ - $FeS_{2.11}$ were measured in a different study (Rakcheyev 1968) and correlated to temperature of formation and activation energy, the pyrite specimens formed at the lowest temperature had the lowest activation energy while the pyrite formed at the highest temperature corresponded to the highest activation energy.

The measured differences in physical properties of pyrite may be partially related to the presence of trace impurities entering into the crystal lattice. In most natural pyrites, impurities constitute only tenths of a percent of the crystalline structure. Molybdenum, arsenic, copper, nickel, zinc, manganese and cobalt have been found intergrown into the pyrite crystals of marine sediments (Raiswell and Plant 1980, Delaney et al. 1987). The occurrence of other elements in pyrite is widespread and dependent on the geochemistry of the environment of formation. Many elements are intergrown into the crystal lattice of pyrite derived from

igneous processes including cobalt, gold, arsenic, zinc, copper, nickel and molybdenum.

Iron monosulfides are also present in marine sedimentary strata and in igneous intrusives. Pyrrhotite is a common mineral in sulfide ore deposits and can occur as an intergrowth with pyrite or in the absence of pyrite. Pyrrhotite is commonly iron deficient relative to a true stoichiometric iron monosulfide (FeS), or troilite. Troilite is rare in terrestrial environments, yet a common constituent in meteorites (Mason and Berry 1968).

Marine depositional sedimentary environments rarely contain pyrrhotite, but other iron sulfide minerals are present. Marcasite (FeS_2), greigite (Fe_3S_4) (Dell 1972), mackinawite ($Fe_{1+x}S$), and other iron sulfides other than pyrite are present in marine environments (Ribbe 1975). These iron sulfides may eventually lead to the synthesis of pyrite or may remain in the sedimentary rock as other sulfide minerals. Iron monosulfides have been shown to form framboidal pyrite (Raiswell 1982). The degree to which iron monosulfides are converted to pyrite is defined as the degree of pyritization (DOP), where iron monosulfides are extracted by HCl:

$$DOP = \frac{Percent\ Pyrite}{Percent\ Pyrite + Percent\ HCl\ Extractable\ Sulfur}$$

Acid Mine Drainage

The degradation of water quality resulting from the oxidation of pyrite is a widespread and persistent problem in many mining environments, both coal and hardrock. As pyrite is brought to the surface by mining activities it is exposed to oxygen and water and subsequently oxidized. The widely accepted reactions for the oxidation of pyrite by oxygen and water can be written as follows.

$$FeS_2 + 3.5\,O_2 + H_2O = Fe^{2+} + 2\,SO_4^{2-} + 2\,H^+ \quad [1]$$

$$Fe^{2+} + 0.25\,O_2 + H^+ = Fe^{3+} + 0.5\,H_2O \quad [2]$$

$$Fe^{3+} + 3\,H_2O = Fe(OH)_3 + 3\,H^+ \quad [3]$$

Summarily, Equations 1-3 can be expressed as Equation 4.

$$FeS_{2(s)} + \frac{15}{4}\,O_2 + \frac{7}{2}\,H_2O = Fe(OH)_3 + 2\,SO_4^{2-} + 4\,H^+ \quad [4]$$

Since there is a seven electron change in the valence state of sulfur from S^{-1} in FeS_2 to S^{+6} in SO_4^{2-} (Equation 4), intermediate reactions in addition to Equations 1-3 may be short lived intermediate steps. Goldhaber (1983) found that meta-stable sulfur oxyanions exist in intermediate oxidation states in the sulfide to sulfate pathway. The intermediate reactions occur quickly, resulting in a 1 to 2 electron oxidation change per reaction. Though the oxidation of iron disulfide to yield acid is not disputed, slight variations in this reaction have been noted including obtaining sulfur as a product of the oxidation of marcasite and pyrite (Lowson 1982).

Ferric iron (Fe^{3+}) can also serve to accelerate the rate at which acid is generated during the oxidation of pyrite. Typically, when pH falls below 3.5, ferric iron oxidation of pyrite can become the dominant process. When sufficient Fe^{3+} is present the oxidation of pyrite can proceed by Equation 5.

$$FeS_{2(s)} + 14\,Fe^{3+} + 8\,H_2O = 15\,Fe^{2+} + 2\,SO_4^{2-} + 16\,H^+ \qquad [5]$$

In Equation 1, 4 moles of H^+ are produced per mole of FeS_2 oxidized by oxygen and water, while in Equation 5, 16 moles H^+ are produced per 1 mole FeS_2 oxidized by ferric iron and water. Equation 5 occurs rapidly (Singer and Stumm 1970) and once initiated becomes self-perpetuating or autocatalytic.

Numerous attempts have been made to establish the rate at which pyrite will oxidize, both in the laboratory (McKibben and Barnes 1986) and in the field (Schuman et al. 1991). One fundamental approach to determination of the rate of pyrite oxidation is to consider acid generation to be a function of surface area. Samples of small particle size will therefore have greater surface area per mass than larger particles, and subsequently more rapid acid production. Framboidal pyrite is an example of pyrite of very small particle size and has been considered to exert strong influence on the rate of acid generation when present. Pugh and others (1981) found that framboidal pyrite has 4-5 times the surface area of massive pyrite in the 20-150 μm size fraction. The same authors (Pugh et al. 1984) examined the oxidation rate of framboidal pyrite and found as surface area doubled, the reaction rate increased by 1.5 times, while a decrease in particle size of massive pyrite had little effect on sulfate production. Caruccio and others

(1976) found that surface and groundwater in Eastern Kentucky contained significant amounts of sulfate when strata containing framboidal pyrite were present in the drainage.

In a laboratory setting, Wiersma and Rimstidt (1984) found no geologically significant differences in the reaction rates of pyrites from different geological environments with ferric iron at pH 2, but found that the surface area for lower temperature/early diagenetic pyrite is an order of magnitude greater than that of higher temperature origin pyrites. This result leads to the conclusion that the lower temperature pyrites have a much greater surface area to mass ratio and consequently greater reactivity per mass.

Though the link between high surface area, high reaction rate and large subsequent acid production is commonly accepted, the findings of all researchers are not in agreement. In an analysis of pyritic coal spoil, the greatest salt content, taken as a measure of pyrite oxidation, was associated with the larger (500-2000 μm) pyrite size fraction when compared to the <500 μm size fraction (Evangelou et al. 1985).

A second approach to prediction of acid generation is to consider both particle size and particle morphology as influencing the rate of acid generation. Hammack (1985) used evolved gas analysis (EGA), x-ray photoelectron spectroscopy (XPS), and x-ray diffraction (XRD) to characterize the differences between "normal" and "aberrant" pyrite. He found that the "aberrant" pyrite samples, which ignited at temperatures of 200° C, yielded higher leachate conductivities in

humidity cell weathering tests than did the "normal" pyrite which ignited at 300° C. Analysis by XPS found that the "aberrant" pyrite samples contained more iron disulfide within 30 angstroms of the surface while reactivity of the "normal" pyrites was limited by the presence of sulfate salt and iron oxide coatings on the mineral surfaces. Weathering experiments using pyritic rock samples performed by Haines (1986) found no useful correlation between particle size or the presence of framboids and acid generation, but found a strong positive correlation between the percentage of massive iron disulfide and the amount of acid and sulfate produced.

The presence of sulfur oxidizing bacteria in mine environments containing pyrite can exert additional influence on the rate of acid generation (Jaynes et al. 1984b). The sulfur oxidizing bacteria *thiobacillus thiooxidans, thiobacillus ferrooxidans* and *ferrobacillus ferrooxidans* have been isolated from acid mine drainage and have been implicated in the oxidation of Fe^{2+} to Fe^{3+} (Colmer and Hinkle, 1947; Leathen et al. 1953; and Beck and Brown 1968). Sulfur oxidizing bacteria are ubiquitous in mine environments and participate to some greater or lesser extent in the oxidation of pyrite depending on the biogeochemical environment.

Additional environmental factors can influence the rate of acid production including the "activity" of the bacteria, oxygen concentration, spoil temperature and solution pH (Jaynes et al. 1984a).

The presence of sulfides other than pyrite or marcasite can influence the rate of acid production. Some hardrock mines may contain from a few to many percent of other minerals which control or contribute to the formation of acid.

Some sedimentary environments may contain HCl soluble sulfide minerals which may contribute to the generation of acidic drainage. The oxidation of FeS (which is soluble in HCl) by weathering is presented by Haines (1986) in Equation 6.

$$FeS + O_2 + 2H_2O = Fe^{2+} + SO_4^{2-} + 4H^+ + 4e^- \qquad [6]$$

In hardrock environments chalcopyrite can be oxidized by ferric iron and water to yield acid (Brierley 1990), Equation 7.

$$CuFeS_2 + 16Fe^{3+} + 8H_2O = Cu^{2+} + 17Fe^{2+} + 2SO_4^{2-} + 16H^+ \qquad [7]$$

The formation of jarosite ($KFe_3(SO_4)_2(OH)_6$) occurs as a consequence of pyrite oxidation under strong oxidizing and acidic conditions (Lindsay 1979), Equation 8.

$$FeS_2 + \frac{15}{4}O_2 + \frac{5}{2}H_2O + \frac{1}{3}K^+ = \frac{1}{3}KFe_3(SO_4)_2(OH)_6 + \frac{4}{3}SO_4^{2-} + 3H^+ \qquad [8]$$

If pH is elevated jarosite becomes thermodynamically unstable and is consumed by hydrolysis yielding ferric oxide (limonite), SO_4^{2-} and K^+. The presence of jarosite in mine waste materials has been implicated in the generation of acidic drainage in accordance with Equations 9, 10 and 11 (Schafer and Associates et al. 1989).

$$KFe_3(SO_4)_2(OH)_6 + 6H^+ = K^+ + 3Fe^{3+} + 2SO_4^{2-} + 6H_2O \qquad [9]$$

$$3Fe^{3+} + 9H_2O = 3Fe(OH)_3 + 9H^+ \qquad [10]$$

$$3Fe(OH)_3 = 3FeOOH + 3H_2O \qquad [11]$$

Although acidity is consumed in Equation 9, hydrolysis of ferric iron in Equation 10 yields a net change of 3 moles H^+ generated per mole of jarosite consumed.

Mineral Dissolution And Surface Chemistry

The generation of acid mine drainage by the weathering of minerals present in mine waste materials occurs as a consequence of the dissolution of the solid mineral phase by an oxidizing agent, commonly water and atmospheric oxygen. As the oxidizing agent comes into contact with the mineral surface, part of the mineral surface is destructively removed and carried away in solution. This process continues as long as the mineral is in contact with the oxidizing agent, until the mineral is entirely consumed by the process.

The process of mineral dissolution has been examined by scanning electron microscopy (SEM) and inferred by scanning tunnelling microscopy (STM) (Eggleston and Hochella 1990). The process of weathering is observed to occur at focused locations on the mineral surface, and not uniformly across the surface. Oxidation is centered on sites of excess energy, or at imperfections in the crystal structure (Lasaga and Blum 1986). The formation of solution cavities or etch pits are the result of this selective attack of the mineral surfaces. The reactive sites on the crystal surface can include lattice defects, dislocations, structural distortions, microcracks, grain edges, corners, cleavage planes, fractures, twinning boundaries, solid and fluid inclusions, and at any site of different activation energy (Hochella and White 1990). The density of reactive sites on mineral surfaces therefore has

important implications to mineral-water geochemistry, where the effective or reactive surface area is different from the total surface area (McKibben and Barnes 1986). Reactive sites may also be induced during sample preparation activities such as grinding (Eggleston et al. 1989). The observation not only of particle, but mineral surface morphology, may subsequently improve our knowledge of mineral-water interactions (Hochella et al. 1989).

In a study of pyrite oxidation in carbonate-buffered solution, Nicholson and others (1988) found the initial rate of pyrite oxidation to be a linear function of surface area. The pyrite oxidation rate dependence on oxygen concentration however was nonlinear, suggesting that the oxidation rate limiting step was not the concentration of oxygen, but the pyrite surface decomposition reaction. The difference in oxidation rate between the five samples used in the study exhibited a maximum oxidation rate difference of approximately 25%, suggesting that the reactive surface area shows linear dependence on the total surface area.

Holdren and Speyer (1987) performed analysis of the dissolution rate of feldspars of different size fractions as a function of surface area, finding that the reaction rates are not related to specific surface area in any simple fashion. Testing the importance of reactive surface area, as opposed to total surface area, Holdren found reproducible decreases in reaction rates with the finer size fractions. The lowest reactivity per mass of any size fraction measured was in the 200-400 mesh size fraction, undermining the assumption that crystalline defects are

uniformly distributed in feldspar crystals, and that the smallest size fraction is the most reactive.

Neutralization

To mitigate the environmental affects of acid formation, neutralization is accomplished through the addition of alkaline materials. Acid producing mine spoil is commonly amended by the addition of $CaCO_3$, CaO and $Ca(OH)_2$ to raise the pH of the material and facilitate the reestablishment of vegetation, decrease the mobility of metals in solution and improve the quality of surface and ground-water resources. The summary reaction detailing the neutralization of acid produced by the oxidation of pyrite is presented in Equation 12.

$$FeS_2 + 2CaCO_3 + 3.75O_2 + 1.5H_2O = Fe(OH)_3 + 2SO_4^{2-} + 2Ca^{2+} + 2CO_2(g) \quad [12]$$

The oxidation of 1 mole of pyrite, which generates 4 moles of acidity, is neutralized by 2 moles of calcium carbonate. It follows that 1 mole of pyrite weighs 120 grams, of which 64 grams are provided by the sulfur fraction. Since 2 moles of calcium carbonate weigh 200 grams, the acidity generated by the oxidation of 1 mole of pyrite (64 grams S) is neutralized by 2 moles of calcium carbonate (200 grams $CaCO_3$), or 1 gram sulfur to 3.125 grams calcium carbonate. Put in the context of the mining industry, 31.25 tons $CaCO_3$ are required to neutralize 1000 tons of waste containing 1 % sulfur as FeS_2 (Sobek et al. 1978).

An alternative scenario to the neutralization of acid produced by the oxidation of pyrite has been put forward by Cravotta and others (1990), where bicarbonate is one of the products of neutralization Equation 13.

$$FeS_2 + 4CaCO_3 + 3.75O_2 + 3.5H_2O = Fe(OH)_3 + 2SO_4^{2-} + 4Ca^{2+} + 4HCO_3^- \quad [13]$$

If this alternative reaction is correct, the 4 moles acidity produced by the oxidation of 1 mole pyrite would require 4 moles calcium carbonate for neutralization, or double the amount in accordance with Sobek and others (1978). In the reclamation of mined lands, 62.5 tons $CaCO_3$ would be required to neutralize 1000 tons waste containing 1% sulfur as FeS_2.

The production of neutral drainage is possible upon addition of neutralizing materials, provided the rate of acid production and rate of neutralization are in balance. Geidel (1979) found that the production of acidity and alkalinity in a simulated weathering test occurred by dissimilar processes. The rate of acid generation was shown to be proportional to the time interval between flushings with water, while the rate of alkalinity produced at various flushing intervals was similar.

Acid-base accounting (ABA) has been used extensively to predict the outcome of potential pyrite oxidation and acidity neutralization (Sobek et al. 1978). Caruccio (1980) found a strong relationship between water quality and the sulfur to carbonate ratio of Pennsylvania shales. While alternative methods for determination of the sulfur forms present in a sample have been suggested (O'Shay et al. 1990, Dacey et al. 1979, Zhabina et al. 1978, Powell 1920, Smitten-

berg et al. 1951), ABA remains the most commonly applied test in the U.S. Acid-base accounting requires laboratory analysis to determine both the maximum potential acidity as pyrite content and neutralization potential as calcium carbonate. Upon calculation of the net ABA, the addition of calcium carbonate or other neutralizing materials may subsequently be required to balance the shortfall of neutralization potential present in the sample analyzed.

Acid-base account is performed in the laboratory to identify the sulfur forms present in a sample considered to be acid forming by using hydrochloric acid and nitric acid extractions to remove sulfur minerals (Sobek et al. 1978). The solid sample remaining after each extraction is analyzed by combustion methodologies to measure the quantity of sulfur in the solid fraction surviving the extraction. Soluble sulfur forms removed during the HCl extraction are considered to be nonacid forming. Sulfur forms removed by nitric acid extraction are considered to be acid producing, while sulfur forms surviving all extractions are categorized as residual sulfur. The residual component is commonly presented as organic sulfur and considered to be nonacid forming (Casagrande et al. 1989). Organic sulfur is a major component of the low-sulfur coals (Casagrande et al. 1980).

An additional hydrochloric acid extraction step is added to ABA in circumstances where jarosite ($KFe_3(SO_4)_2(OH)_6$) is believed to add additional acidity upon addition of lime and dissolution of jarosite at neutral pH (Schafer et al. 1987). The HCl extraction removes jarosite from a sample during ABA analysis and allows for additional neutralizing minerals to be added during reclamation to

account for acid generation attributed to the presence of jarosite. The Schafer Method (1987) of ABA calculation uses a hot water extraction to remove nonacid producing sulfur forms, in addition to the HCl and HNO_3 extractions. The hot water extraction is intended to remove nonacid generating sulfate minerals such as gypsum and anhydrite.

DESCRIPTION OF MINERALS USED IN THIS INVESTIGATION

Mineral samples used in this investigation were obtained from commercial suppliers and operational mines. Operational coal and metal mines located in Montana, Idaho, Wyoming, South Dakota, Colorado, New Mexico, Arizona, Texas and Nevada provided materials for this project. At the request of participating mines, samples are not identified by source.

Sulfide bearing minerals were obtained from mines in a variety of forms including coal cleanings, coal overburden, coal, tailings, mine ore and waste rock. These diverse materials were subsequently crushed and high-graded. Samples were first high graded by using a water supplied shaker table, while the second high-grading resulted from heavy liquid separation (O'Meara et al. 1928).

Samples of sulfide and sulfate minerals were also obtained from Ward's Natural Science Establishment, a commercial mineral supplier. The geological history for these minerals is unknown. These samples were relatively pure and did not require high-grading procedures.

Identification Of Minerals Obtained From Operational Mines

The following descriptions of sulfide minerals used in this research are presented to provide insight into the geological character of the environment of formation.

- **Control** - The control sample was comprised of ground silica sand and contained no sulfide minerals. The control sample was commer-

cial grade 10/20 silica sand used for water well installations containing little impurity.

- **Copper Mine Tailings (Hardrock Pyrite)** - This sample was derived from a large open pit copper mine. Mineralization was hosted in coarse grained igneous rock. The tailing material lacked significant quantities of waste sulfide minerals other than pyrite. Pyrite particles were entirely euhedral morphology and typically less than 500 μm in diameter. The acid-base account (ABA) of the tailings was -31 tons $CaCO_3$ per 1000 tons waste material.
- **Metal Mine Tailings** - An historic metal mining district was the source of this sample. Pyrite was the dominant waste sulfide mineral present in these tailings which had a pH that ranged from 3 to 5. The mineralization was hosted in a coarse grained igneous rock, while the ABA was -51 tons $CaCO_3$ per 1000 tons waste material.
- **Montana Gold Mine Tailings** - Pyrite was the dominant sulfide waste mineral in this sample. Pyrite was disseminated throughout an igneous body which intruded the surrounding sedimentary formations. The particles were entirely euhedral in morphology and typically less than 250 μm in diameter. The ABA of the concentrated sulfide material from tailings was -891 tons $CaCO_3$ per 1000 tons waste material.

- **Gold Mine Tailings I** - Waste tailing material was obtained from this large open pit gold mine. Pyrite was the dominant sulfide material in tailings, but lesser amounts of chalcopyrite, covelite and enargite were present. The pyrite particles were entirely euhedral morphology, and typically less than 250 μm in diameter. The ABA of the tailing material was -78 tons $CaCO_3$ per 1000 tons waste material.
- **Gold Mine Tailings II (Hardrock Pyrrhotite)** - Pyrrhotite was the dominant waste iron sulfide mineral in the tailings though pyrite and marcasite were present in portions of the ore body. The sulfide sample material used in experimentation was entirely pyrrhotite. The gold mineralization was hosted in calcareous country rock. Waste sulfide material piles demonstrate exothermic reaction of pyrrhotite with atmospheric conditions. The pyrrhotite particles were entirely euhedral in morphology and typically less than 250 μm in diameter. The ABA of this was -137 tons $CaCO_3$ per 1000 tons waste material.
- **Gold Mine Ore** - Even dissemination of pyrite through the ore was common at this mine site. The mineralization occurred in coarse grained igneous rock. The pyrite particles were 65% euhedral and 35% massive particle morphology at this location, with some pyrite particles present in the ore as large as a few millimeters in diameter.

The ABA of the ore material was -178 tons $CaCO_3$ per 1000 tons waste material.

- **Molybdenum Mine Tailings** - The tailings were derived from the coarse grained igneous ore body where pyrite was evenly disseminated. Pyrite was the dominant waste mineral, comprising 0.50-0.75% of the ore body. The pyrite particles were 62% euhedral and 38% massive particle morphology. The tailing sample used in research had an ABA of -18 tons $CaCO_3$ per 1000 tons waste material.
- **Wyoming Coal Overburden** - The coal at this location averaged less than 1% sulfur, which tended to increase to greater than 1% sulfur in the overburden. The sulfur forms in the coal were three parts organic sulfur to one part pyritic sulfur, which was evenly disseminated throughout the overburden. Pyrite particles were dominantly massive in morphology and typically less than 500 μm in diameter. The ABA of the sulfide material submitted was -42 tons $CaCO_3$ per 1000 tons waste material.
- **Texas Coal Overburden** - The pyrite which comprised this sample was collected from overburden shale material containing large concretionary masses of massive morphology pyrite. Samples contained pyrite masses lacking definite crystal faces, 3 mm to 10 mm in thickness by 2 cm to 6 cm in length. This sample was comprised of 12% euhedral particles and 88% massive particles, though the

euhedral particles were only evident upon microscopic examination. This sample was not submitted for ABA analysis since it contained no minerals other than pyrite.

- **Nevada Gold Ore** - The dominant iron sulfide mineral from this location was pyrite, though orpiment and realgar were abundant in the waste material. The pyrite particles were dominantly massive particle morphology, and typically less than 500 μm in diameter. The ABA for the ore was -118 tons $CaCO_3$ per 1000 tons material.
- **Coal Cleaning Waste I (Coal Pyrite)** - Pyrite was the dominant waste mineral in this sample which consisted of massive particle morphology pyrite. This material was the reject material from a coal cleaning operation prior to crushing of the coal. Pyrite commonly occurs as concretionary masses of pyrite one to four centimeters in diameter. The ABA of the concentrated reject material was -734 tons $CaCO_3$ per 1000 tons waste material.
- **Coal Cleaning Waste II** - Platy secondary massive pyrite was present in this sample material which was the reject material from coal cleaning processes. Particle size was typically less than 2000 μm and occurred in thin layers within "cleats", or on the faces of vertical fractures within the coal. The ABA of the material was -944 tons $CaCO_3$ per 1000 tons waste material.

- **Underground Coal Waste** - Entirely massive pyrite particle morphology was present in this sample collected from an underground coal mine. Particle size was typically less than 500 μm in diameter. The sample used was from coal partings that were not planned for mining and were adjacent to the major coal seam. Analysis of ABA was not performed.

Identification Of Pure Mineral Samples By Source

Sulfide and sulfate minerals were obtained primarily from Ward's Natural Science Establishment for use in research. These mineral samples were provided as pure mineral samples lacking significant impurity.

A description of the mineral name used in the report, chemical composition, and geographic location of the source is presented.

- Barite ($BaSO_4$) - Madison County, Montana. This sample was provided by Dr. David Mogk, Montana State University, Geology Department.
- Anhydrite ($CaSO_4$) - Hants County, Nova Scotia, Canada.
- Gypsum ($CaSO_4 \cdot 2H_2O$) - Edmonton, Alberta, Canada.
- Anglesite ($PbSO_4$) - Chihuahua, Mexico.
- Jarosite ($KFe_3(SO_4)_2(OH)_6$) - Gila County, Arizona.
- Arsenopyrite (FeAsS) - Chihuahua, Mexico.
- Ward's pyrite (FeS_2) - Huanzala, Peru.

- Chalcocite (Cu_2S) - Butte, Montana.
- Ward's pyrrhotite - ($Fe_{1-x}S$) - Chihuahua, Mexico.
- Chalcopyrite ($CuFeS_2$) - Messina, Transvaal, Republic of South Africa.
- Galena (PbS) - Brushy Creek, Missouri.
- Marcasite (FeS_2) - Coconino County, Arizona.
- Sphalerite ((Zn,Fe)S) - Source unknown. This sample was provided by Dr. Lloyd Hossner, Texas A & M University.

THE INFLUENCE OF PARTICLE SIZE AND MORPHOLOGY ON SULFIDE MINERAL WEATHERABILITY

Acid Generation By Sulfide Mineral Oxidation

Sulfide minerals are commonly present in mining environments. Pyrite is the most common sulfide mineral and occurs in association with hardrock mineral assemblages and in depositional sedimentary environments. The oxidation of sulfide minerals, dominantly pyrite, has been implicated in the generation of acid upon mineral dissolution in the presence of oxygen and water. The generation of acid as a consequence of sulfide mineral oxidation is responsible for the degradation of thousands of miles of surface water streams, and tens of thousands of acres of land. The prevention of uncontrolled pyrite oxidation is, therefore, important in the prevention of potential negative environmental consequences. The prevention of pyrite oxidation is not always possible, so liming minerals are commonly added to sites containing sulfide minerals as pyrite to ameliorate the effects of pyrite oxidation.

Analysis of pyrite containing mine wastes is consequently very important to understanding the net potential acidity and rate of oxidation, such that adequate liming materials are present to neutralize acidity generated by pyrite oxidation. Net potential acidity is typically estimated by laboratory determination of the total sulfide sulfur content attributed to pyrite. The rate of oxidation of pyrite is poorly

understood, though field observation of the consequences of acid generation suggest that great variation occurs in the rate of pyrite oxidation.

The influence of sulfide particle size and morphology may be an important mineral physical property pertaining to the rate of sulfide mineral oxidation. The importance of total sulfide mineral surface area has been implicated in the rate of mineral oxidation (Pugh et al. 1984), though mineral surface area alone is an insufficient method of estimating the rate of sulfide mineral oxidation. The morphology of sulfide particles found in mining environments may exert a fundamental influence on the rate of oxidation in addition to surface area.

Pyrite is found in mining environments in many crystal forms as the dominant sulfide mineral, where crystal morphological characteristics are controlled by the environment of formation. Though great variation exists in pyrite particle morphology, three general classes of particle morphology were identified: euhedral, massive and framboidal. Euhedral particles are well formed crystals of regular atomic arrangement, typically found in hardrock mining environments. Massive particles are noncrystalline masses of mineral matter lacking regular atomic arrangement. Framboidal particles are a unique morphological class of spherical aggregates of crystalline pyrite typically less than 25 μm in diameter.

In this investigation, sulfide particles of different morphology from dissimilar mine environments were related to the acid generation ability of each morphological type by particle size. Sulfide minerals were submitted to oxidation by both H_2O/O_2, and by 10% H_2O_2 to assess the influence of particle size and morphology

on rate of acid generation. The evolution of chemicals in the resulting leachate was measured, and surface mineral dissolution behavior documented by scanning electron microscopy.

Methods

A diversity of samples was obtained from operational coal and metal mines in the western United States. The sample materials provided for use in research shared the common physical characteristic of containing sulfide minerals. The material provided included tailings, overburden, run of mine ore, coal, coal cleanings, processed concentrates, and diverse waste products suspected to contain sulfide minerals, dominantly as pyrite.

A subsample of each material was collected and analyzed for acid-base account by methods described by Schafer and others (1987).

Sample preparation

Waste materials were processed to remove the sulfide material from associated silicates. Initially, all the large sample material was crushed with a jaw crusher, and subsequently with a roller mill to reduce the particle size to approximately minus 500 μm. The crushed sample material was then subjected to gravimetric separation by a water-supplied shaker table which readily separated particles of the same size by density. The shaker table successfully high-graded sulfide mineral samples to 90% purity.

The high-graded sulfide material was then subjected to a second high-grading process (O'Meara 1928). A heavy organic liquid (1,1,2,2 tetrabromo-ethane, density = 2.96 g cm^{-3}), was placed in a separatory funnel. The sample material was added incrementally to the separatory funnel, and after agitation, heavy particles were allowed to settle from solution. Pyrite was the most common sulfide waste mineral and has a density of 5.01 g cm^{-3}, while most silicates present as an impurity have a density of 2.65 g cm^{-3}. Since the density of 1,1,2,2 tetra-bromoethane is intermediate between the two minerals, separation is accomplished by flotation of the lighter minerals. The heavy fraction passing through the liquid was collected from the bottom of the separatory funnel, rinsed with acetone and dried. Though the purity of samples surviving both high-grading steps was variable depending on minerals present and intergrowth of impurities, the mean percent impurity of 11 samples used was 5.1%, excluding the two samples which contained significant impurities.

Upon high-grading the sulfide fraction to approximately 95% purity, the removal of sulfates present as weathering products on pyrite crystals was initiated by HCl rinsing. The high-graded samples were rinsed for two hours in 6 M HCl, using five grams of sample material per 100 ml of 6 M HCl. During the rinsing step, the sample was agitated by a magnetic stir bar mixer. At the termination of two hours, the sample was poured into a filter paper to remove the HCl and subsequently rinsed with deionized water and allowed to air dry.

Particle Morphology Identification

After processing the mineral samples, identification of sulfide particle morphology was accomplished by reflected light microscopy. A subsample of the high-graded sample was placed on a glass slide and viewed with reflected light between 15 and 300 power magnification. Particles were classified as either massive or euhedral based on the structure of the crystals. No framboidal pyrite was observed.

After identification of the particle morphology, the high-graded samples were sieved and crushed by mortar and pestle into four size fractions: > 250 μm, 106-250 μm, 38-106 μm and <38 μm.

Sample Oxidation by 10% H_2O_2

From each of the four characteristic size fractions, one gram (1.000 ± 0.001 g) samples were weighed into weighed Erlenmeyer flasks. The flasks were then placed in an ice bath at 0° C. A 10% H_2O_2 solution was prepared using reagent grade hydrogen peroxide (30%) and deionized water. Fifty ml of 10% H_2O_2 was subsequently added to each sample and the ensuing reaction monitored and allowed to run to completion. The time of completion was recorded as the point at which effervescence or bubbling ceased in the reaction vessel.

Filtration of the residual sample material from the leachate was initiated at the point of completion of the reaction. Filtration was accomplished when the leachate and sample were poured into a weighed 11 cm Whatman No. 40 filter paper and allowed to drain by gravity. Ten milliliters of deionized water were

added to the Erlenmeyer flask as a rinsing step. The 10 ml deionized water rinse was added to the leachate sample in the filter paper, diluting the original 50 ml sample to 60 ml. The leachate was retained for subsequent analysis. The flask, residual sample, and filter paper were air dried for two hours at 40° C in a forced air oven and reweighed.

The leachate resulting from oxidation of each sample by 10% H_2O_2 was analyzed for pH and electrical conductivity, and for concentrations of sulfur, iron, and titratable acidity (Franson et al. 1989). Statistical comparisons between treatments for each response variable were made by the General Linear Model for unbalanced ANOVA (SAS 1985). Mean separation tests were performed by the Student-Newman-Keuls Method (Miller 1981).

Sample Examination By Scanning Electron Microscopy

The mineral material residual after oxidation was retained for examination by scanning electron microscopy (SEM) and energy dispersive analysis of x-rays (EDAX). Polished aluminum stub mounts were prepared for submission to the SEM by application of a thin film of colloidal graphite paint to the stub followed by sprinkling of the sample material on the wet paint. A conductive coating of Neutrastat was applied to the surface of the aluminum stub, and images collected at various magnifications. Images were collected from the mineral samples before and after oxidation with H_2O_2.

Examination of Surface Weathering Processes by SEM

A second set of unweathered mineral samples was prepared for SEM imaging by casting mineral samples in a 32 mm diameter epoxy mold. After the epoxy hardened, the surface was polished and coated with a conducting gold film. Polaroid images of fresh, unweathered, clean mineral surfaces were collected by SEM for particles of the same size from different sources. The epoxy pod was removed from the SEM and replaced in the sample cup from which the pod was cast with the fresh mineral surface facing up. Hydrogen peroxide (10 or 30%) was then placed in contact with the mineral surfaces and allowed to react. After a period of time (10 to 60 minutes), the unconsumed H_2O_2 was removed from the sample, which was then rinsed with deionized water, dried, recoated with gold, and replaced in the SEM. Polaroid images of the same mineral surfaces photographed before oxidation were collected to contrast the surface specific removal of mass from the mineral surface.

Water Weathering of Pyrite

Upon completion of hydrogen peroxide oxidation of the 13 member sulfide mineral sample set, a subset of four samples was subjected to oxidation by water. High-graded samples were crushed and sieved to obtain sufficient sample material less than 149 μm (Standard U.S. Sieve Number 100). A one gram sample (1.000 $\pm$ 0.001 g) was weighed into a 100 ml beaker and placed in a hot water bath at 35° C. Incremental additions of deionized water were added 2 ml at a time and allowed to air dry. The alternate wet-dry cycle was repeated 106 times over a 116

day period. Upon termination of the wet-dry cycle, 50 ml deionized water were added to the beaker. After 30 minutes, the sample was poured through a weighed 11 cm Whatman No. 40 filter paper. The leachate was retained for measurement of pH, electrical conductivity, titratable acidity, and determination of iron and sulfur levels by inductively coupled plasma emission spectroscopy (ICP). The filter paper and sample were dried in a forced air oven at 40° C for two hours and reweighed. Statistical comparisons were made by one-way analysis of variance (Snedecor and Cochran 1989).

Particle Morphology Identification

Each mineral sample was studied by optical and scanning electron microscope (SEM) to determine the relative compositional and morphological proportion of the particles comprising each high graded sample. Several published papers have identified many morphological forms of pyrite and numerous SEM photographs presented that have substantiated specific classes (Arora et al. 1978, Caruccio 1970 and 1976, Grady 1977, Haines 1986, Pugh et al. 1981, and Williams et al. 1982). In this investigation, the very specific morphological classes have been grouped into three broad morphological classes: euhedral, massive and framboidal.

Euhedral morphology particles exhibit a definite crystal face, developed by the growth of a regular crystalline lattice (Figure 1). Pyrite crystals do not break

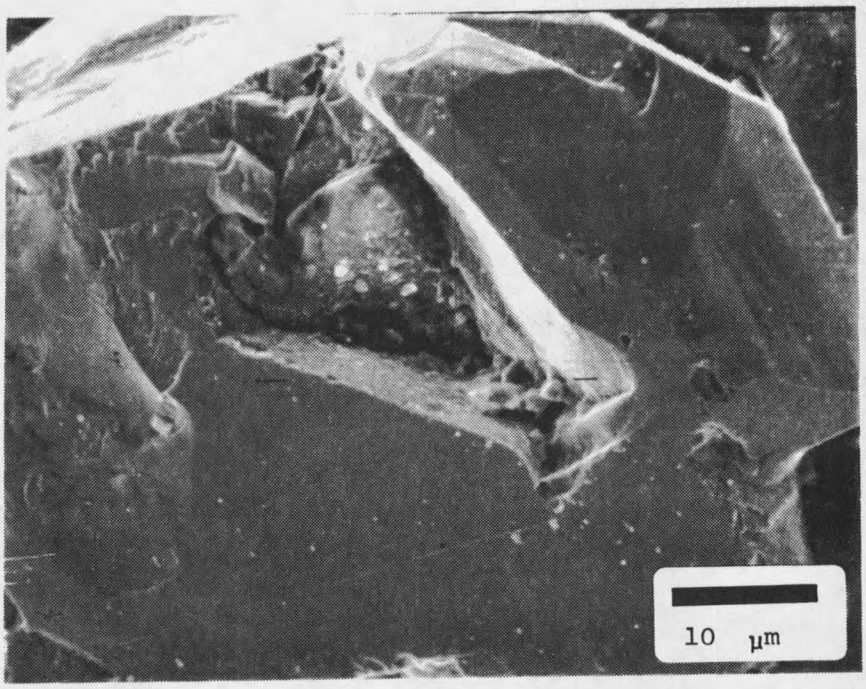

Figure 1. Scanning electron micrograph of a euhedral pyrite particle from Molybdenum Mine Tailings, (650X Magnification).

preferentially along the atomic lattice, so euhedral particles often exhibit a fractured crystal face not coincident with the crystalline structure. The fracture of euhedral pyrite is conchoidal, or smoothly curved. Euhedral particles commonly have high reflectivity and exhibit the characteristic brassy yellow color of pyrite in visible light. Crystal growth faces and regular linear surface features are commonly associated with euhedral pyrite particles. The development of euhedral pyrite is common in metalliferous mine environments, though the microcrystalline structure is dependent on the geochemical and thermodynamic conditions present at the time of mineral formation.

Massive pyrite particles are amorphous particles which have the chemical composition FeS_2, yet do not have regular crystalline structure (Figure 2). Massive particles are sometimes incorrectly considered large particles, but in the geologic usage of the word, massive only implies amorphous crystalline structure and not size [Throughout this thesis, massive morphology particles are considered to be amorphous to x-rays though this was not determined experimentally]. Massive particles do not commonly exhibit the characteristic brassy yellow color attributed to pyrite, though secondary massive pyrite formed in the cleats of coal can exhibit high reflectivity and brassy yellow color. Primary massive pyrite is pyrite which formed at the time of formation of the host rock, while secondary massive pyrite was formed at some time after initial lithification of the host rock. Massive pyrite is not distinguished by color, but entirely by the lack of crystalline structure.

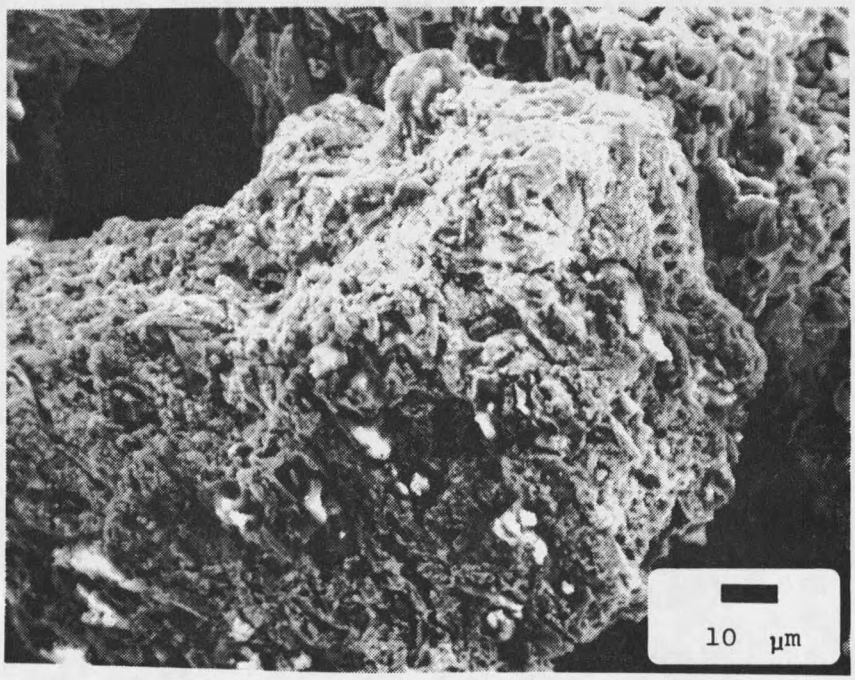

Figure 2. Scanning electron micrograph of massive pyrite from Coal Cleaning Waste I, (490X magnification).

Massive pyrite is common in depositional sedimentary environments which favor the formation of pyrite, though massive pyrite is also found in hardrock mine environments.

Framboidal pyrite is a special morphological form comprised of spherical aggregates of microcrystalline pyrite typically less than 25 μm in diameter. Framboidal pyrite is common in pyritic depositional sedimentary environments, and frequently implicated in the generation of acidic drainage under oxidizing conditions. Though framboidal pyrite was considered as a particle morphology of interest, none was identified in the sample set used for experimentation. Very small pyrite particles less than 1 μm in diameter were identified by SEM which may be the disaggregated remnant microcrystals which previously had been incorporated into the characteristic spherical framboidal structure. Figure 3 shows many μm and smaller size pyrite particles on the surface of a larger pyrite particle. Since no framboidal spheres were identified intact, no assumption was made that framboidal pyrite had been present. The sample set used during experimentation may have contained no framboidal pyrite, or the aggressive processing techniques used to high grade the sulfides may have disaggregated the framboids that were present. Regardless of the reason for the absence of framboidal pyrite, none was identified in the classification of particle morphology.

Particle morphology by sample source is identified in Table 1 inclusive of the presence of impurity. The mean percentage impurity for 11 of 13 samples listed is 5.1%, excluding the samples Gold Mine Tailings II and Nevada Gold Ore.

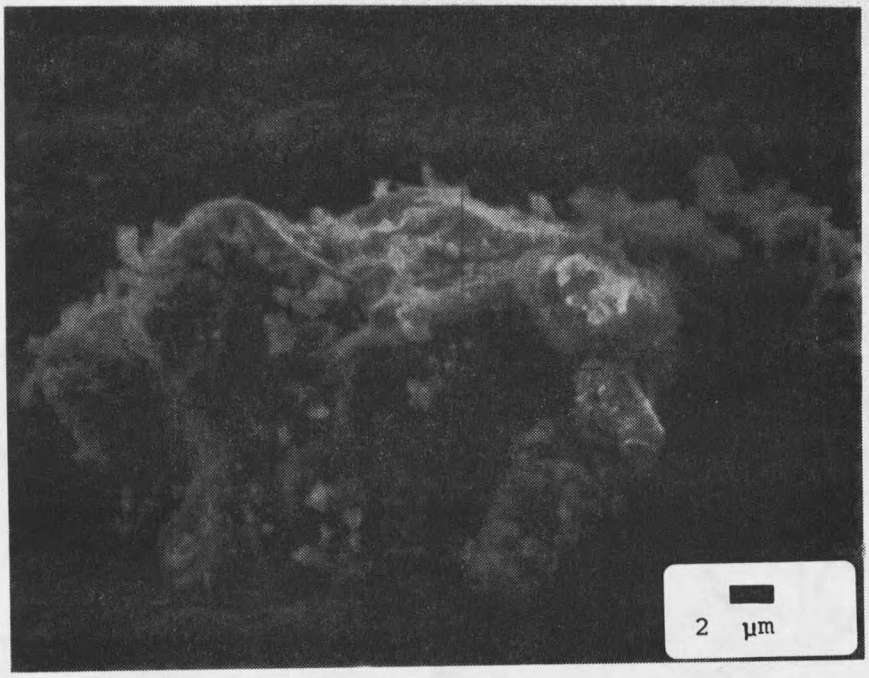

Figure 3. Scanning electron micrograph of 1 μm size pyrite particles on the surface of a larger pyrite particle, (2000X magnification).

Typically, the impurities were quartz and feldspars which were intergrown with pyrite, and were not removed by heavy liquid separation. The Gold Mine Tailings II sample contained 58% impurity due to the encapsulation and intergrowth of silicates with the sulfides which prevented disaggregation without crushing to a smaller particle size. The Nevada Gold Ore sample contained sulfide minerals other than iron sulfides which were more dense than the organic liquid used for final separation of the sulfides, and consequently were included in the final high graded sample and considered as impurities.

Table 1. Summary of particle morphology identification.

Sample Name	Number of Observations	Probable Mineral Impurities	Sample Particle Composition			
			% Impurity	Pyrite Particle Morphology		
				% Euhedral	% Massive	% Framboidal
Gold Mine Tailings II	324	quartz, anorthite	58	42	0	0
Wyoming Coal Overburden	334	orthoclase, barite, quartz	15.5	11.4	73	0
Underground Coal Waste	305	orthoclase, quartz	7.5	0	93	0
Gold Mine Ore	349	orthoclase, quartz	1.7	64.5	35.5	0
Molybdenum Mine Tailings	318	orthoclase, quartz	0	61.6	38.4	0
Gold Mine Tailings I	258	orthoclase, quartz, barite, sphalerite	10.5	89.5	0	0
Coal Cleaning Waste II	356	not analyzed	4.8	0	95.2	0
Metal Mine Tailings	290	not analyzed	0	100	0	0
Nevada Gold Ore	366	unspecified sulfides, quartz	70.2	0.8	28.1	0
Texas Coal Overburden	395	not analyzed	0.5	11.4	88.6	0
Montana Gold Mine Tailings	367	orthoclase, quartz	12.8	87.2	0	0
Copper Mine Tailings	364	not analyzed	1.6	98.4	0	0
Coal Cleaning Waste I	262	not analyzed	1.5	3	95.5	0

Three general classes of pyrite particle morphology are observed in Table 1: dominantly euhedral, dominantly massive and mixed (approximately 65% euhedral, 35% massive) morphology classes. The dominantly euhedral particle morphology class includes only samples derived from hardrock mine environments, while the dominantly massive particle morphology class includes both hardrock

and coal environment samples. The mixed morphology class is comprised of only two samples, both from hardrock mine environments.

The samples considered dominantly euhedral particle morphology include Gold Mine Tailings II (pyrrhotite), Gold Mine Tailings I, Metal Mine Tailings, Montana Gold Mine Tailings and Copper Mine Tailings (Table 1). All of these samples are from hardrock mineral mining environments.

The dominantly massive particle morphology samples are Wyoming Coal Overburden, Underground Coal Waste, Coal Cleaning Waste II, Nevada Gold Ore, Texas Coal Overburden and Coal Cleaning Waste I (Table 1). Five of six samples in this class are from depositional sedimentary environments, while the Nevada Gold Ore sample is derived from a hardrock mine environment.

The mixed morphology class has two members, Gold Mine Ore and Molybdenum Mine Tailings. Both of these samples have between 60 and 65% euhedral pyrite particles, while the balance are massive. Some of the samples classified as dominantly massive morphology also contain euhedral particles. The Texas Coal Overburden sample contains 11.4% euhedral particles (Table 1), as well as the Wyoming Coal Overburden sample which contains 11.4% euhedral particles. The relative abundance of any particle morphology is entirely a function of the physical conditions present in the environment of formation, so particles of varying morphologies may be present within a waste sample containing pyrite.

Acid-Base Account Of Natural Samples

The acid generation potential of materials present at mine sites is commonly assessed to determine which materials are suitable for placement in the plant root zone during site remediation. Acid forming materials are also selectively placed above aquifers to prevent or reduce water quality degradation. The acid-base account (ABA) method is used to ascertain the *potential acidity* of mine wastes, but does not indicate whether the material will be *acid generating*. One objective of this research was to develop an understanding of the process of acid generation from samples having potential acidity measured by ABA.

Prior to separation of the sulfide minerals from the natural sample, a subsample of the natural material was analyzed for ABA. Due to the diversity of the natural samples, some of the samples were previously processed (e.g. tailings and coal cleanings) prior to submission for use in research, so the ABA analysis was performed on the sample as received.

Acid-base account (Sobek et al. 1978, Schafer et al. 1987) is an analytical technique used to assess the acid generating potential of a sample. Potential acidity (PA) is identified by the fractionation of acid generating and nonacid forming sulfur forms. Neutralization potential (NP) is expressed as the proportion of calcium carbonate present, and considered to neutralize acid formed by the oxidation of pyrite (Equation 14).

$$ABA = NP - PA \qquad [14]$$

A negative ABA occurs when PA exceeds NP, while a positive ABA is indicative of neutralization ability in excess of the potential acidity. The units of ABA are expressed as tons $CaCO_3$ required to neutralize the acidity generated by 1000 tons waste material (e.g. -16 tons $CaCO_3$/1000 tons).

All of the natural samples listed in Table 2 have negative ABA values, meaning the PA exceeds the NP for all samples. The total sulfur range of the samples is from 0.96% sulfur for the Molybdenum Mine Tailings to 33.1% sulfur for the Coal Cleaning Waste II sample, while the ABA range was from -17 tons $CaCO_3$/1000 tons waste material for the Coal Barite sample to -944 tons $CaCO_3$/-1000 tons waste material for the Coal Cleaning Waste II sample.

The determination that the entire sample set was potentially acid forming by ABA sets the stage for the characterization of the acid producing processes associated with each sample. Since the subsequent treatment of samples deals only with maximum potential acidity and not neutralization potential, the influence of calcium carbonate on acid generation is considered only in Table 2.

Weatherability Of Sulfide Minerals By Oxidation With Hydrogen Peroxide

The weathering of sulfides, primarily pyrite, and subsequent generation of acid is a significant source of resource degradation in areas disturbed by mining. Characterization of the problem is difficult because mines which have similar laboratory analyzed potential acidity levels may yield acid during mining and land

Table 2. Acid-base account results of samples as received, prior to high-grading.

Mine Name	Neutralization Potential tons $CaCO_3$ per 1000 tons	Hot Water Extractable SO_4-S	HCl Extractable SO_4/Sulfide-S	HNO Extractable Sulfide-S	Residual S	Total Sulfur (%)	Acid[1] Base Account tons $CaCO_3$ per 1000 tons
		%					
Underground Coal Waste	11	0.00	0.00	0.98	0.30	1.28	-29
Wyoming Coal Overburden	8	0.21	0.00	0.91	0.69	1.81	-42
Gold Mine Ore	0	0.82	0.00	5.00	0.68	6.50	-178
Nevada Gold Ore	31	0.34	0.00	3.39	1.38	5.11	-118
Metal Mine Tailings	0	0.00	0.16	1.41	0.06	1.63	-51
Gold Mine Tailings I	0	0.00	0.03	2.38	0.08	2.49	-78
Coal Barite	0	0.66	0.01	0.23	0.30	1.20	-17
Molybdenum Mine Tailings	11	0.02	0.00	0.93	0.01	0.96	-18
Gold Mine Tailings II	71	0.00	0.00	0.65	6.03	6.68	-137
Coal Cleaning Waste I	0	0.20	0.00	20.9	2.64	23.7	-734
Coal Cleaning Waste II	19	2.30	0.00	28.7	2.09	33.1	-944
Copper Mine Tailings	8	0.00	0.00	1.21	0.00	1.24	-31
Montana Gold Mine Tailings	24	0.00	0.00	25.6	3.71	29.3	-891

[1] ABA = Neutralization Potential - {(HNO_3 ext. S + Residual S) (31.25) + (HCl ext. S) (23.44)}.

remediation at very different rates. The oxidation of pyrite by oxygen and water is presented in Equation 15.

$$FeS_2 + \frac{15}{4} O_2 + \frac{7}{2} H_2O = Fe(OH)_3 + 2\,SO_4^{2-} + 4\,H^+ \qquad [15]$$

The simulation of natural weathering in the laboratory by H_2O in the presence of O_2 has been attempted with limited success. The great length of time required to attain a laboratory response to H_2O/O_2 weathering limits the practicality of water weathering tests for assessment of acid generation. Hydrogen peroxide is a stronger oxidizer than the H_2O/O_2 redox pair, so rapid characterization of potentially acid producing samples can be accomplished (Equation 16) (O'Shay et

$$FeS_2 + \frac{15}{2} H_2O_2 = Fe(OH)_3 + 2\,SO_4^{2-} + 4\,H^+ + 4\,H_2O \qquad [16]$$

al. 1990). The weathering of sulfides by hydrogen peroxide accentuates the differences between samples when compared to H_2O weathering, and facilitates the understanding of acid generation principles.

High graded sulfide minerals, dominantly pyrite, were subjected to oxidation by 10% H_2O_2 under laboratory conditions. The evolution of chemical constituents to the resulting leachate was recorded in parallel with the mass removed during oxidation. All leachate parameters (pH, electrical conductivity, iron, sulfate, and titratable acidity) as well as mass loss and reaction time parameters were recorded by sample source and particle size. The dominant crystal morphology of each sample was recorded for each sample. Four particle size fractions were used consistently, >250 μm, 106-250 μm, 38-106 μm and <38 μm. Wherever

sufficient sample material was available, three replications were performed for each sample by particle size class. Raw data are shown in Table 19, Appendix.

Sulfide Mineral Mass Change After Weathering

The change in mass during oxidation of 1.000 gram of high graded sulfide mineral was recorded by retaining and weighing the mineral sample mass residual after oxidation by 10% H_2O_2. The mass lost by all sulfide mineral samples was referenced to the control sample which was silica sand (Table 3), and to the original 1.000 gram mass. Mass loss is a function of the reactivity of each sample to 50 ml 10% H_2O_2. Since all samples were submitted to oxidation under the same conditions (0° C), the ease of oxidation, or reactivity, of a sample can be measured directly by the mass lost during treatment.

The mean Copper Mine Tailings sample mass lost during oxidation was 2.97%, while the mean sample mass lost by the Texas Coal Overburden was 60.19% (Table 3). These two samples are the endpoints of a broad range. The mean mass loss data by sample source demonstrated many levels of significance among the 14 samples. At the 95% confidence level, 10 of 14 samples were significantly different from one another.

Mass loss by particle size fraction was compared and reported in Table 3. The overall mean mass loss data demonstrates significant differences ($p \leq 0.05$) between all of the particle size fractions. The mean mass lost by the >250 μm size fraction was 39.42%, while the mass lost by the 106-250 μm, 38-106 μm and <38 μm size fractions was 27.83%, 26.47% and 16.04%, respectively. Therefore,

Table 3. Mean sample mass lost (%) following laboratory weathering by 10% hydrogen peroxide at 0° C by particle size.

Sample	Crystalline Form (% Euhedral/% Massive)	MASS LOST (%) Particle Size Fraction (μm) > 250	106-250	38-106	< 38	Mean
Control	100 / 0	- 0.97 Aa*†‡	- 0.86 Aa	- 1.10 Aa	- 1.20 Aa	- 1.03 A
Copper Mine Tailings	100 / 0	- 2.07 Aa	- 2.69 Bb	- 2.36 Aab	- 4.45 Bc	- 2.97 B
Metal Mine Tailings	100 / 0	---	-20.92 Fc	-17.78 Db	-10.53 Da	-16.41 F
Montana Gold Mine Tailings	100 / 0	---	-12.22 Eb	-13.88 Cc	- 8.16 Ca	-11.42 E
Gold Mine Tailings I	100 / 0	---	- 3.64 Ba	- 3.81 Aa¶	- 4.25 Ba	- 3.91 B
Gold Mine Tailings II	100 / 0	---	- 7.65 Cb	- 9.58 Bc	- 5.20 Ba	- 7.47 C
Gold Mine Ore	65 / 35	- 8.40 Ba	-10.19 Dc	- 9.27 Bb	-11.13 Dd	- 9.75 D
Molybdenum Mine Tailings	62 / 38	-10.56 Bb	- 9.91 Da	- 9.46 Ba	-14.65 Ec	-11.15 E
Wyoming Coal Overburden	14 / 86	-42.17 Cb	-40.62 Hb	-36.32 Fa§	---	-40.67 H
Texas Coal Overburden	12 / 88	-67.34 Fcb	-69.33 Lc	-64.77 Ib	-39.34 Ha	-60.19 L
Nevada Gold Ore	3 / 97	-74.57 Gd	-32.88 Gc	-25.15 Eb	- 6.98 Ca	-34.89 G
Coal Cleaning Waste I	3 / 97	-59.40 Eb	-59.60 Jb	-58.86 Hb	-33.43 Fa	-52.82 J
Coal Cleaning Waste II	0 / 100	-49.65 Dc	-53.55 Id	-48.48 Gb	-36.01 Ga	-46.92 I
Underground Coal Waste	0 / 100	-66.59 Fb	-65.53 Kb	-68.81 Jb	-33.15 Fa	-58.52 K
Mean		-39.42 d	-27.83 c	-26.47 b	-16.04 a	---

* Mean of three replications, unless otherwise noted.

† Means in the same *column* followed by the same *uppercase* letter are not significantly different ($p \leq 0.05$).

‡ Means in the same *row* followed by the same *lowercase* letter are not significantly different ($p \leq 0.05$).

¶ Mean of two replications.

§ N = 1.

the largest size fraction, which lost the greatest mass, was the most acid generating.

The overall mean differences are also reflected by statistically significant differences between samples of the same particle size. In the >250 μm particle size class the samples lost 0.97%, 2.07%, 8.40%, 10.56%, 42.17%, 49.65%, 59.40%, 66.59%, 67.34% and 74.57% of their original mass in ascending order (Table 3). The Gold Mine Ore sample (8.40%) and Molybdenum Mine Tailings sample (10.56%) are not significantly different ($p \leq 0.05$), which is also true of the Control sample (silica sand, 0.97%) and Copper Mine Tailings sample (2.07%), as well as the Texas Coal Overburden (67.34%) and Underground Coal Waste sample (66.59%). The balance of the sample set is significantly different from each other member.

Particle morphology was found to exert a strong influence on the sample mass lost by oxidation. The massive particle morphology samples lost more mass than the euhedral particle morphology samples when subjected to the same treatment. For example, the Copper Mine Tailing sample is comprised of 100% euhedral pyrite particles and lost the least mass (Table 3), while the samples with dominantly massive particle morphology lost the greatest amount of their original mass (42.17% to 74.57%). The Gold Mine Ore sample and Molybdenum Mine Tailings sample were mixed euhedral and massive particle morphology samples, and had measured mass loss values intermediate, and significantly different from, the dominantly euhedral and dominantly massive particle morphology samples.

The difference in mass loss by particle size from a specific source is also dependent on the particle morphology. Euhedral particles typically exhibited little difference in mass loss between the particle size classes. For example, the Gold Mine Tailings I sample (Table 3), which was 100% euhedral, lost a mean 3.64%, 3.81% and 4.25% of the original mass for each size fraction, none of which were statistically different ($p \leq 0.05$). While the Gold Mine Tailings II sample, which was also 100% euhedral particle morphology, lost a mean 7.65%, 9.58% and 5.20% of the original mass for each size fraction. Each of the Gold Mine Tailings II particle size fractions were significantly different from one another ($p \leq 0.05$).

Massive morphology particles typically demonstrate a marked decrease in mass loss for the smallest size fraction (Table 3) when compared to the three largest size fractions. Underground Coal Waste is a dominantly massive particle morphology sample. The mean mass loss for the Underground Coal Waste sample from largest to smallest size fraction was 66.59%, 65.53%, 68.81% and 33.15%. Only the smallest size fraction is significantly different ($p \leq 0.05$) from the others. The trend toward decreasing mass loss for the smallest size fraction is repeated by the other dominantly massive morphology samples. It is believed that the reason for small particle size resistance to oxidation relates to the particle morphology and crystallization history of the sample. It is not uncommon to see an occasional small reflective euhedral crystal face entombed in a larger massive pyrite particle. These small euhedral particles likely formed initially when thermo-dynamic and geochemical conditions were such that crystalline euhedral pyrite had

the opportunity to grow. Subsequent to formation of the small euhedral particles, thermodynamic and geochemical conditions changed and late stage massive pyrite formed around the previously formed euhedral particles. The smallest size fraction consequently had a greater proportion of better formed crystals which were relatively more resistant to oxidation. This hypothesis is further supported by SEM observation of samples before and after weathering. Figure 2 illustrates a typical massive pyrite particle prior to weathering, while Figure 4 illustrates the residual sample material from the same sample set after oxidation by 10% H_2O_2. Note that the particles in Figure 4 have been attacked by oxidation, as is evident from the formation of etch pits, but that the residual material particle morphology demonstrates linear surface features characteristic of euhedral pyrite which were not evident in Figure 2. The material in Figure 4 is considered relatively resistant to oxidation since it survived treatment with hydrogen peroxide.

Both coal and hardrock mineral mine environments have particles of different morphologies, massive and euhedral. In general the hardrock mine environments are dominantly euhedral morphology and the coal bearing depositional sedimentary environments are dominantly massive particle morphology. This generality is highly variable. The Nevada Gold Ore, for example, is dominantly massive pyrite though the pyrite is not from a depositional sedimentary environment, rather the pyrite is associated with gold mineralization from an igneous intrusive.

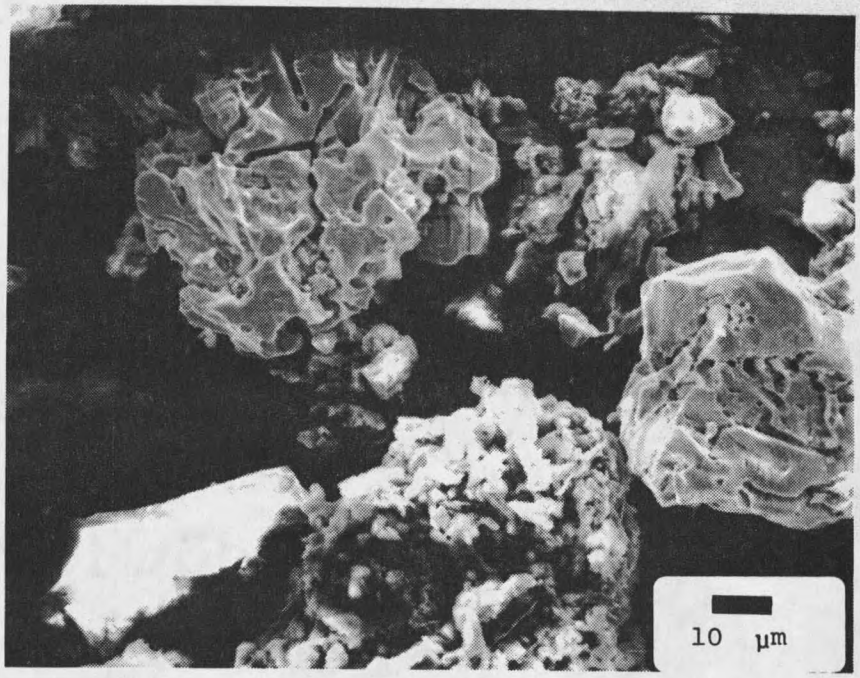

Figure 4. Scanning electron micrograph of pyrite particles from Coal Cleaning Waste I which survived oxidation by 10% H_2O_2, (490X magnification).

Regardless of the environment of formation, the largest massive pyrite particles have the greatest rate of acid generation. The largest three of four size fractions of the dominantly massive morphology samples lost the greatest fraction of their original mass (Table 3) during treatment with 10% H_2O_2. Massive pyrite particles of any size fraction are also more readily oxidized, and generate acid more quickly than the euhedral pyrite particles (Table 3). All of the dominantly massive morphology samples lost significantly more mass than the dominantly euhedral morphology samples when subjected to the identical treatment.

Sulfide Mineral Leachate pH After Weathering

Leachate pH was measured after collection of a leachate sample at the point of termination of the reaction of the sample material with 10% H_2O_2. The leachate parameters are based on the observation that all the hydrogen peroxide has been consumed at the point of completion of the reaction. Reaction completion was identified as the point at which bubbling ceased in the reaction vessel.

The 10% H_2O_2 had the least effect on the Control sample (silica sand) pH during treatment (Table 4). The pH of the hydrogen peroxide prior to addition to the sample material was approximately 4.50. After reaction, the Control sample mean pH was 3.68. The Control sample mean pH was not significantly different ($p \leq 0.05$) from the Copper Mine Tailings mean pH which was 2.61. The most acidic pH was attributed to the Nevada Gold Ore sample which had a mean pH of 1.35. The general trend established by the mass loss data was followed by the pH data, where samples which lost the greatest mass during reaction had the lowest leachate pH.

Using the 106-250 μm size fraction as an example of leachate pH by sample source for a specific size class, the most acidic leachate was measured in the Coal Cleaning Waste (I and II) samples which had a mean pH of 1.37 and 1.38 and were not significantly different ($p \leq 0.05$) (Table 4). The Wyoming Coal Overburden had a leachate pH of 1.46, which was significantly different from the Texas Coal Overburden, Nevada Gold Ore and Underground Coal Waste samples which had mean leachate pH values of 1.53, 1.50 and 1.53, respectively. These

Table 4. Mean sample extract pH following laboratory weathering by 10% hydrogen peroxide at 0° C by particle size.

Sample Source	Crystalline Form (% Euhedral/% Massive)	pH Particle Size Fraction (μm) > 250	106-250	38-106	< 38	Mean
Control	100 / 0	3.83 Db*†‡#	3.70 Gb	3.78 Ib	3.41 Ga	3.68 I
Copper Mine Tailings	100 / 0	2.73 Dd	2.58 FGb	2.66 HIc	2.48 Ga	2.61 HI
Metal Mine Tailings	100 / 0	---	1.67 Da	1.62 Ea	1.79 Eb	1.69 E
Montana Gold Mine Tailings	100 / 0	---	1.93 Ea	1.81 Fa	1.98 Fa	1.91 F
Gold Mine Tailings I	100 / 0	---	2.38 Fa	2.35 Ha¶	2.45 Ga	2.40 H
Gold Mine Tailings II	100 / 0	---	2.07 Ea	2.07 Ga	2.01 Fa	2.05 G
Gold Mine Ore	65 / 35	1.88 Ca	1.95 Ea	1.95 Ga	1.94 Fa	1.93 FG
Molybdenum Mine Tailings	62 / 38	2.02 CDb	2.03 Eb	2.00 Gb	1.80 Ea	1.96 FG
Wyoming Coal Overburden	14 / 86	1.53 Ba	1.46 Ba	1.50 CDa§	---	1.50 C
Texas Coal Overburden	12 / 88	1.49 Ba	1.53 Cb	1.60 Ec	1.55 Cb	1.54 D
Nevada Gold Ore	3 / 97	1.24 Aa	1.50 Cb	1.54 Db	1.14 Aa	1.35 A
Coal Cleaning Waste I	3 / 97	1.46 Bb	1.37 Aa	1.37 Aa	1.54 Cc	1.44 B
Coal Cleaning Waste II	0 / 100	1.39 Bab	1.38 Aa	1.42 Bab	1.49 Bb	1.42 B
Underground Coal Waste	0 / 100	1.54 Ba	1.53 Ca	1.48 Ca	1.68 Db	1.56 D
Mean		1.91 a	1.94 b	1.95 b	1.94 b	---

* Mean of three replications, unless otherwise noted.

† Means in the same *column* followed by the same *uppercase* letter are not significantly different ($p \leq 0.05$).

‡ Means in the same *row* followed by the same *lowercase* letter are not significantly different ($p \leq 0.05$).

¶ Mean of two replications.

§ N = 1.

\# Statistics calculated from hydrogen ion content (mg l^{-1}).

five samples are dominantly massive particle morphology and have leachate pH values significantly less than the dominantly euhedral particle morphology samples.

The overall influence of particle size, regardless of particle morphology, suggests that the largest size fraction (>250 μm) generated the most acidic leachate. The mean leachate pH for the >250 μm size fraction was 1.91 while the other size fractions had leachate pH means of 1.94 or 1.95, both of which were significantly higher. These pH data strongly support the contention that the samples which lost the greatest mass generate the greatest acidity, since the lowest leachate pH is associated with the samples which lost the greatest amount of their original mass (Table 3).

Sulfide Mineral Leachate Electrical Conductivity After Weathering

Upon collection of a leachate sample at the termination of the reaction of the sample with 10% H_2O_2 the electrical conductivity was measured and recorded. The leachate electrical conductivity was measured at the same time as the pH and parallels the trend established by pH and mass loss. The samples which lost the largest fraction of their original mass resulted in the lowest pH values and highest leachate electrical conductivities.

The control sample (silica sand) mean electrical conductivity was 0.11 dS m^{-1} which was significantly less than any of the other sample sources. Of the sulfide material submitted to oxidation by 10% H_2O_2 the Copper Mine Tailings had the lowest mean leachate electrical conductivity (2.28 dS m^{-1}), while the

Nevada Gold Ore had the highest leachate electrical conductivity (37.76 dS m^{-1}) (Table 5).

Many of the samples from geographically different mining environments were significantly different from one another, suggesting that *site specific variation* in sulfide particle physical properties will result in dissimilar response to oxidizing conditions. The electrical conductivity results further support the contention that particle morphology exerts a strong influence on pyrite oxidation. The dominantly massive particle morphology samples achieved the highest leachate electrical conductivity while all of the dominantly euhedral morphology samples had leachate electrical conductivities which were significantly less ($p \leq 0.05$) than the dominantly massive samples.

The result of particle size variation on leachate electrical conductivity demonstrates a trend of decreasing electrical conductivity with decreasing particle size (Table 5). The greatest mean leachate electrical conductivity is attributed to the largest size fraction (>250 μm), while the lowest leachate electrical conductivity is attributed to the smallest size fraction (<38 μm). All of the overall mean leachate electrical conductivity values by particle size fraction are significantly different ($p \leq 0.05$) from one another, indicating that evolution of chemical constituents is greatest in the largest size fraction.

Table 5. Mean sample extract electrical conductivity (dS m^{-1}) following laboratory weathering by 10% hydrogen peroxide at 0° C by particle size.

Sample Source	Crystalline Form (% Euhedral/% Massive)	Electrical Conductivity (dS m^{-1}) Particle Size Fraction (μm) > 250	106-250	38-106	< 38	Mean
Control	100 / 0	0.10 Ib*†‡	0.07 Lb	0.06 Mb	0.22 Ia	0.11 L
Copper Mine Tailings	100 / 0	1.52 Hc	2.11 Kb	2.00 Lb	3.49 GHa	2.28 K
Metal Mine Tailings	100 / 0	---	13.73 Fa	12.50 Gb	7.85 Ec	11.36 F
Montana Gold Mine Tailings	100 / 0	---	8.43 Gb	9.30 Ha	5.65 Fc	7.79 G
Gold Mine Tailings I	100 / 0	---	2.77 Kb	3.19 Ka¶	2.97 Hab	2.95 J
Gold Mine Tailings II	100 / 0	---	3.81 Jb	3.47 Kc	4.36 Ga	3.88 I
Gold Mine Ore	65 / 35	6.53 Gb	7.69 Ha	6.93 Ib	7.99 Ea	7.28 H
Molybdenum Mine Tailings	62 / 38	6.82 Gb	6.40 Ic	6.16 Jc	9.00 Da	7.10 H
Wyoming Coal Overburden	14 / 86	19.27 Fb	22.91 Ea	20.92 Fab§	---	21.07 E
Texas Coal Overburden	12 / 88	34.52 Cb	35.45 Ba	33.01 Bc	22.25 Bd	31.31 C
Nevada Gold Ore	3 / 97	60.48 Aa	29.92 Cc	24.79 Ed	34.92 Ab	37.76 A
Coal Cleaning Waste I	3 / 97	28.96 Da	29.36 CDa	28.74 Ca	18.68 Cb	26.43 D
Coal Cleaning Waste II	0 / 100	27.41 Eb	28.63 Da	26.80 Db	21.41 Bc	26.06 D
Underground Coal Waste	0 / 100	37.28 Bb	37.63 Ab	40.48 Aa	18.13 Cc	33.38 B
Mean		22.29 a	16.35 b	15.64 c	11.47 d	---

* Mean of three replications, unless otherwise noted.

† Means in the same *column* followed by the same *uppercase* letter are not significantly different ($p \leq 0.05$).

‡ Means in the same *row* followed by the same *lowercase* letter are not significantly different ($p \leq 0.05$).

¶ Mean of two replications.

§ N = 1.

Sulfide Mineral Leachate Iron Content After Weathering

The summary of leachate iron data is presented in Table 6, and supports the preceding discussion and results from mass loss, pH and electrical conductivity. The samples which lost the greatest proportion of their original mass had the lowest leachate pH, highest leachate electrical conductivity and highest leachate iron.

Comparisons of mean leachate iron content by sample source reveal a range from 1 mg l^{-1} to 5766 mg l^{-1} (Table 6). The lowest leachate iron content resulted from the attempted oxidation of the silica sand control, which resulted in very low levels of leachate iron. The lowest leachate iron content from one of the pyrite treatments (Copper Mine Tailings), 183 mg l^{-1} was not significantly different from the Control. The greatest mean leachate iron was attributed to the Underground Coal Waste sample which had a mean leachate iron content of 5766 mg l^{-1}.

The influence of particle size on leachate iron follows the same trend as the mass loss data. The overall mean leachate iron content increases from small particle size to large. The mean leachate iron measured in the four size fractions was 1497 mg l^{-1}, 2629 mg l^{-1}, 2694 mg l^{-1}, and 3680 mg l^{-1}, for the respective size fractions <38 μm, 38-106 μm, 106-250 μm and >250 μm (Table 6). The 106-250 μm and 38-106 μm size fractions are not different ($p \leq 0.05$). The trend toward decreasing leachate iron content with decreasing particle size is most strongly supported by the dominantly massive particle morphology samples, and not well supported by the dominantly euhedral morphology samples.

Table 6. Mean sample extract iron (mg l^{-1}) following laboratory weathering by 10% hydrogen peroxide at 0° C by particle size.

Sample Source	Crystalline Form (% Euhedral/% Massive)	Iron (mg l^{-1}) Particle Size Fraction (μm) > 250	106-250	38-106	< 38	Mean
Control	100 / 0	0 Hb*†‡	0 Ib	0 Gb	5 Ja	1 I
Copper Mine Tailings	100 / 0	120 Hc	179 HIb	165 Gb	268 Ia	183 HI
Metal Mine Tailings	100 / 0	---	2188 Da	1936 DEb	1060 Fc	1728 E
Montana Gold Mine Tailings	100 / 0	---	1239 Eb	1405 EFa	758 Gc	1134 F
Gold Mine Tailings I	100 / 0	---	315 Hc	404 FGa¶	353 Hb	351 H
Gold Mine Tailings II	100 / 0	---	641 Gc	1002 EFGa	768 Gb	803 G
Gold Mine Ore	65 / 35	840 Gc	989 Fb	940 EFGb	1162 Ea	983 FG
Molybdenum Mine Tailings	62 / 38	1011 Gb	964 Fb	927 EFGb	1460 Da	1090 F
Wyoming Coal Overburden	14 / 86	3365 Fb	3863 Ca	3371 Cb§	---	3579 D
Texas Coal Overburden	12 / 88	6024 Cb	6253 Aa	5744 Bc	3300 Bd	5330 B
Nevada Gold Ore	3 / 97	8054 Aa	3726 Cb	2698 CDc	253 Id	3683 D
Coal Cleaning Waste I	3 / 97	5760 Da	5444 Ba	5491 Ba	3086 Cb	4945 C
Coal Cleaning Waste II	0 / 100	5186 Ea	5488 Ba	5656 Ba	3620 Ab	4988 C
Underground Coal Waste	0 / 100	6441 Bb	6431 Ab	6826 Aa	3365 Bc	5766 A
Mean		3680 a	2694 b	2629 b	1497 c	---

* Mean of three replications, unless otherwise noted.

† Means in the same *column* followed by the same *uppercase* letter are not significantly different ($p \leq 0.05$).

‡ Means in the same *row* followed by the same *lowercase* letter are not significantly different ($p \leq 0.05$).

¶ Mean of two replications.

§ N = 1.

Sulfide Mineral Leachate Sulfate Content After Weathering

Sulfate in leachate was measured after completion of the reaction of the mineral material with 10% H_2O_2. Laboratory analysis for the determination of sulfate was performed by Inductively Coupled Plasma Emission Spectroscopy (ICP). Speciation of leachate sulfur was performed by Ion Chromatography on a subset of the total sample set to confirm that the dominant sulfur species in leachate was sulfate. Consequently, laboratory results were reported as leachate sulfate.

The result of sulfate analysis strongly supports the previous results measured by the parameters mass loss, leachate pH, leachate electrical conductivity and leachate iron. Samples which lost the greatest proportion of their original mass resulted in the lowest leachate pH, highest leachate electrical conductivity, and highest iron and sulfate content.

The influence of sample source on leachate sulfate is presented in Table 7. The control sample mean leachate sulfate was 15 mg l^{-1} which was significantly different ($p \leq 0.05$) from all other sample sources. The Copper Mine Tailings pyrite sample had the lowest mean leachate sulfate content after oxidation, 762 mg l^{-1}, while the Texas Coal Overburden pyrite sample had the highest mean leachate sulfate content, 20641 mg l^{-1}. Within the range established by the two extremes, the remaining samples were intermediate and all were significantly different ($p \leq 0.05$) from one another except for the Montana Gold Mine Tailings and Molybdenum Mine Tailings sample sources. The statistical comparison of

Table 7. Mean sample extract sulfate (mg l^{-1}) following laboratory weathering by 10% hydrogen peroxide at 0° C by particle size.

Sample Source	Crystalline Form (% Euhedral/% Massive)	Sulfate (mg l^{-1}) Particle Size Fraction (μm) > 250	106-250	38-106	< 38	Mean
Control	100 / 0	0 Hb*†‡	2 Lb	2 Mb	54 Ka	15 M
Copper Mine Tailings	100 / 0	496 Hc	690 Kb	672 Lb	1191 Ja	762 L
Metal Mine Tailings	100 / 0	---	7609 Ga	6499 Gb	3544 Gc	5884 G
Montana Gold Mine Tailings	100 / 0	---	3975 Hb	4484 Ha	2677 Hc	3712 H
Gold Mine Tailings I	100 / 0	---	1143 Kc	1397 Ka¶	1312 Jb	1270 K
Gold Mine Tailings II	100 / 0	---	1926 Jb	2408 Ja	2407 Ia	2247 J
Gold Mine Ore	65 / 35	2842 Gd	3334 Ib	3092 Ic	3797 Ga	3266 I
Molybdenum Mine Tailings	62 / 38	3508 Gb	3226 Ic	2996 Ic	4583 Fa	3578 H
Wyoming Coal Overburden	14 / 86	10561 Fb	12085 Fa	10737 Eb§	---	11239 F
Texas Coal Overburden	12 / 88	23640 Ba	24127 Aa	22111 Bb	12684 Ac	20641 A
Nevada Gold Ore	3 / 97	26306 Aa	12919 Eb	9283 Fc	5693 Ed	13550 E
Coal Cleaning Waste I	3 / 97	19031 Da	18098 Db	17901 Cb	9930 Dc	16240 D
Coal Cleaning Waste II	0 / 100	18204 Eb	19281 Ca	16376 Dc	12332 Bd	16548 C
Underground Coal Waste	0 / 100	22485 Cb	22503 Bb	24105 Aa	11309 Cc	20101 B
Mean		12707 a	9351 b	8803 c	5501 d	---

* Mean of three replications, unless otherwise noted.

† Means in the same *column* followed by the same *uppercase* letter are not significantly different ($p \leq 0.05$).

‡ Means in the same *row* followed by the same *lowercase* letter are not significantly different ($p \leq 0.05$).

¶ Mean of two replications.

§ N = 1.

leachate sulfate by sample source within a particle size fraction is similar to the statistical comparison of the overall mean independent of particle size.

Ignoring the influence of sample source, the overall mean leachate sulfate results by particle size demonstrate the recurring trend of decreasing concentration with decreasing particle size. The overall mean leachate sulfate content for the >250 μm size fraction was 12707 mg l^{-1}, while the 106-250 μm, 38-106 μm and <38 μm size fractions were 9351 mg l^{-1}, 8803 mg l^{-1} and 5501 mg l^{-1}, respectively. All the particle size fractions demonstrated statistically significant differences ($p \leq 0.05$) among each of the members.

Sulfide Mineral Leachate Titratable Acidity After Weathering

Titratable acidity was measured in the leachate after termination of the reaction of the mineral sample with 10% H_2O_2. The results of titratable acidity measurement are reported in Table 8. Titratable acidity is considered the response variable of greatest importance in the investigation of the oxidation of sulfide materials and their subsequent generation of acid. The titratable acidity results are supported by the analysis of mass loss, pH, electrical conductivity, leachate iron and leachate sulfate, but titratable acidity is treated as the primary variable since it directly measures the acidity of a solution in relation to neutralizing requirement. Titratable acidity results parallel the previously discussed response variables. Samples which lost the greatest portion of their original mass during treatment had the lowest measured pH values, highest electrical conductivities and highest leachate iron, sulfate and titratable acidity values.

Table 8. Mean sample extract titratable acidity (mg $CaCO_3$ l^{-1}) to pH 7 following laboratory weathering by 10% hydrogen peroxide at 0° C by particle size.

Sample Source	Crystalline Form (% Euhedral/% Massive)	Titratable Acidity (mg $CaCO_3$ l^{-1}) to pH 7 — Particle Size Fraction (μm) > 250	106-250	38-106	< 38	Mean
Control	100 / 0	35 Gb*†‡	28 Ib	28 Lb	44 La	34 M
Copper Mine Tailings	100 / 0	535 Gc	762 HIb	689 KLb	1181 Ka	792 L
Metal Mine Tailings	100 / 0	---	7506 Fa	7128 Ga	3629 Hb	6088 G
Montana Gold Mine Tailings	100 / 0	---	4306 Gb	4826 Ha	2616 Ic	3916 H
Gold Mine Tailings I	100 / 0	---	1202 Hb	1437 Ka¶	1283 Kab	1291 K
Gold Mine Tailings II	100 / 0	---	1637 Hc	2380 Ja	1976 Jb	1998 J
Gold Mine Ore	65 / 35	2954 Fc	3435 Gb	3187 Ibc	4147 Ga	3430 I
Molybdenum Mine Tailings	62 / 38	3500 Fb	3297 Gb	3343 Ib	4955 Fa	3774 HI
Wyoming Coal Overburden	14 / 86	12605 Ea	13364 Ea	11801 Ea§	---	12815 F
Texas Coal Overburden	12 / 88	23201 Ba	23909 Aa	22385 Ba	14204 Ab	20924 A
Nevada Gold Ore	3 / 97	28293 Aa	12967 Eb	9874 Fc	9264 Ec	15099 E
Coal Cleaning Waste I	3 / 97	20437 Ca	19719 Ca	19315 Ca	10817 Db	17572 C
Coal Cleaning Waste II	0 / 100	18200 Dab	18750 Da	17483 Db	12682 Bc	16779 D
Underground Coal Waste	0 / 100	22482 Bb	22018 Bb	23566 Aa	11407 Cc	19868 B
Mean		13224 a	9493 b	9161 c	6015 d	---

* Mean of three replications, unless otherwise noted.

† Means in the same *column* followed by the same *uppercase* letter are not significantly different ($p \leq 0.05$).

‡ Means in the same *row* followed by the same *lowercase* letter are not significantly different ($p \leq 0.05$).

¶ Mean of two replications.

§ N = 1.

The comparison of mean leachate titratable acidity by sample source demonstrates many levels of significance across all sample sources. The control sample mean leachate titratable acidity was 34 mg $CaCO_3$ l^{-1} which was significantly less ($p \leq 0.05$) than all of the other treatments (Table 8). The titratable acidity of the 10% H_2O_2 prior to addition to the sample material was 28 mg $CaCO_3$ l^{-1}, so the Control treatment generated essentially no additional titratable acidity. The control treatment was silica sand and not sulfide material, so the generation of acid was not expected.

The sulfide samples, dominantly pyrite, were expected to generate acidic leachate upon oxidation, which they did readily. The range of leachate titratable acidity is reported in Table 8 as 792 mg $CaCO_3$ l^{-1} for the Copper Mine Tailings sample to 20924 mg $CaCO_3$ l^{-1} for the Texas Coal Overburden sample. The broad range of response of sulfide material to oxidation and subsequent generation of acidity is entirely a function of the inherent physical properties of the sulfide materials. Physical properties include particle size and morphology which are readily observed, but additionally include relatively salient and less easily observed physical properties like mineral electrical conductivity, microcrystalline form, presence of impurity, presence of defects and the density and spatial variance of the physical properties within the crystal.

The sulfide samples, dominantly pyrite, responded to oxidation by 10% H_2O_2 in a manner dependent on the sample source. Many levels of significance were recorded for titratable acidity across all sample source comparisons, indicat-

ing that nearly all the sample sources are significantly different ($p \leq 0.05$) from one another. Therefore, sulfide samples of the same particle size and particle morphology will yield acidic leachate at a different rate when submitted to the identical treatment. Table 8 demonstrates many significant differences ($p \leq 0.05$) between sample sources and between particle sizes.

Comparing the overall mean titratable acidity between particle sizes, each of the four particle sizes is significantly different from the other, with the largest particle size fraction being the strongest acid producer. The >250 μm size fraction yielded the highest mean titratable acidity (13224 mg $CaCO_3$ l^{-1}) while the 106-250 μm, 38-106 μm and <38 μm size fractions yielded a mean 9493 mg $CaCO_3$ l^{-1}, 9161 mg $CaCO_3$ l^{-1} and 6015 mg $CaCO_3$ l^{-1}, respectively. The trend toward increasing reactivity with increasing particle size is demonstrated by titratable acidity, but also by the other response variables (mass loss, pH, electrical conductivity, leachate iron and leachate sulfate). The trend toward increasing reactivity with larger particle size is especially pronounced for the dominantly massive particle morphology samples.

The influence of particle morphology has exerted a strong influence on all response variables, yet leachate titratable acidity clearly sets forth the importance of particle morphology on the rate of pyrite oxidation. The dominantly euhedral particle morphology samples (Copper Mine Tailings, Metal Mine Tailings, Montana Gold Mine Tailings, Gold Mine Tailings I and Gold Mine Tailings II (pyrrhotite)) generated mean leachate titratable acidity values between 792 mg

$CaCO_3$ l^{-1} and 6088 mg $CaCO_3$ l^{-1} (Table 8). By comparison, the greatest mean leachate titratable acidity attributed to a dominantly euhedral morphology is significantly less than the smallest mean leachate titratable acidity attributed to a dominantly massive particle morphology sample. The smallest mean leachate titratable acidity for a dominantly massive particle morphology sample is 12815 mg $CaCO_3$ l^{-1} which was generated by the Wyoming Coal Overburden sample. The dominantly massive particle morphology samples are Wyoming Coal Overburden, Texas Coal Overburden, Nevada Gold Ore, Coal Cleaning Waste I, Coal Cleaning Waste II and Underground Coal Waste. The mean titratable acidity for the dominantly massive particle morphology samples is prominently greater than the mean titratable acidity for the dominantly euhedral samples, which were not as easily oxidized as the massive particle morphology samples.

Sulfide Mineral Reaction Time During Oxidation

The period of time required for the reaction of 10% H_2O_2 with the mineral sample to run to completion was recorded for each sample. Completion was determined as the point at which bubbling ceased in the reaction vessel as hydrogen peroxide was consumed by oxidation of the sulfide material. The strength of the reaction over time was variable, but typically the reaction was strongest during the first minute of reaction then tapered off slowly. This generalization holds true for most of the samples, the exception being samples which ran to completion during the first minute of reaction. The strength of reaction during

the first minute was also variable, but typically the massive morphology samples initially reacted most strongly to the addition of hydrogen peroxide.

All samples were oxidized with the reaction vessel placed in an ice bath to control the rate of reaction and prevent boiling. The temperature of reaction was maintained at 0° C throughout the reaction, with the exception of the first few minutes of reaction where the reaction was rapidly proceeding and strongly exothermic. During the first few minutes the temperature did rise because the rate of cooling in the ice bath was insufficient to offset the rate of heat generation.

The duration of these reactions ranged from a mean of 0.35 days to 1.12 days and is reported in Table 9. Unlike the previous response variables no general trend is evident in the reaction time data between sample sources. Many levels of significance ($p \leq 0.05$) are noted between sample sources, but the trend is counter to the previously demonstrated response variables. There is no effect of particle morphology on reaction time.

Particle size statistical comparisons do reveal a trend which has been previously observed. All the mean reaction time particle size fractions are different and statistically significant ($p \leq 0.05$). The shortest overall mean reaction time is associated with the smallest size fraction (<38 μm) (Table 9). The larger particles apparently are able to sustain an oxidizing environment longer than the small particles. The mean length of reaction may relate to the evolution of chemical constituents most strongly released in the largest size fraction, though reaction time is not a reliable predictor of leachate chemistry.

Table 9. Mean sample reaction time (days) during laboratory weathering by 10% hydrogen peroxide at 0° C by particle size.

Sample Source	Crystalline Form (% Euhedral/% Massive)	Reaction Time (Days) - Particle Size Fraction (μm) > 250	106-250	38-106	< 38	Mean
Control[#]	100 / 0	---	---	---	---	---
Copper Mine Tailings	100 / 0	0.64 Da[*†‡]	0.64 Fa	0.11 Hb	0.001 Ic	0.35 I
Metal Mine Tailings	100 / 0	---	1.36 Ba	0.78 Dc	1.09 Ab	1.07 B
Montana Gold Mine Tailings	100 / 0	---	1.53 Aa	0.61 Eb	0.14 Hc	0.76 EF
Gold Mine Tailings I	100 / 0	---	0.65 Fa	0.02 Ib[¶]	0.004 Ic	0.25 J
Gold Mine Tailings II	100 / 0	---	0.77 Ea	0.48 Fc	0.72 Cb	0.66 G
Gold Mine Ore	65 / 35	1.39 Aa	0.91 Db	0.63 Ec	0.006 Id	0.73 F
Molybdenum Mine Tailings	62 / 38	0.46 Ea	0.34 Hb	0.23 Gc	0.004 Id	0.26 J
Wyoming Coal Overburden	14 / 86	0.83 Ca	0.54 Gc	0.59 Eb[§]	---	0.67 G
Texas Coal Overburden	12 / 88	0.81 Ca	0.91 Da	0.91 Ca	0.48 Eb	0.78 E
Nevada Gold Ore	3 / 97	1.13 Ba	0.90 Db	0.92 Cb	0.65 Dc	0.90 D
Coal Cleaning Waste I	3 / 97	0.92 Ca	0.66 Fb	0.47 Fc	0.24 Gd	0.57 H
Coal Cleaning Waste II	0 / 100	1.13 Bb	1.15 Cb	1.26 Aa	0.95 Bc	1.12 A
Underground Coal Waste	0 / 100	1.20 Ba	1.19 Ca	1.19 Ba	0.30 Fb	0.97 C
Mean		0.95 a	0.89 b	0.65 c	0.38 d	---

* Mean of three replications, unless otherwise noted.
† Means in the same *column* followed by the same *uppercase* letter are not significantly different ($p \leq 0.05$).
‡ Means in the same *row* followed by the same *lowercase* letter are not significantly different ($p \leq 0.05$).
¶ Mean of two replications.
§ N = 1.
# Control sizes >250, 106-250 and 38-106 μm had not run to completion after 20 days and were terminated at that time. Control run time is not included in this table.

The inability to use reaction time data for prediction of leachate chemistry is illustrated by comparing the overall mean reaction time for the Montana Gold Mine Tailings sample, which took a mean 0.76 days to run to completion, to the Texas Coal Overburden sample which took a mean 0.78 days to run to completion (Table 9). These two samples are not significantly different ($p \leq 0.05$). If reaction time were to be a reasonable predictor of leachate chemistry, then leachate chemistry results would be expected to be similar since the mean reaction time was not different. Using titratable acidity as a basis for comparison, the Montana Gold Mine Tailings sample had a mean of 3916 mg $CaCO_3$ l^{-1} compared to the Texas Coal Overburden sample which had a mean of 20924 mg $CaCO_3$ l^{-1} (Table 8). These two samples are observationally and statistically very different, demonstrating the lack of usefulness of reaction time data to predict or assist in assessment of leachate chemistry. No further reaction time data interpretation is applied to the assessment of sulfide size and morphology characteristics for understanding acid generation processes.

Weatherability of Different Sulfide Mineral Morphologies

The morphology of the sulfide particles from each sample source exerted a fundamental influence on the response to oxidation. Table 10 further details the importance of particle morphology on generation of acidic conditions. Graphical presentation of the overall experimental results presented in Table 10 are presented in Figures 5 through 8.

Table 10. Summary of response to oxidation by 10% H_2O_2 by crystal morphology.

Particle Size Fraction (μm)/Dominant Crystal Morphology		Mass Loss (%)	Response Variable (Mean of All Measurements) EC (dS m^{-1})	Titratable Acidity (mg $CaCO_3$ l^{-1})	SO_4^{2-} (mg l^{-1})	Fe (mg l^{-1})	pH	Reaction Time (Days)
> 250	Euhedral[1/]	-7.01[+§] a	4.96 a	2330 a	2282 a	657 a	2.21 a	0.83 ab[++]
> 250	Massive[2/]	-59.95 B[•]	34.65 A	20870 B	20040 B	5805 B	1.44 A	1.00 B[++]
106-250	Euhedral	-9.60 a	6.42 a	3164 a	3129 a	931 a	2.09 a	0.89 b[++]
106-250	Massive	-53.59 B	30.65 A	18450 AB	18170 B	5201 B	1.46 A	0.89 AB[++]
38-106	Euhedral	-9.45 a	6.22 a	3284 a	3078 a	968 a	2.07 a	0.41 ab
38-106	Massive	-50.40 B	29.12 A	17400 AB	16750 AB	4964 B	1.48 A	0.89 AB
< 38	Euhedral	-8.34 a	5.90 a	2827 a	2787 a	832 a	2.06 a	0.28 a[++]
< 38	Massive	-29.78 A	23.08 A	11670 A	10390 A	2725 A	1.48 A	0.52 A[++]
Mean of All Particle Size Fractions								
Euhedral		-8.60	5.87	2901	2819	847	2.11	0.60[++]
Massive		-48.43	29.38	17100	16340	4675	1.46	0.83[++]

[•] Massive means in the same *column* followed by the same *uppercase* letter are not significantly different ($p \leq 0.05$).

[§] Euhedral means in the same *column* followed by the same *lowercase* letter are not significantly different ($p \leq 0.05$).

[+] Euhedral and massive means are significantly different ($p \leq 0.05$) within each size fraction for each response variable except where denoted by [++] where massive and euhedral means are not significantly different ($p \leq 0.05$).

[1/] N = 24 observations for all euhedral means.

[2/] N = 23 observations for all massive means.

Particle morphology, as distinguished between the two broad classes massive and euhedral, is a very important consideration in the classification of the acid producing potential of sulfides, dominantly as pyrite. Within each size fraction, >250 μm, 106-250 μm, 38-106 μm and <38 μm, for each of seven different response variables, the massive and euhedral morphology samples are

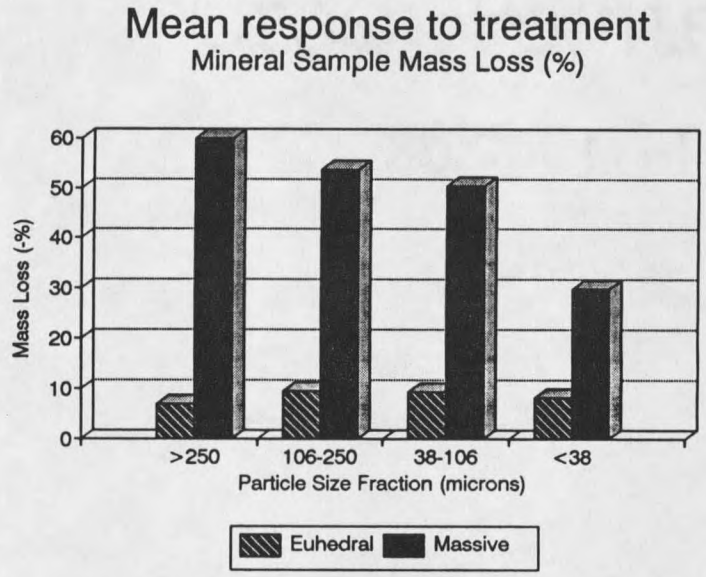

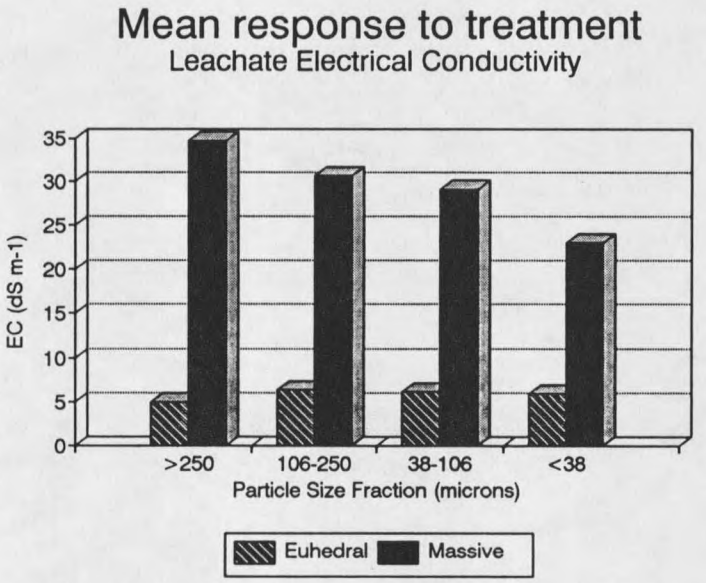

Figure 5. Experimental mean mass loss and leachate electrical conductivity for all samples by particle size and morphology.

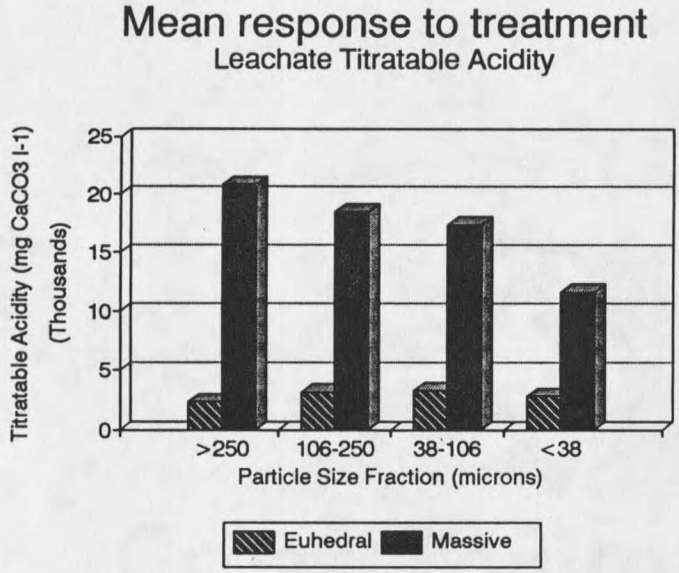

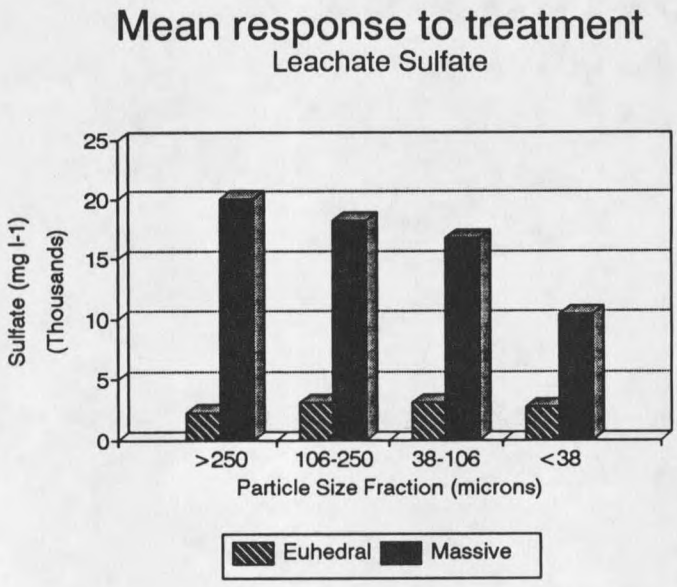

Figure 6. Experimental mean leachate titratable acidity and sulfate for all samples by particle size and morphology.

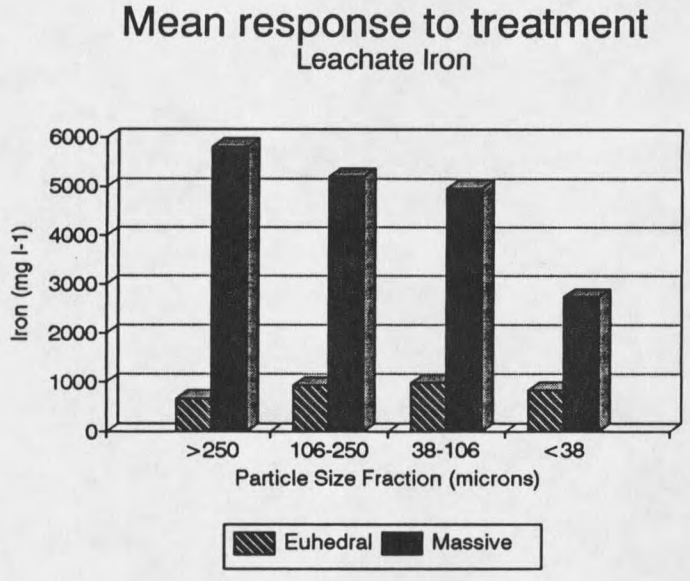

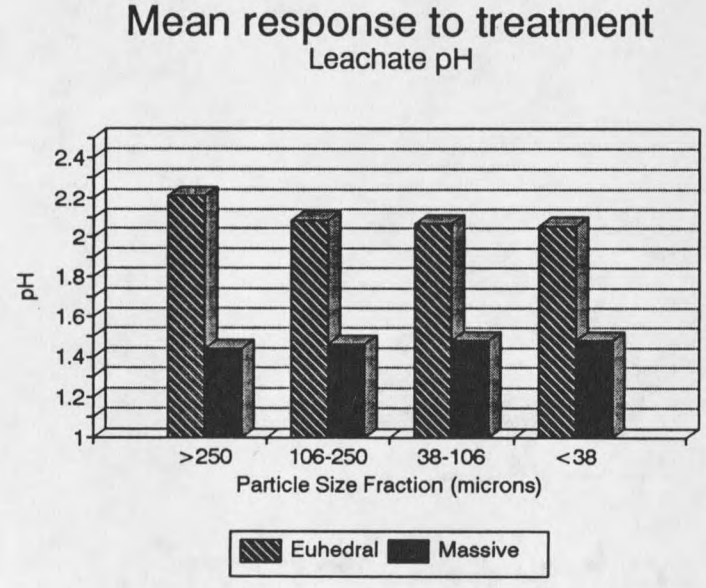

Figure 7. Experimental mean leachate iron and pH for all samples by particle size and morphology.

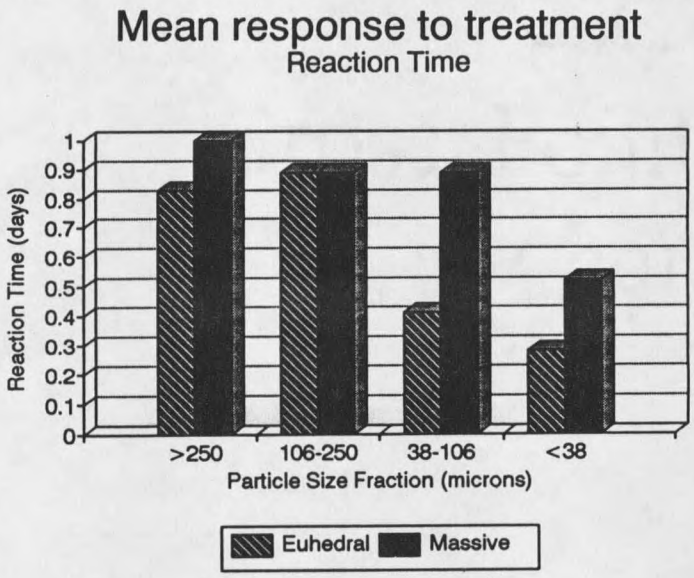

Figure 8. Experimental mean reaction time for all samples by particle size and morphology.

significantly different ($p \leq 0.05$) for every comparison except reaction time. The differences between massive and euhedral morphology samples are prominent.

Comparing the titratable acidity of massive and euhedral particle morphologies in the >250 μm size fraction (Table 10), the euhedral morphology samples generated a mean 2330 mg $CaCO_3$ l^{-1} titratable acidity while the massive morphology samples generated a mean 20870 mg $CaCO_3$ l^{-1}, a nearly 10 fold difference. In the 38-106 μm size fraction the mean electrical conductivity of the euhedral morphology samples was 6.22 dS m^{-1} while the massive morphology mean electrical conductivity was 29.12 dS m^{-1}. In the 106-250 μm size fraction the mean leachate sulfate for the euhedral morphology samples was 3129 mg l^{-1}, as com-

pared to the massive morphology samples which had a mean leachate sulfate content of 18170 mg l^{-1}. Leachate chemistry measured as a response to pyrite oxidation demonstrates large differences in the weatherability of euhedral and massive morphology samples.

The reason for dissimilar oxidation between euhedral and massive morphology particles is attributed to differences in the atomic structure of the crystals. Since massive particles are amorphous and noncrystalline, the iron and sulfur atoms are not located in a regular crystalline lattice as they are in euhedral particles. Since the massive particles do not have regular crystalline structure, the iron and sulfur electrons are not shared uniformly through the crystalline structure. The presence of irregular electron distribution provide many sites on massive particles for attack and removal of the crystal by oxidation. Euhedral particles can also have defects in the crystalline structure which become sites of excess energy and sites which become the focus of oxidation, but the frequency of imperfection in euhedral particles is small compared to massive particles. The reactivity of massive morphology pyrite to oxidation is subsequently a consequence of the atomic structure of the crystal, which is characteristic to the specific environment of formation. Therefore, characterization of the acid generation potential of a sample by acid-base account analysis would identify the quantity of the sulfur component present as pyrite, but would fall short of understanding the acid generation potential of the sample since no assessment of particle morphology would be made.

Stoichiometric Balance of Pyrite Oxidation

Pyrite is oxidized under natural conditions where 1 mole of pyrite is oxidized by oxygen and water to produce 4 moles of acidity (Equation 15).

$$FeS_2 + \frac{15}{4} O_2 + \frac{7}{2} H_2O = Fe(OH)_3 + 2\,SO_4^{-2} + 4\,H^+ \qquad [15]$$

Under simulation of natural weathering by hydrogen peroxide, 1 mole of pyrite when oxidized will also yield 4 moles of acidity (Equation 16, O'Shay et al. 1990).

$$FeS_2 + \frac{15}{2} H_2O_2 = Fe(OH)_3 + 2\,SO_4^{-2} + 4\,H^+ + 4\,H_2O \qquad [16]$$

Since the rate of natural weathering by water and oxygen is slower than the rate of simulated weathering by hydrogen peroxide, hydrogen peroxide was chosen as the laboratory oxidant.

Under oxidation of sulfide samples by 10% H_2O_2, differences in the rate of oxidation of sulfide samples of different size and morphology have been established in previous thesis sections. For each sample material used, the response variables mass loss, leachate sulfur, leachate iron and leachate titratable acidity were recorded. Though significant differences have been noted in the quantity of mineral material removed during oxidation and significant differences have been noted in the quality of the leachate, it has not been established that the oxidation of sulfide material occurred in accordance with Equations 15 and 16. Confirmation of the expected reaction products was performed by normalizing all leachate response variables to a leachate analyte per 1% mass loss basis.

Using the Molybdenum Mine Tailings sample as an example, the 106-250 μm size fraction lost a mean 9.91% of the original 1.000 gram mass during oxidation (Table 3). This loss in mass resulted in a mean 3226 mg l^{-1} sulfate (Table 7) and 964 mg l^{-1} iron (Table 6) in the leachate. Dividing each of the leachate parameters by 9.91 puts the leachate chemistry results in terms of leachate analyte per 1% mass lost by the mineral sample. Per 1% mass loss, the leachate sulfate is 325 mg l^{-1} and the leachate iron is 97 mg l^{-1}. Since the volume of leachate generated by consumption of hydrogen peroxide was 50 ml, each of the leachate parameters is divided by 20 to put the leachate chemistry results in terms of leachate analyte per 1% mass loss per actual leachate volume. The leachate results are now recorded as 16.25 mg sulfate per 50 ml and 4.85 mg iron per 50 ml volume. These are the leachate constituents per .01 gram, or 10 mg, FeS_2 oxidized. Since pyrite has an atomic weight of 119.97 grams per mole, and iron has an atomic weight of 55.847 grams per mole, iron represents 46.55% of the mass. Ten milligrams of pyrite would then be comprised of 4.65 mg iron and 5.35 mg sulfur. By comparison to the leachate findings, 10 mg FeS_2 when oxidized by 10% H_2O_2 yielded 4.85 mg Fe and 16.25 mg SO_4^{2-} in the example case. Since $Fe(OH)_3$ is not stable at low pH, the iron in leachate was present as ferric ion and not ferric hydroxide. Therefore, the predicted leachate iron content was 4.65 mg Fe while the experimentally observed leachate iron was 4.85 mg Fe, or a 4.2% relative difference. For comparison of sulfate, the predicted leachate sulfur content was 5.35 mg S, while the experimentally observed value was 16.25 mg

SO_4^{-2}, or expressed as sulfur, 5.42 mg S. The relative percentage difference for sulfur between predicted and observed values is 1.3%.

To further understand the stoichiometric relations of pyrite oxidation, pyrite and leachate constituents are expressed on a molar basis. One mole of pyrite has a mass of 119.97 grams per mole, or .01 grams pyrite can be expressed as 0.083 moles FeS_2. The experimentally observed oxidation of pyrite resulted in 4.85 mg Fe, 16.25 mg SO_4^{2-} and 33.30 mg acidity (expressed as mg $CaCO_3$) in the leachate per oxidation of .01 g FeS_2. Expressing the masses of each constituent on a molar basis gives Equation 17.

.083 mmol FeS_2 + .623 mmol H_2O_2 = .087 mmol Fe + .168 mmol SO_4^{2-} + .333 mmol H^+ [17]

Dividing each constituent by .083 mmol to balance the FeS_2, reveals the stoichiometric relationship of the products of the oxidation of pyrite observed experimentally (Equation 18). The close agreement of Equation 16 and 18, suggests that the

$$FeS_2 + \frac{15}{2} H_2O_2 = 1.05\,Fe + 2.02\,SO_4^{2-} + 4.01\,H^+ \qquad [18]$$

predicted and experimentally observed reactions for pyrite oxidation for the Molybdenum Mine Tailings sample by hydrogen peroxide are very similar.

To confirm that the dissolution of sulfides from different mine environments yielded acid in accordance with Equation 16, the preceding normalization of response variables to a per 1% mass loss basis and calculation of stoichiometric relationships was performed for all sample sources (Table 11). The predicted generation of products is in accordance with Equation 16, while the experimentally

observed stoichiometry is presented in Table 11 (see Table 20, Appendix for support data).

Four moles of acidity were anticipated as the product of oxidation of 1 mole pyrite (Equation 16). The comparison of moles H^+ generated by FeS_2 oxidation by sample source reveals no significant differences ($p \leq 0.05$) between any of the sulfide treatments except the control which is not a sulfide (Table 11). The range of H^+ generation is from 3.32 moles H^+ for the Copper Mine Tailings sample to 7.51 moles H^+ for the Nevada Gold Ore sample. The Nevada Gold Ore sample results may not be accurate due to the presence of the nonpyritic sulfide minerals orpiment and realgar which are dense arsenic sulfide minerals which could not be readily separated for pyrite.

Two moles of sulfate in leachate were expected per mole FeS_2 oxidized (Equation 16). The comparison of leachate results by sample source for stoichiometric sulfate component (Table 11) reveals that the Control sample was significantly different ($p \leq 0.05$) from each other and the remainder of the sample sources.

The oxidation of 1 mole FeS_2 was expected to yield 1 mole iron as $Fe(OH)_3$ (Equation 16), while experimental results closely approximate the expected finding independent of sample source (Table 11). The Control sample was significantly different from all other sample sources.

The results of Table 11 are important to a discussion of pyrite oxidation because they demonstrate that independent of the environment of formation, and

Table 11. Mass balance for stoichiometric oxidation of pyrite by H_2O_2.

Sample Source	Moles H^+ Generated By Oxidation of 1 Mole FeS_2	Moles SO_4^{2-} Generated By Oxidation of 1 Mole FeS_2	Moles Fe Generated By Oxidation of 1 Mole FeS_2
Control	0.39 B[§‡]	0.07 C[§]	0.01 C[§]
Copper Mine Tailings	3.31 AB	1.64 B	0.69 B
Metal Mine Tailings	4.43 AB[•]	2.23 AB[•]	1.13 A[•]
Montana Gold Mine Tailings	4.10 AB[•]	2.04 AB[•]	1.06 A[•]
Gold Mine Tailings I	4.05 AB[•]	2.07 AB[•]	0.99 AB[•]
Gold Mine Tailings II	3.38 AB[•]	2.02 AB[•]	1.21 A[•]
Gold Mine Ore	4.23 AB	2.10 AB	1.09 A
Molybdenum Mine Tailings	4.08 AB	2.02 AB	1.05 A
Wyoming Coal Overburden	3.82 AB[•]	1.76 B[•]	0.96 AB[•]
Texas Coal Overburden	4.72 AB	2.13 AB	0.95 AB
Nevada Gold Ore	7.51 A	3.02 A	0.98 AB
Coal Cleaning Waste I	4.60 AB	1.92 AB	1.01 AB
Coal Cleaning Waste II	4.30 AB	2.21 AB	1.14 A
Underground Coal Waste	3.56 AB	2.15 AB	1.06 A
Mean[▲]	4.31	2.10	1.02

[§] Mean of 12 replications, unless otherwise noted.

[‡] Means in the same *column* followed by the same *uppercase* letter are not significantly different ($p \leq 0.05$).

[•] Mean of 9 replications.

[▲] Overall means exclude the control treatment.

independent of the rate of oxidation, a 1.000 gram sample of pyrite will yield the same amount of acid, iron and sulfur upon complete oxidation. Additionally, the Gold Mine Tailings II sample has the dominant sulfide mineral pyrrhotite present and not pyrite. The products of pyrrhotite oxidation are not significantly different from pyrite (Table 11).

SEM/EDAX Examination Of Weatherability Of Different Pyrite Morphologies

Two fundamental approaches to visually understand the oxidation of sulfide materials and process of mineral dissolution were applied. The first approach consisted of examining whole mineral particles by scanning electron microscopy (SEM) and energy dispersive analysis of x-rays (EDAX), before and after oxidation by 10% H_2O_2. Mineral samples were prepared by sprinkling sulfide particles on conductive graphite paint and collecting photographic images of characteristic particles.

The second approach to collection of visual evidence pertaining to the process of mineral dissolution was to cast particles derived from different sources in an epoxy mount. The epoxy casting was prepared by sanding and polishing until fresh unweathered particle surfaces were evident, then collecting photographic images of the particles by SEM. The exposed mineral surfaces were then subjected to oxidation by hydrogen peroxide, and a second set of photographs was collected of the same particles. This approach allows for the particles derived

from different sources to be subjected to the identical treatment since they are exposed to exactly the same conditions, being cast in the same epoxy pod.

The destruction of sulfide minerals by oxidation has been observed to occur nonuniformly across the surface of mineral samples. The removal of mass from the solid mineral phase does not occur by the sequential removal of thin layers from the mineral, rather oxidation is focused at sites of excess energy on the crystal surfaces. Sites of excess energy include any feature which is not a contiguous part of the atomic lattice, including cleavage planes, steps, grain edges, microcracks, dislocations, defects and inclusions. At these sites of excess energy, an etch pit or cavity will form as weathering of the mineral proceeds. As weathering continues, etch pits continue to grow and interconnect until complete mineral dissolution is attained. Figure 9 illustrates the formation of etch pits on pyrite

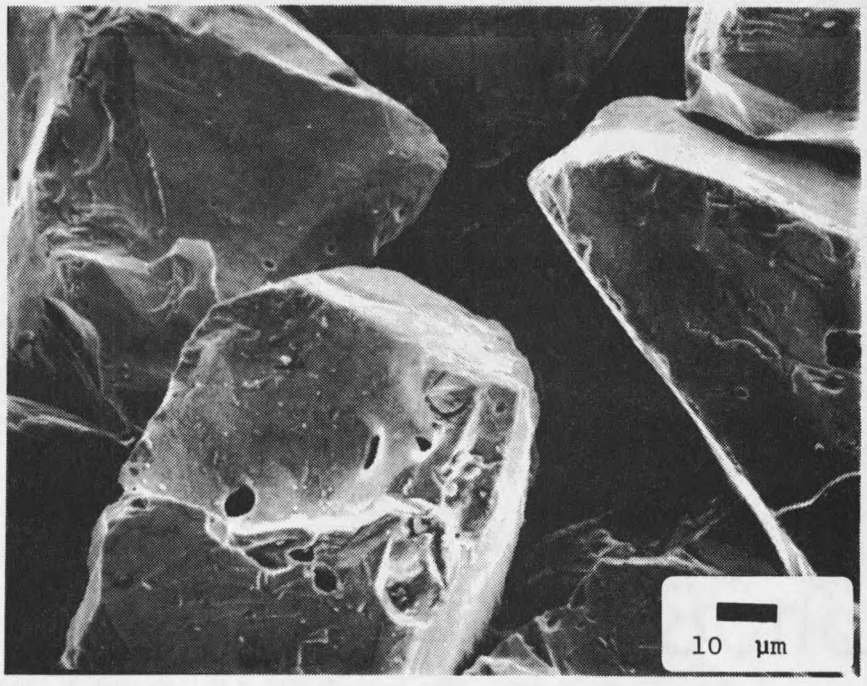

Figure 9. Etch pit formation on Copper Mine Tailings euhedral pyrite after oxidation by 10% H_2O_2, (490X magnification).

particles submitted to weathering by 10% H_2O_2. The density of defects on the mineral surface therefore exerts an important influence on the rate of mineral dissolution. The extreme case of mineral surface morphologies containing defects are massive pyrite particles which are composed entirely of defects and do not have any regular crystalline lattice. Massive pyrite therefore is likely to oxidize easily due to the high density defect of sites for oxidation.

The development of etch pits on pyrite is displayed in Figure 10 and 11. Figure 10 shows pyrite of two morphologies from the Gold Mine Ore sample from the 106-250 μm size fraction. The particle in the lower left corner of Figure 10 is a massive morphology particle while the particles in the center and upper portion

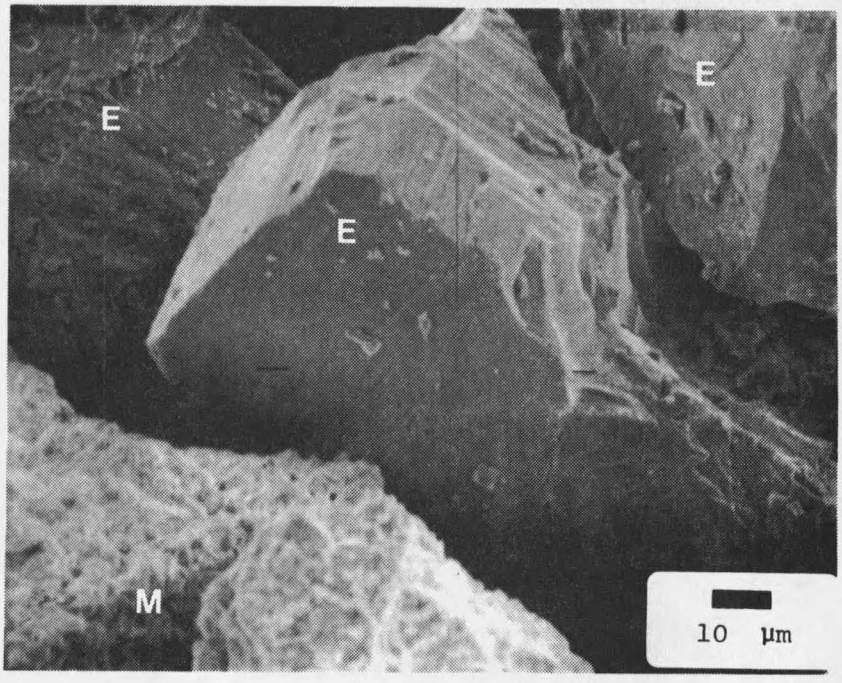

Figure 10. Unweathered pyrite particles from Gold Mine Ore, 106-250 μm size fraction, (490X magnification) (E = Euhedral, M = Massive).

of Figure 10 are euhedral morphology. Small particles (5 μm and smaller) are present on the surface of the euhedral particles in Figure 10, but the development of etch pits is not evident.

After oxidation by 10% H_2O_2 the Gold Mine Ore sample material was reexamined by SEM. Prominent etch pits developed on the surfaces of euhedral pyrite are evident in Figure 11 after oxidation. Etch pit development in Figure 11 on the euhedral pyrite particle in the lower right follows a linear trend, possibly parallel to crystallographic planes within the particle.

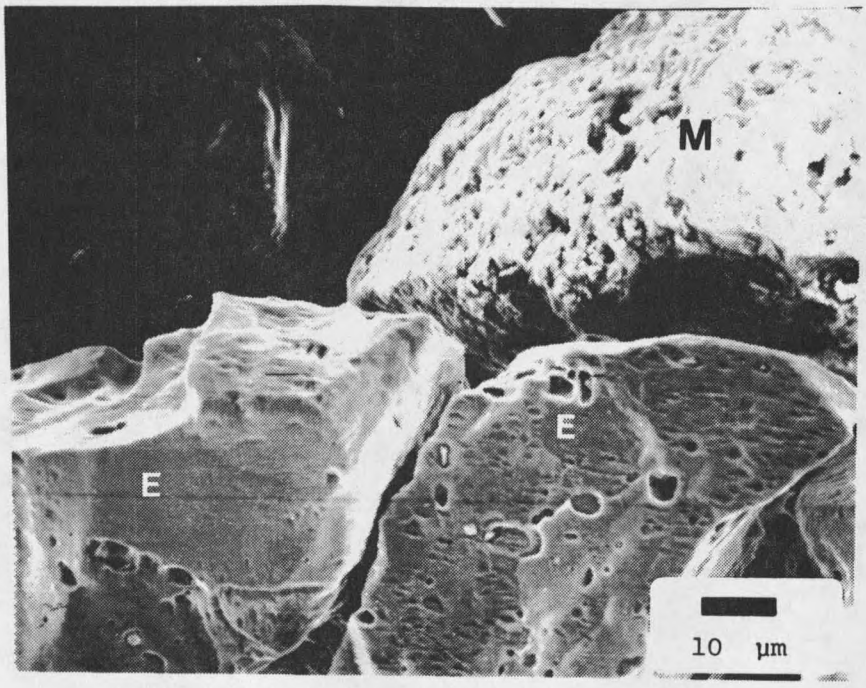

Figure 11. Etch pit development on euhedral pyrite from Gold Mine Ore, 106-250 μm size fraction, (490X magnification), photograph taken after oxidation by 10% H_2O_2 (E = Euhedral, M = Massive).

The weathering of massive pyrite particles also results in the nonuniform destruction of the mineral surface. Figure 12 displays a massive pyrite particle, in the upper right corner of the figure, which has been attacked by 10% H_2O_2 during this experiment. The surface of the massive pyrite particle, upper right particle, is much rougher than the euhedral particles from the same sample submitted to the same treatment, lower right corner (Figure 12).

A higher magnification (1270X) photographic image (Figure 13) was collected from the surface of the massive pyrite particle in the upper right corner

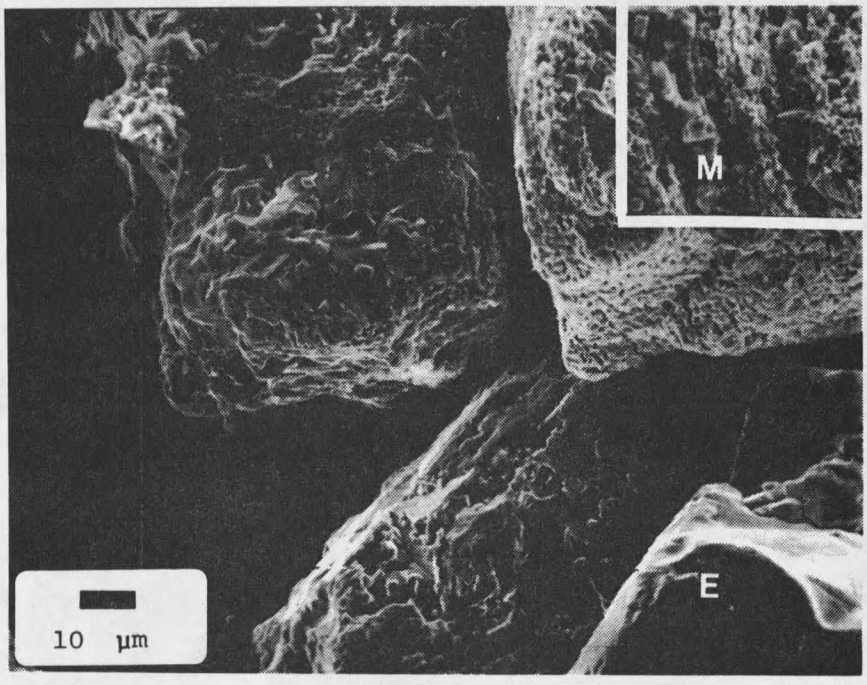

Figure 12. Pyrite particles from Molybdenum Mine Tailings (470X), 106-250 μm size fraction, after oxidation by 10% H_2O_2 (E = Euhedral, M = Massive). Box indicates the location of Figure 13.

of Figure 12. Figure 13 demonstrates the small scale characteristic rough surface features of massive pyrite.

The surface structure of natural pyrite particles was also examined by Scanning Tunnelling Microscopy (STM) to ascertain mineral surface morphology at the atomic scale. Though STM does not collect actual photographs of the mineral surface, the morphology of the surface can be observed through computer image processing of data collected by the microscope. Successful resolution of the surface morphology of sulfide minerals at the scale of tons of Angstroms was performed, but due to inherent physical properties of pyrite no relevant STM images of atomic surface morphology were obtained.

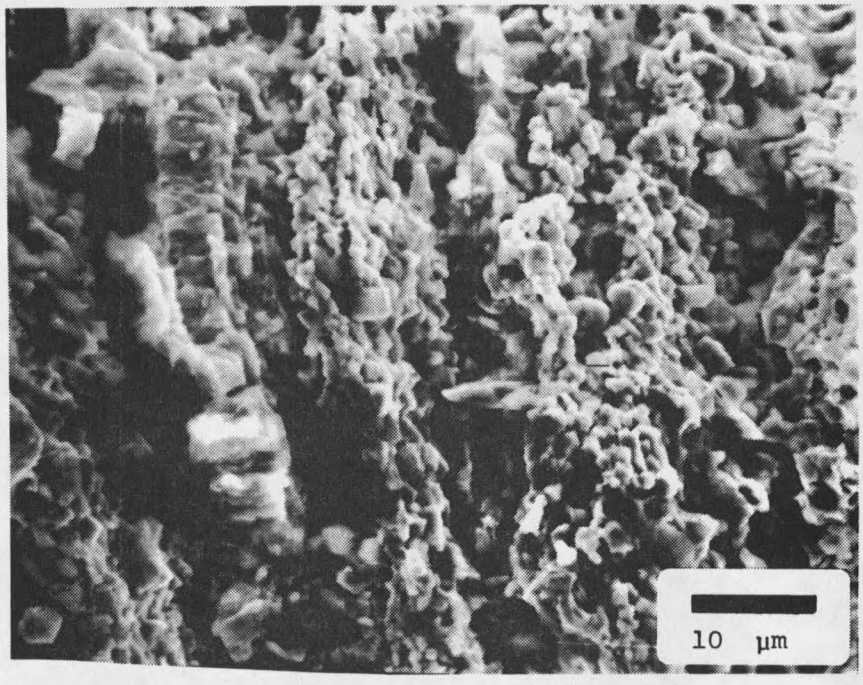

Figure 13. Surface structure of massive pyrite from Molybdenum Mine Tailings (see Figure 12) at 1270X magnification, after oxidation by 10% H_2O_2.

The most revealing evidence pertaining to the dissolution of pyrite, and resulting surface morphologies, by hydrogen peroxide was obtained by the SEM. The change, or lack thereof, of the fresh mineral surface was clearly observable since it was possible to relocate the same particle surfaces previously photographed.

After casting pyrite particles from different sources in a single epoxy mold, the casting was sanded with progressively finer sandpaper until smooth, fresh, unoxidized mineral surfaces were evident. Figure 14 illustrates a pyrite particle cast in epoxy prior to treatment with hydrogen peroxide. The dark material containing large air bubbles is the epoxy. The pyrite particles are approximately 1 mm (1000 μm) in diameter, euhedral morphology particles, containing crystalline imperfections (microcracks and small pits). Figure 15 displays the same particles after oxidation by 2 ml 30% H_2O_2 for 45 minutes.

The destructive removal of mass from the sample is clearly demonstrated by Figure 15. The removal of mass did not occur uniformly across the mineral surface, rather mass removal was focused at sites containing crystalline imperfection. The mineral microcracks evident before oxidation became fissures during oxidation and the small pits prior to oxidation became large etch pits during oxidation. While mass was destructively removed from portions of the crystal containing imperfections, regions of the mineral surface lacking imperfection were relatively unaltered. Further detail of the mineral surface where aggressive attack

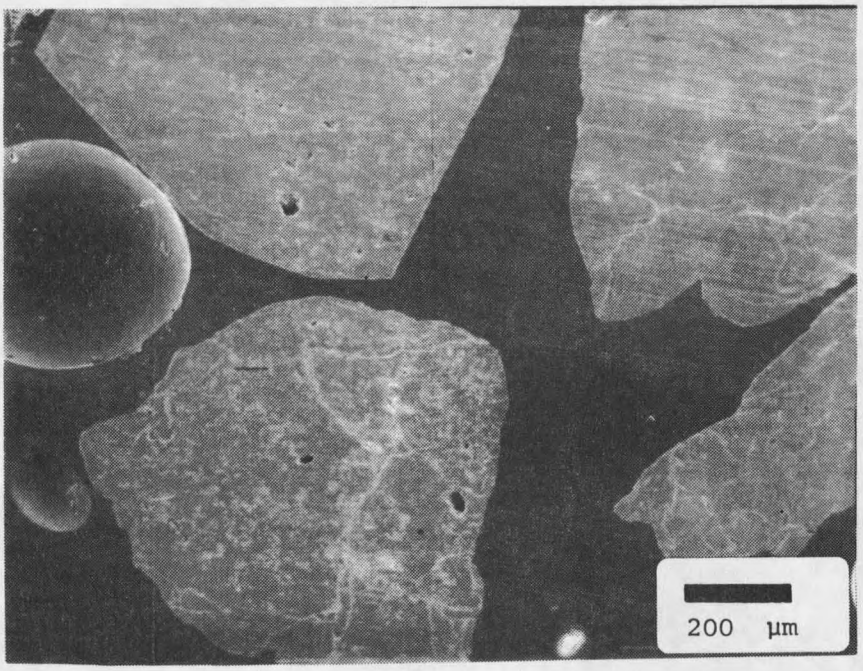

Figure 14. High reactive surface area euhedral morphology pyrite particles (1000 μm) cast in epoxy prior to oxidation (45X magnification).

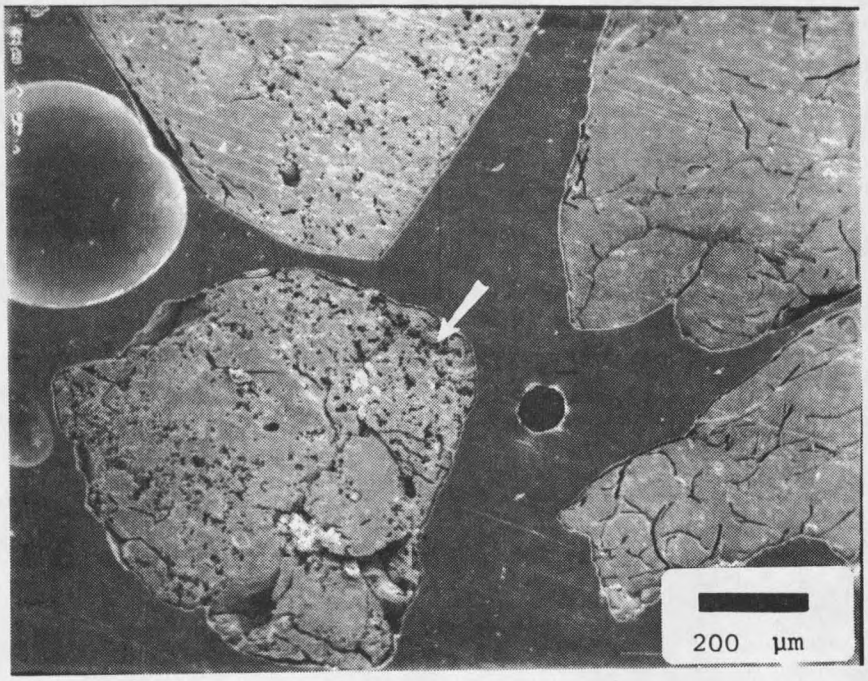

Figure 15. High reactive surface area euhedral morphology pyrite particles (1000 μm) cast in epoxy after oxidation by 30% H_2O_2 (45X magnification). White arrow indicates location of Figure 16.

of the mineral occurred is presented in Figure 16, demonstrating the depth of mineral dissolution. Defects in the crystalline structure of the mineral are distributed throughout the entire crystal, so though oxidation is initiated on the crystal surface the process of oxidation can rapidly penetrate into the particle. Though much attention has been paid to the surface area of pyrite as it pertains to the generation of acidic drainage, the implication from Figures 15 and 16 is that the reactive exposed surface area may exert a stronger influence on the generation of acid than the total exposed surface area. The reactive surface area is defined as the surface area which is readily chemically reactive to oxidation. Potentially, the

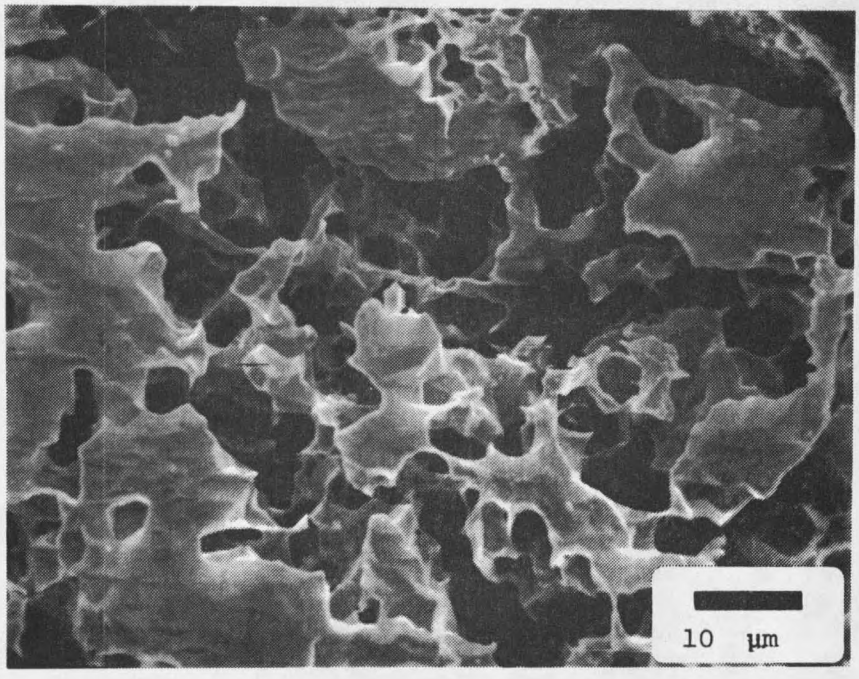

Figure 16. Pyrite surface morphology (from Figure 15, see arrow) after exposure to 30% H_2O_2 demonstrating innerpenetrating destructive removal of mineral material (630X magnification).

reactive surface area is the dominant control on generation of acidic drainage by pyrite oxidation.

By contrast, Figures 17 and 18 are SEM photographs taken before and after oxidation by 30% H_2O_2 of euhedral pyrite derived from a different environment. The treatment of the pyrite samples in Figures 15 and 18 was identical, since both samples were in contact with the same 2 ml 30% H_2O_2 for the same interval of time. The response of the pyrite particles in Figure 18 was markedly less than the response of the particles in Figure 15. The reactive surface area was not measured for either of the sample sources, but Figures 15 and 18 suggest that the difference in reactive surface between the two sources is distinct. The low reactive surface area euhedral morphology pyrite (Figure 18) is comprised of crystals relatively free from defects or microcracks which were exploited by oxidation in the high reactive surface area euhedral morphology pyrite in Figure 15. Upon close examination of Figure 18, the removal of mass is evident at the boundary between the epoxy and the pyrite grain, where a relatively uniform thickness of material was removed from the particle surface, but not at reactive locations within the crystal.

The process of mass removal from pyrite samples of the same morphology is apparently strongly correlated to the reactive surface area of the mineral, which is a physical property indigenous to a specific source. To provide additional insight into the removal of mass from diverse sources and visual confirmation of

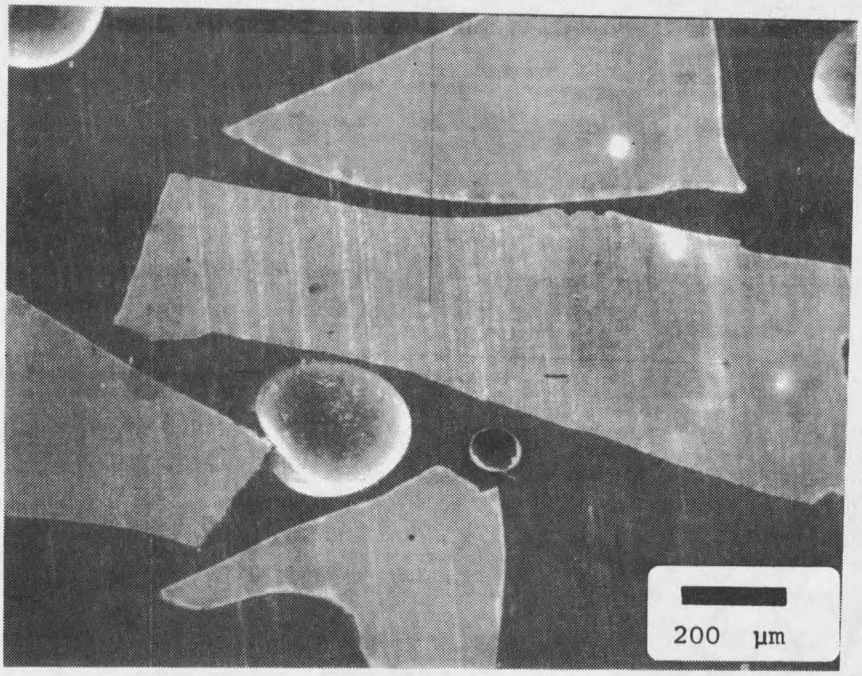

Figure 17. Low reactive surface area euhedral morphology pyrite particles (1000 μm) cast in epoxy prior to oxidation (45X magnification).

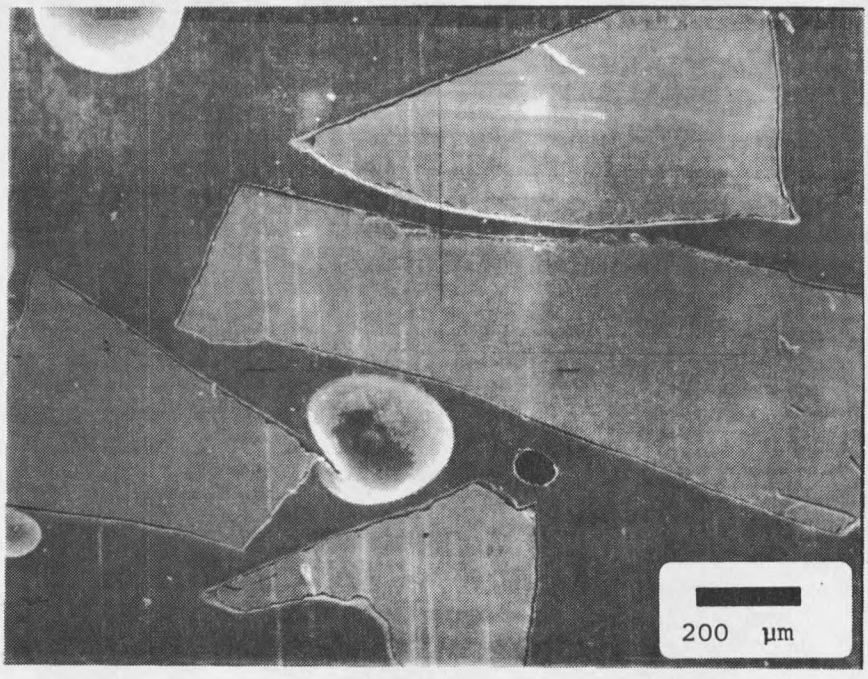

Figure 18. Low reactive surface area euhedral morphology pyrite particles (1000 μm) cast in epoxy after oxidation by 30% H_2O_2 (45X magnification).

leachate chemistry results, the Montana Gold Mine Tailings sample and Texas Coal overburden sample were cast in the same epoxy mold as the low reactive surface area and high reactive surface area samples (Figures 14-18). The Texas Coal Overburden sample is a dominantly massive particle morphology sample which was strongly acid producing during laboratory weathering with 10% H_2O_2. The Montana Gold Mine Tailings sample is a dominantly euhedral morphology sample which was significantly less ($p \leq 0.05$) acid generating than the Texas Coal Overburden samples (Tables 3-9). The response to oxidation by 30% H_2O_2 for 45 minutes was very different between the Texas Coal Overburden and Montana Gold Mine Tailings sample (Figures 19-22).

Microcracks evident in the unoxidized Montana Gold Mine Tailings pyrite crystals (Figure 19) were the focus of attack by hydrogen peroxide (Figure 20). Mass was also removed along the grain edges of all particles.

The Texas Coal Overburden sample was a massive morphology sample, so the pyrite crystals prior to oxidation were permeated with defects and crystallographic imperfections. Figure 21 reveals hints of the crystalline nonhomogeneity, while Figure 22 demonstrates the result of oxidation.

The difference between the oxidation of the Montana Gold Mine Tailings and Texas Coal Overburden samples by 30% H_2O_2 is not quantified by the SEM, but the photographic evidence supports the previous findings where both samples were oxidized by 10% H_2O_2 and leachate chemistry subsequently analyzed. The

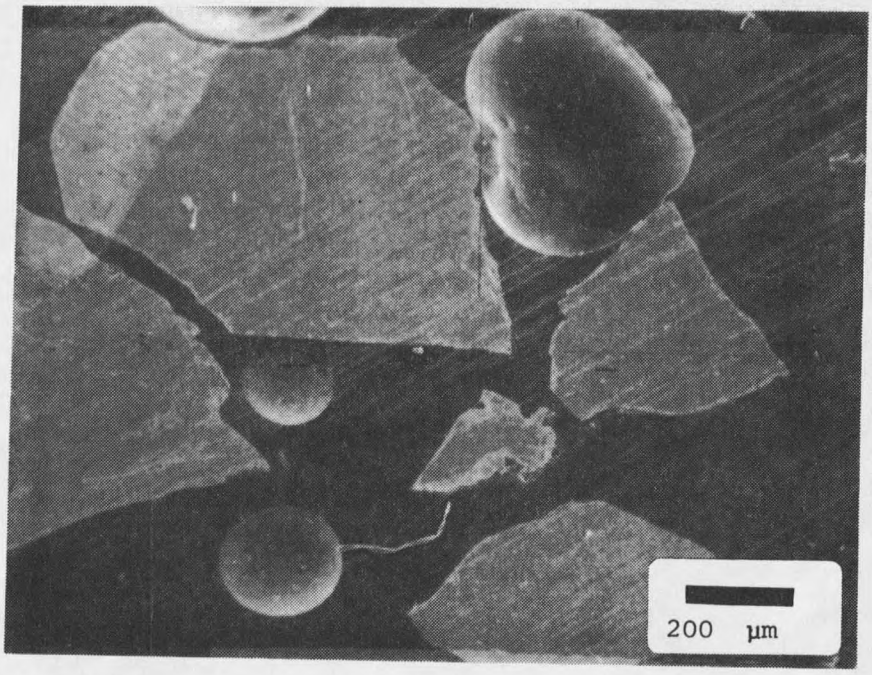

Figure 19. Montana Gold Mine Tailings pyrite (1000 μm) prior to oxidation (45X magnification).

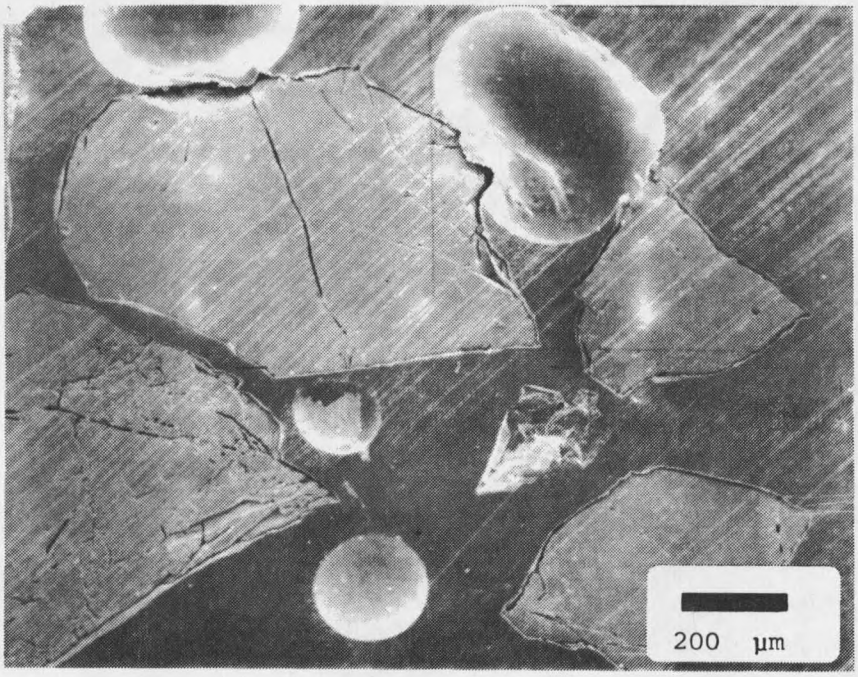

Figure 20. Montana Gold Mine Tailings pyrite (1000 μm) after oxidation by 30% H_2O_2 (45X magnification).

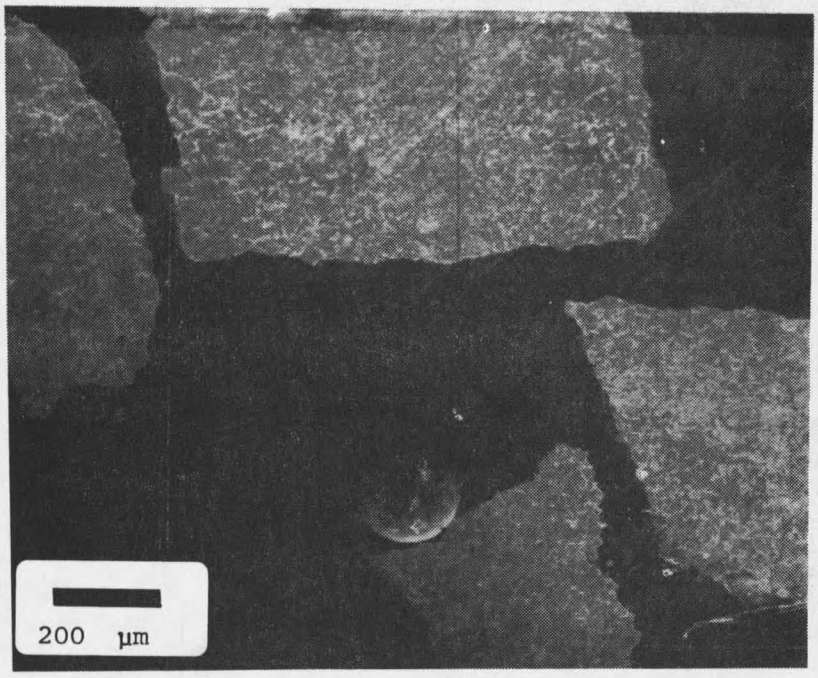

Figure 21. Texas Coal Overburden pyrite (1000 μm) prior to oxidation (45X magnification).

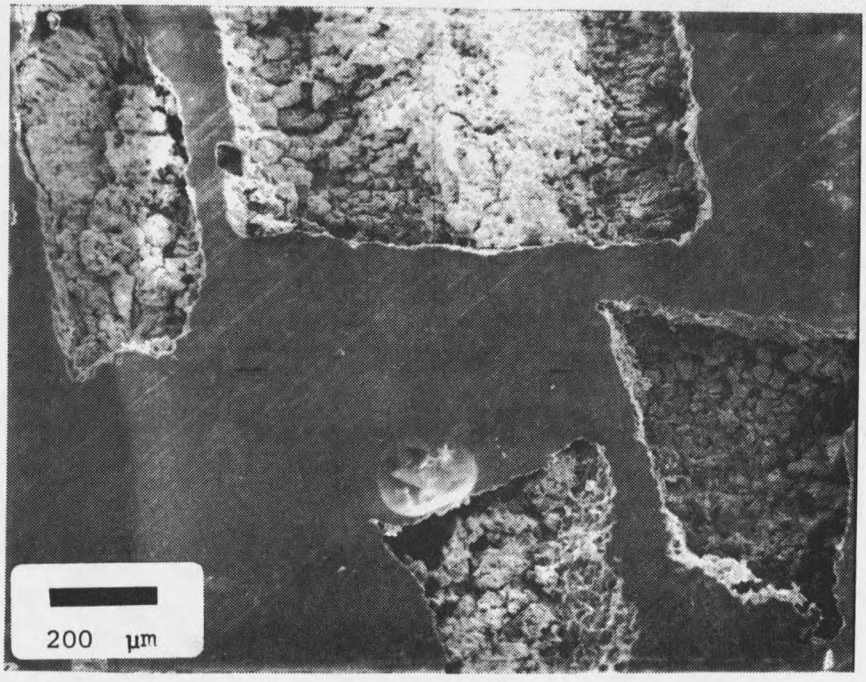

Figure 22. Texas Coal Overburden pyrite (1000 μm) after oxidation by 30% H_2O_2 (45X magnification).

Texas Coal Overburden had significantly more mass removed (60.19%) than the Montana Gold Mine Tailings sample (11.42%) (Table 3). The mass removed from the Montana Gold Mine Tailings sample was limited to attack of microcracks present on the mineral surface (Figure 20), while the Texas Coal Overburden sample was nearly entirely consumed (Figure 22). The SEM has tremendous depth of field resolution, so Figure 22 is slightly misleading since the mineral surface and epoxy surface are both in focus though the mineral surface is well below the epoxy surface after oxidation.

The influence of particle size on pyrite surface oxidation processes was also investigated by SEM. Epoxy castings were made of four size fractions of samples from different sources and submitted to oxidation by 10% H_2O_2. Supporting photographic evidence was collected by SEM. No visual evidence of differences between the oxidation of particles of different sizes from the same source were observed. Differences between oxidation of pyrite derived from different sources overshadowed any difference between particle size differences in oxidation within the same sample.

The sequential removal of mass by 10% H_2O_2 is highly variable between sample sources, and variable between particles from the same source. The sequential removal of pyrite by 10% H_2O_2 from massive pyrite particles derived from the Coal Cleaning Waste I sample is presented in Figures 23, 24 and 25. Figure 23 shows a set of massive pyrite particles shortly after preparation and

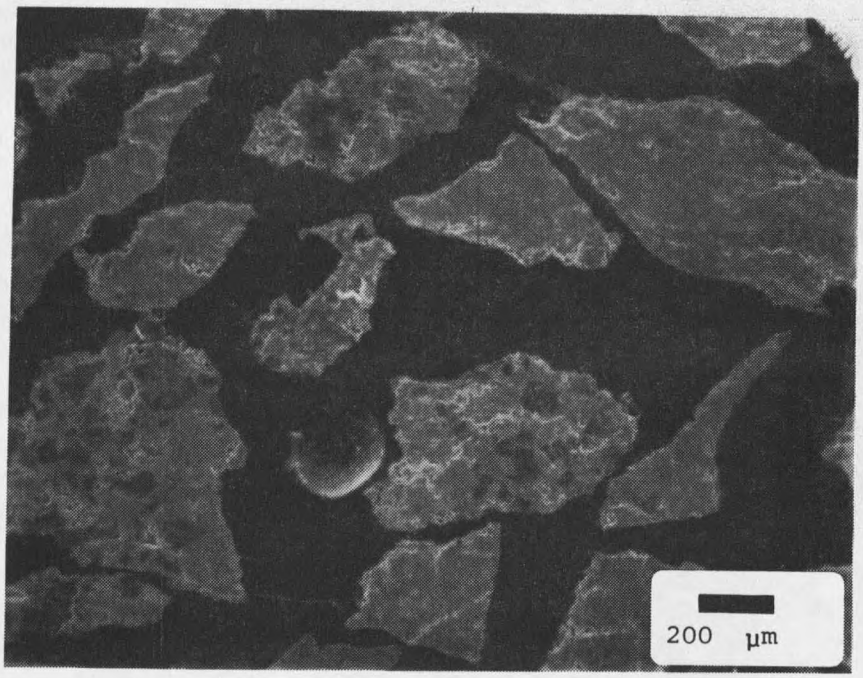

Figure 23. Pyrite particles from Coal Cleaning Waste I cast in epoxy prior to oxidation, 106-250 μm size fraction (250X magnification).

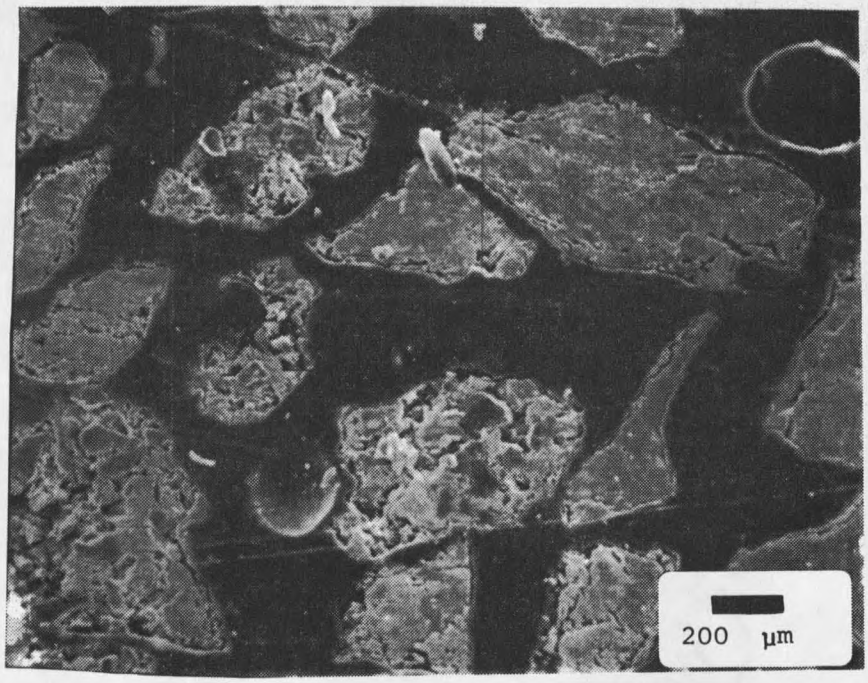

Figure 24. Pyrite particles from Coal Cleaning Waste I cast in epoxy after oxidation by 10% H_2O_2 for 10 minutes, 106-250 μm size fraction (250X magnification).

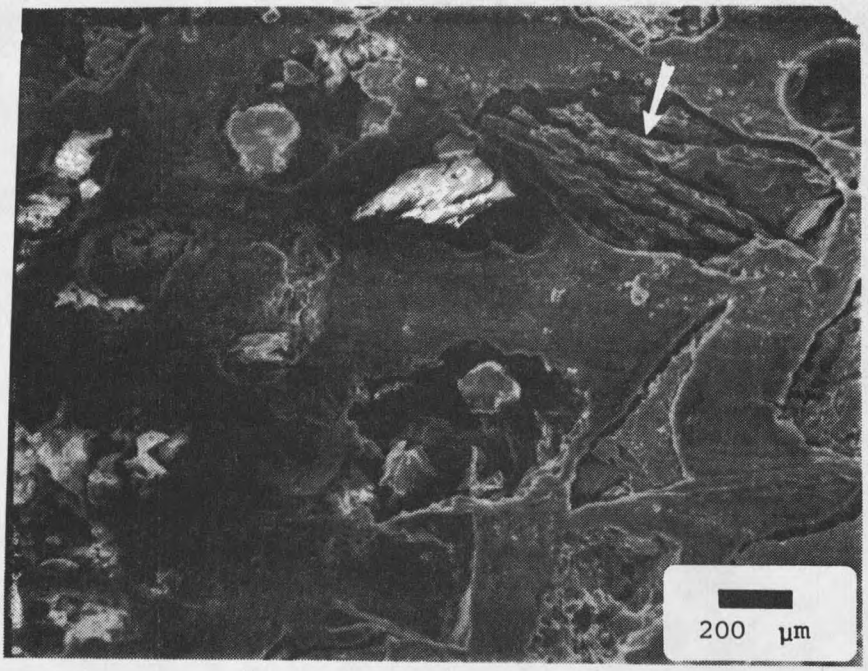

Figure 25. Pyrite particles from Coal Cleaning Waste I cast in epoxy after oxidation by 10% H_2O_2 for 60 minutes, 106-250 μm size fraction (250X magnification). White arrow indicates location of Figure 22.

prior to oxidation. Figure 24 displays the same particles after oxidation by 10% H_2O_2 for ten minutes, while Figure 25 shows the surface morphologies after 60 minutes of treatment with 10% H_2O_2. The dark material encapsulated by some of the pyrite particles in Figure 23 is silica. Since massive pyrite can form in the interstices of sediments and grow around silicates present in the sediment, the inclusion of nonpyritic material within individual particles is expected. Note that during oxidation of the sample by 10% H_2O_2 the silica particles are unaltered.

The destruction of pyrite particles from Coal Cleaning Waste I by 10% H_2O_2 oxidation spanned a range from complete to minimal destruction, depending

on the individual particle (Figure 25). The surface morphology of the pyrite particle in the upper right hand corner (white arrow) of Figure 25 is shown at higher magnification in Figure 26.

The implication of SEM pyrite particle oxidation photography for understanding acid generation processes, is that inherent crystalline physical properties exert a strong influence on the reactivity of pyrite to oxidizing conditions. Differences in the crystalline structure of pyrite particles of the same size are most prominent between samples from different geologic environments, though differences exist in the reactivity of particles derived from the same geologic environment depending on their morphology. The prominent differences between the

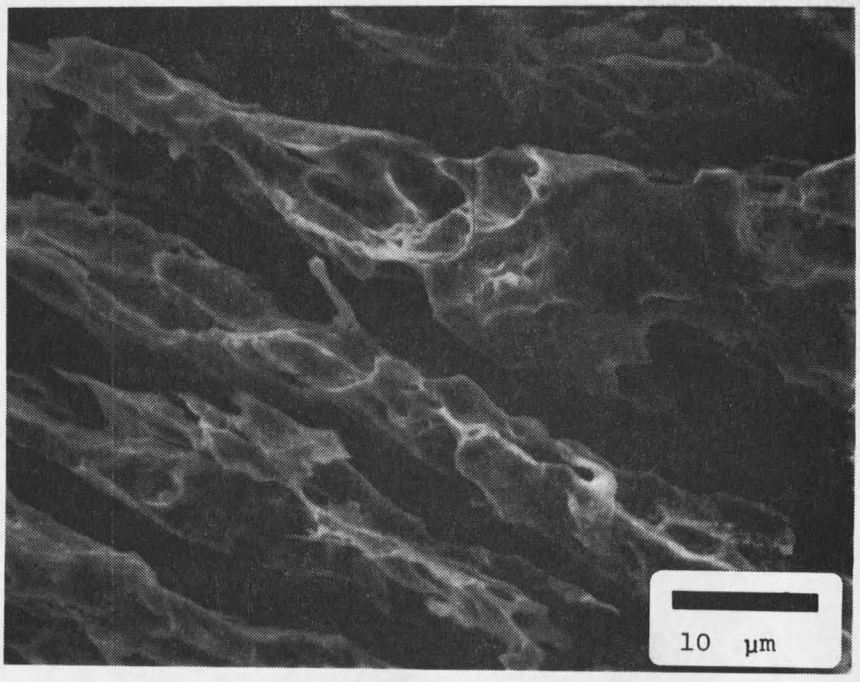

Figure 26. Pyrite surface morphology developed after 60 minutes of oxidation by 10% H_2O_2 (1250X magnification). Location of photograph indicated by white arrow on Figure 25.

crystalline structure of pyrite result in very dissimilar reactivity to oxidizing conditions for particles of the same size, undermining the assumption that the total surface area of pyrite will exert the dominant control on evolution of acid (Caruccio 1968, Pugh et al. 1981 and 1984).

Oxidation Of Pyrite By Deionized Water

Pyrite samples were submitted to oxidation by deionized water by the initiation of repeated wet/dry cycles to evaluate whether hydrogen peroxide and water weathering methods would yield comparable results. At the termination of experimentation after 106 wet/dry cycles with deionized water, six response variables were measured (Table 12). The dominantly massive morphology samples (Coal Cleaning Waste I and Coal Cleaning Waste II) were significantly different ($p \leq 0.05$) from the dominantly euhedral morphology samples (Gold Mine Ore and Copper Mine Tailings) for all response variables measured at the termination of oxidation by deionized water, indicating their greater reactivity (Table 12). Raw data are shown in Table 21, Appendix.

Mass Change

At the termination of oxidation by deionized water, the residual mass was measured and compared to the original 1.000 gram mass. The Gold Mine Ore and Copper Mine Tailings sample demonstrated very little change in mass during

Table 12. Response of mineral samples to oxidation by deionized water at 35° C.

Sample Source	Crystal Form (% Euhedral / % Massive)	Particle Size Fraction (μm)	Sample Response to Oxidation					
			Mass Change (%)	Leachate pH	Leachate EC (dS m^{-1})	Leachate Fe (mg l^{-1})	Leachate SO_4^{2-} (mg l^{-1})	Titratable Acidity (mg $CaCO_3$ l^{1})
Gold Mine Ore	65 / 35	<149	+0.01 C*+	4.20 C	0.10 A	1 A	29 A	12 A
Copper Mine Tailings	100 / 0	<149	-0.01 C	4.78 D	0.08 A	0 A	25 A	8 A
Coal Cleaning Waste I	3 / 97	<149	-7.79 A	2.65 A	3.02 C	862 C	1855 C	1067 C
Coal Cleaning Waste II	0 / 100	<149	-0.55 B	3.33 B	0.45 B	75 B	188 B	171 B

* Mean of three replications.

+ Means in the same column followed by the same uppercase letter are not significantly different ($p \leq 0.05$).

treatment (±0.01%) (Table 12). The Coal Cleaning Waste I and II samples lost 7.79% and 0.55% of their respective masses during treatment. Both Coal cleaning waste samples are significantly different ($p \leq 0.05$) from each other and from the dominantly euhedral morphology samples.

The mass loss results are supported by visual observation of the formation of white salt crusts on the minerals during application of wet/dry cycles. The Coal Cleaning Waste I sample rapidly developed a distinct white salt crust which became progressively more evident over time, while the Coal Cleaning Waste II sample developed a faint salt crust upon drying nearer to the end of experimentation. The dominantly euhedral morphology samples never developed visible salt crusts.

Leachate pH

The mean measured leachate pH values for all samples demonstrate significant differences ($p \leq 0.05$) between all treatments (Table 12). The Copper Mine Tailings mean pH was highest (4.78), followed by the Gold Mine Ore sample (4.20). The dominantly massive morphology samples had the lowest mean pH. The Coal Cleaning Waste II mean sample pH was 3.33 while the Coal Cleaning Waste I sample mean pH was 2.65. The Coal Cleaning Waste I sample lost the greatest amount of the original sample mass during treatment and had the lowest pH.

Leachate Electrical Conductivity

The trend in electrical conductivity parallels the trend established by other variables where samples which lost the most mass had the lowest mean pH and highest mean electrical conductivity (Table 12). The Gold Mine Ore sample and Copper Mine Tailings sample were not significantly different ($p \leq 0.05$) from each other, yet significantly lower than the Coal Cleaning Waste I and II samples. The Coal Cleaning Waste I sample had the highest mean electrical conductivity, 3.02 dS m^{-1}, which was significantly different ($p \leq 0.05$) than the Coal Cleaning Waste II sample mean electrical conductivity of 0.45 dS m^{-1}.

Leachate Iron

The dominantly euhedral morphology samples yielded nearly no iron to the leachate. The Gold Mine Ore sample mean leachate iron content was 1 mg l^{-1} while the Copper Mine Tailings mean leachate iron content was 0 mg l^{-1} (Table 12). Both the dominantly massive particle morphology samples (Coal Cleaning Waste I and II) were significantly different ($p \leq 0.05$) from each other and from the dominantly euhedral morphology samples. The Coal Cleaning Waste I sample, which demonstrated the greatest mass loss, lowest pH and highest electrical conductivity also had the highest mean leachate iron content (862 mg l^{-1}).

Leachate Sulfate

The statistical result of leachate sulfate comparisons is identical to the statistical result for leachate iron (Table 12). The dominantly euhedral morphol-

ogy samples have low levels of leachate sulfate and are not statistically different ($p \leq 0.05$), while the dominantly massive morphology samples are significantly different from each other and from the dominantly euhedral morphology samples. The Coal Cleaning Waste I sample had the highest leachate sulfate content of 1855 mg l^{-1}.

Leachate Titratable Acidity

The statistical result of leachate titratable acidity comparisons is identical to the statistical result for leachate iron and sulfate (Table 12), continuing the trend established for all response variables. The dominantly euhedral morphology samples have very low levels of leachate titratable acidity and are not statistically different ($p \leq 0.05$), while the dominantly massive morphology samples are significantly different from each other and from the dominantly euhedral morphology samples. The Coal Cleaning Waste I sample had the highest leachate titratable acidity of 1067 mg $CaCO_3$ l^{-1}.

There is not a quantifiable comparison to be made between the results of sulfide oxidation, dominantly pyrite, by deionized water at 35° C and 10% H_2O_2 at 0° C. No attempt was made to derive a rate constant specific to any one material at a given set of conditions, rather the intent was to contrast the differences in oxidation of particles of different size and morphology from diverse mine environments, both coal and hardrock. The oxidation of the same sample material under two different conditions yielded two different responses, yet the general trends are comparable (Table 13). The Coal Cleaning Waste I sample lost the most mass

Table 13. Comparison of mineral response to H_2O/O_2 and H_2O_2 simulated weathering techniques.

Sample Source	Crystal Form (% Euhedral / % Massive)	Mean Mass Change (%)		Mean Titratable Acidity (mg $CaCO_3$ l^{-1})	
		10% H_2O_2 Treatment	H_2O/O_2 Treatment	10% H_2O_2 Treatment	H_2O/O_2 Treatment
Gold Mine Ore	65/35	-9.75[+]	+0.01[•]	3430[••]	12[•]
Copper Mine Tailings	100/0	-2.97	-0.01	792	8
Coal Cleaning Waste I	3/97	-52.82	-7.79	17572	1067
Coal Cleaning Waste II	0/100	-46.92	-0.55	16779	171

[+] From Table 3.
[•] From Table 12.
[••] From Table 8.

and had the highest mean titratable acidity by both oxidation treatments, while the Copper Mine Tailings sample had the lowest mean titratable acidity by both oxidation treatments. An important general observation is that massive morphology particles are more readily oxidized than euhedral particles under both deionized water and hydrogen peroxide oxidizing conditions, though weathering differences between euhedral morphology samples are difficult to detect with water weathering due to the minimal response.

Discussion

Particle morphology, whether massive or euhedral, exerted the dominant control on sulfide oxidation, while particle size influenced the rate of oxidation to a lesser degree. The process of sulfide mineral dissolution occurred at focused

locations on the mineral surface where imperfections in the crystalline structure occurred. The development of crystalline imperfection was a consequence of the unique environment of formation and the thermodynamic and geochemical setting at the time of formation of the mineral. Locations where oxidation was initiated included cleavage planes, steps, fractures, dislocations, inclusion and defects. The result of oxidation at these reactive sites on the surface of the mineral was the formation of an etch pit. The frequency of etch pit formation was a function of the density of defects on the surface of the mineral. Since particles with massive morphology lack regular crystalline structure they are defect laden and have many sites for attack by oxidizing agents. Sulfide particles with euhedral morphology typically exhibit defects in the crystalline structure, but many fewer than the particles with massive structure. The relative ease of oxidation of the sulfide particles at any location is a function of the geologic history, and characteristic physical properties of the sulfides inherent to the specific location.

The oxidation of sulfide minerals was recorded for each of four distinct size fractions to assess the importance of particle size to the generation of acid. Particles of smaller size have greater surface area per mass than larger particles, therefore, potentially greater acid generation might be expected from the smaller size particles. The result of experimentation revealed that in fact the smallest size fraction was the *least* acid producing, and particle morphology exerted the dominant influence on rate of acid generation. The *reactive* surface area, meaning

surface area containing imperfections in the crystalline structure, is more important than the *total* surface area.

The implication to remediation of sites containing sulfide minerals is that though a laboratory analysis of acid-base account provides an estimate of the total potential acidity in a sample, no knowledge of the rate of oxidation is implied. For example, the Underground Coal Waste sample was dominantly massive particle morphology and had an ABA of -29 tons $CaCO_3$/1000 tons waste (Table 2). The Copper Mine Tailings sample was dominantly euhedral particle morphology and had a similar ABA of -31 tons $CaCO_3$/1000 tons waste. On the basis of ABA, those two samples would be expected to have similar acid producing characteristics based on potential acidity. This assumption is grossly in error, since when both samples were oxidized by the identical treatment, the generation of acid was significantly different (Table 8). When 1.000 gram pyrite from each of these environments was oxidized in the laboratory with 10% H_2O_2, the Copper Mine Tailings mean titratable acidity was 792 mg $CaCO_3$ l^{-1} while the Underground Coal Waste mean titratable acidity was 19868 mg $CaCO_3$ l^{-1}, or a 25 fold difference. The result of the oxidation of pyrite samples from different geological environment of the same particle size was the generation of acidity which may vary by an order of magnitude between samples, resulting in very different environmental consequences. A mining environment dominated by euhedral sulfide morphology may require decades or centuries of time to impact site acidity. However, a mining environment dominated by a massive sulfide morphology may

reveal acid remediation problems in a few years. The ultimate generation of acidity from 1.000 gram of massive pyrite will be the same as the acidity generated by oxidation of 1.000 gram of euhedral pyrite, but the rate of dissolution may be very dissimilar. The acid load to surface water resources or impact to plant growth may be entirely a function of the rate of oxidation. If oxidation should proceed rapidly, negative environmental consequence may accrue, while if the oxidation of sulfides occurs slowly, the addition of acid load may be diluted to the point where aquatic or vegetative mortality does not occur. Remediation of sulfide containing environments should therefore reflect knowledge of the differential weathering characteristics of pyrite of varying morphology.

ACID PRODUCTION FROM DIFFERENT SULFUR BEARING MINERALS DURING OXIDATION

Distribution Of Sulfur Minerals In Mine Environments

Sulfur is an abundant element in the lithosphere. Sulfur can occur in many forms including native sulfur, inorganic minerals and in organic compounds. In mining environments, sulfur compounds are typically enriched relative to the average crustal composition. In hardrock mining, metals and metals of economic interest occur naturally as sulfides or in association with sulfide and sulfate mineral assemblages. In depositional sedimentary environments where coal deposits are found, sulfur is a common element, both as sulfide and sulfate minerals, as well as sulfur incorporated into the chemical structure of various organic compounds.

In order to remediate lands disturbed by mining, understanding sulfur form distribution in materials is essential for effective land reclamation. The presence of pyrite and marcasite is especially important since prior to mining, sulfur is present in a reduced form and may generate acidic drainage upon exposure to atmospheric conditions. Sulfate minerals, where sulfur is in an oxidized form are not expected to generate acidic drainage though they may contribute to the sulfur content of waters originating in an area disturbed by mining due solely to their solubility in water.

Though pyrite and marcasite are commonly accepted as being acid producing minerals in oxidizing conditions, the reaction of other sulfur containing

minerals (e.g. galena, chalcopyrite) to oxidizing conditions is unknown. Since many sulfur containing minerals in addition to pyrite and marcasite are found in mining environments, knowledge of the fate of these minerals in oxidizing conditions is required for effective land remediation when pyrite and marcasite do not constitute the entirety of the sulfur component.

The purpose of this investigation was to determine which of the sulfur bearing minerals found in both coal and hardrock mine environments will generate acid upon weathering. Pyrite and marcasite are common minerals and generally believed responsible for the generation of acidic drainage, but the acid generating potential of other sulfur bearing minerals upon weathering is unknown.

Methods

Pure mineral samples containing sulfur as a constituent in the chemical structure were obtained from Wards Scientific Establishment and from operational coal and metal mines from the western United States. The mineral samples included both sulfide and sulfate minerals. Samples obtained from operational mines were waste materials containing a few percent sulfur. This material was subsequently high-graded by water separation methods (shaker table) followed by heavy liquid separation by 1,1,2,2 tetrabromoethane (density = 2.96 g cm^{-3}) (O'Meara et al. 1928). Heavy liquid separation allows for the flotation of silicates (density = 2.65 g cm^{-3}) and their subsequent removal, while the heavier sulfides

(pyrite density = 5.01 g cm^{-3}) pass through the liquid. Some impurities will not be removed by this method when light and dense particles are intergrown and not disaggregated.

All samples were crushed to minus 100 mesh (<149 μm) by mortar and pestle and passed through a U.S. Standard Sieve Number 100.

A total of 17 mineral samples were used, with three replications of each. The treatments were barite, anhydrite, gypsum, anglesite, jarosite, arsenopyrite, Ward's pyrite, chalcocite, Ward's pyrrhotite, chalcopyrite, galena, marcasite, sphalerite, coal barite, hardrock pyrite, hardrock pyrrhotite, and coal pyrite. The first 13 samples were pure minerals while the last four samples were obtained from operational mines and contained impurity. One gram (1.000 ± 0.001 g) samples of each mineral were weighed into 250 ml Erlenmeyer flasks. The flasks were then placed in an ice bath at 0° C. A 10% H_2O_2 solution was prepared using reagent grade hydrogen peroxide (30%) and deionized water. Fifty milliliters 10% H_2O_2 was subsequently added to each sample, and the ensuing reaction allowed to run to completion. If no discernable reaction was generated upon addition of 10% H_2O_2 to the sample at the end of 72 hours the solution was removed from contact with the sample by filtration. The pH of the 10% H_2O_2 was 4.52, while the titratable acidity was 28 mg $CaCO_3$ l^{-1} prior to addition to the treatments.

Filtration was accomplished upon completion of the reaction by gravity drainage of the solution through a weighed 11 cm Whatman 40 filter paper. Reaction completion was identified as the point at which bubbles or effervescence ceased in the flask. Upon pouring the solution from the 250 ml Erlenmeyer flask through the filtration apparatus, an additional 10 ml deionized water was added to the residual material in the flask as a rinsing step. The 10 ml deionized water was then filtered into the leachate recovered from the reaction, diluting the original 50 ml sample to 60 ml. The leachate was retained for subsequent analysis. The flask, residual sample and filter paper were air dried for two hours at 40° C in a forced air oven, and then reweighed.

The leachate resulting from oxidation of each sample by 10% H_2O_2 was analyzed for pH, electrical conductivity and titratable acidity. A split of the leachate was analyzed for total sulfur by inductively coupled plasma emission spectroscopy (ICP).

Acid Generation By Sulfur Bearing Minerals

The acid generation, mass loss and leachate chemistry for each mineral when treated with 10% H_2O_2 is presented in Table 14. Raw data for this experiment are shown in Table 22, Appendix.

Table 14. Response to simulated weathering of sulfate and sulfide minerals by 10% hydrogen peroxide at 0° C.

Mineral Sample Name	Sample Chemical Composition	Mass Change (%)*	Leachate pH*	Leachate Electrical Conductivity (dS m^{-1})*	Leachate Sulfur (mg l^{-1})*	Leachate Titratable Acidity to pH 7 (mg $CaCO_3$ l^{-1})*
Barite	$BaSO_4$	0 e**	4.07 e	0.01 a	2 a	36 b
Anhydrite	$CaSO_4$	-13.50 cde	7.03 f	2.45 d	575 gf	3 a
Gypsum	$CaSO_4 \cdot 2H_2O$	-14.30 cde	4.20 e	2.49 d	566 gf	47 cb
Anglesite	$PbSO_4$	-1.60 de	4.57 e	0.03 ab	14 c	33 b
Jarosite	$KFe_3(SO_4)_2(OH)_6$	-2.95 de	4.10 e	0.02 a	6 b	35 b
Arsenopyrite	FeAsS	+4.71 e	1.69 b	18.07 e	1250 h	4365 fgh
Ward's Pyrite	FeS_2	-27.56 cb	1.82 b	13.27 e	2360 i	7362 hi
Chalcocite	Cu_2S	+3.04 e	4.54 e	0.33 c	37 d	128 c
Ward's Pyrrhotite	$Fe_{(1-x)}S$	-2.28 de	2.69 cd	2.26 d	372 g	1089 e
Chalcopyrite	$CuFeS_2$	-5.16 de	2.73 cd	3.52 d	729 g	1995 ef
Galena	PbS	+8.89 e	4.07 ce	0.06 b	33 d	71 cb
Marcasite	FeS_2	-36.47 b	1.83 b	12.39 e	1963 hi	6501 ghi
Sphalerite	(Zn, Fe)S	-24.14 cbd	4.30 e	2.61 d	1611 hi	4645 fgh
Hardrock pyrite	FeS_2 + Impurities	-2.28 de	2.93 d	1.15 d	105 e	316 d
Hardrock pyrrhotite	$Fe_{(1-x)}S$ + Impurities	-5.16 de	2.59 e	2.97 d	528 fg	2552 efg
Coal pyrite	FeS_2 + Impurities	-52.90 a	1.51 a	26.92 e	5333 j	17660 i

* Geometric mean of three observations.

** Mean values in the same column followed by the same letter are not significantly different ($p \leq 0.05$). ANOVA mean separation tests performed by Newman-Keuls tests of significance.

- Barite ($BaSO_4$) - Barite is not an acid forming mineral. Though barite was treated with 10% H_2O_2, which is a strong oxidizer, no measurable mass loss was detected. The insolubility and resistance to oxidation of barite is supported by the leachate electrical conductivity, which was very low (0.01 dS m^{-1}) (Table 14). The mean leachate sulfur content was 2 mg l^{-1}, which is very low compared to the other mineral treatments, and significantly different ($p \leq 0.05$) from all the other mineral treatments. The mean titratable acidity of the barite sample was 36 mg $CaCO_3$ l^{-1}, which is close to the measured titratable acidity of the 10% H_2O_2 prior to addition to the mineral treatments (28 mg $CaCO_3$ l^{-1}). Since barite is common in mine environments, not acid forming, and tremendously resistant to weathering, it is likely to be present in waste materials. Though barite does not represent a problem to site remediation, it may interfere with accurate acid-base account (ABA) analysis.
- Anhydrite ($CaSO_4$) - Anhydrite is very soluble in water and not an acid forming mineral. The mean leachate pH after treatment was elevated (7.03) compared to the pH of the H_2O_2 prior to addition to the mineral treatments (4.52). The mean titratable acidity was 3 mg $CaCO_3$ l^{-1}, which was significantly different ($p \leq 0.05$) from all other mineral treatments (Table 14). The anhydrite samples lost a mean

13.5% of their original mass, resulting in 575 mg S l^{-1}, and an electrical conductivity of 2.45 dS m^{-1}.

- Gypsum ($CaSO_4 \cdot 2H_2O$) - Gypsum is very similar to anydrite; not acid forming and very soluble in water. The mean mass loss attributed to gypsum when treated with 50 ml 10% H_2O_2 was 14.30%, resulting in a mean 566 mg S l^{-1} in the leachate. The mean leachate electrical conductivity was 2.49 dS m^{-1}, which was not significantly different ($p \leq 0.05$) from the anhydrite sample. The mean leachate pH was 4.20 and the mean titratable acidity was 47 mg $CaCO_3$ l^{-1}.
- Anglesite ($PbSO_4$) - Anglesite is a common sulfate mineral in lead mining districts resulting from the weathering of galena. Anglesite is not an acid forming mineral. Anglesite was minimally affected by H_2O_2 oxidation, resulting in a mean leachate electrical conductivity of 0.03 dS m^{-1} (Table 14). The mean titratable acidity was 33 mg $CaCO_3$ l^{-1}, ranking anglesite as a nonacid generating sulfate mineral.
- Jarosite ($KFe_3(SO_4)_2(OH)_6$) - Jarosite is a common secondary mineral formed in association with pyrite, and is considered acid forming upon elevation of soil solution pH by the addition of liming materials during site remediation (Schafer et al. 1989). Acidity is generated as Fe^{3+} is oxidized to Fe^{2+} at near neutral pH since Fe^{2+} is the stable species of iron at this pH. When treated with 10% H_2O_2 in a laboratory setting jarosite was not acid forming, and was little affect-

ed by the treatment. The mean leachate electrical conductivity was 0.02 dS m^{-1} while the mean leachate sulfur content was 6 mg l^{-1} (Table 14). The mean titratable acidity was similarly low (35 mg $CaCO_3$ l^{-1}) compared to other mineral treatments. Upon partial oxidation of pyrite in the presence of potassium the formation of jarosite can occur (Equation 19).

$$FeS_2 + \frac{15}{4}O_2 + \frac{5}{2}H_2O + \frac{1}{3}K^{+1} = \frac{1}{3}KFe_3(SO_4)_2(OH)_6 + \frac{4}{3}SO_4^{-2} + 3H^+ \qquad [19]$$

If jarosite had not formed and pyrite oxidation had run to completion, 4 moles acidity would have been generated by pyrite oxidation (Equation 20) instead of 3 moles acidity (Equation 19). The addi-

$$FeS_2 + \frac{15}{4}O_2 + \frac{7}{2}H_2O = Fe(OH)_3 + 2SO_4^{-2} + 4H^+ \qquad [20]$$

tional 1 mole of acidity is predicted to be released upon elevation of pH resulting in the destruction of jarosite, which is not thermodynamically stable at pH levels near neutral (Equations 21 and 22).

$$KFe_3(SO_4)_2(OH)_6 + 6H^+ = K^+ + 3Fe^{+3} + SO_4^{-2} + 6H_2O \qquad [21]$$

$$3Fe^{+3} + 9H_2O = Fe(OH)_3 + 9H^+ \qquad [22]$$

- Arsenopyrite (FeAsS) - Arsenopyrite is an acid producing sulfide mineral. The mean leachate pH was 1.69 and the mean titratable acidity was 4365 mg $CaCO_3$ l^{-1} (Table 14). Arsenopyrite reacted aggressively to oxidation by 10% H_2O_2 and is expected to yield acid when present in a natural oxidizing environment. The reaction of

the mineral with hydrogen peroxide yielded the formation of presumed metallic oxide precipitates as is evident by the gain in mass of the sample while the leachate mean electrical conductivity was 18.07 dS m^{-1}.

- Ward's pyrite (FeS_2) - Pyrite is an acid producing sulfide mineral and is oxidized under atmospheric conditions in accordance with Equation 20. Equation 23 presents the oxidation of pyrite by hydrogen peroxide (O'Shay et al. 1990).

$$FeS_2 + \frac{15}{2} H_2O_2 = Fe(OH)_3 + 2SO_4^{-2} + 4H^+ + 4H_2O \qquad [23]$$

The Ward's pyrite sample is a "museum grade" pyrite sample purchased for use in research for comparison to the mining environment pyrite samples; Hardrock pyrite and Coal pyrite (Table 14). Using mass loss as an indication of the differences between the three pyrite samples, the mean Hardrock pyrite sample lost 2.28% of the original mass while the Ward's pyrite sample mean mass loss was 27.56%, and the mean Coal pyrite mass loss was 52.90%. These three samples were significantly different ($p \leq 0.05$) for the response variables mass change, pH and leachate sulfur.

- Chalcocite (Cu_2S) - Chalcocite is a nonacid forming sulfide mineral as was determined experimentally. The mean leachate pH was 4.54 after treatment, while the 10% H_2O_2 pH was 4.52 prior to addition to the chalcocite sample (Table 14). The mean titratable acidity was

128 mg $CaCO_3$ l^{-1} which is not significantly different from gypsum which was also nonacid generating. The mean mass change for chalcocite was a gain of 3.04% relative to the original mass. The formation of insoluble metallic oxide compounds during oxidation may be the cause of sample mass gain.

- Ward's pyrrhotite ($Fe_{1-x}S$) - Pyrrhotite is a common acid forming mineral. The oxidation of pyrrhotite, or FeS minerals, is presented in Equation 24 (Haines 1986).

$$FeS + O_2 + 2H_2O = Fe^{+2} + SO_4^{-2} + 4H^+ + 4e^- \quad [24]$$

The Ward's pyrrhotite sample lost a mean 2.28% of the original mass, resulting in a mean leachate pH of 2.69 (Table 14). The mean titratable acidity was 1089 mg $CaCO_3$ l^{-1}. Coincidentally, the Hardrock pyrite lost an identical mean 2.28% of the original sample mass and the resulting leachate pH, electrical conductivity and sulfur content were not significantly different ($p \leq 0.05$) from the Ward's pyrrhotite sample, though the titratable acidity was significantly less.

- Chalcopyrite ($CuFeS_2$) - Chalcopyrite is an acid generating sulfide mineral. The oxidation of chalcopyrite in the presence of ferric iron and water is presented in Equation 25 (Brierley 1990).

$$CuFeS_2 + 16Fe^{3+} + 8H_2O = Cu^{2+} + 17Fe^{2+} + 2SO_4^{2-} + 16H^+ \quad [25]$$

Chalcopyrite lost a mean 5.16% of the original sample mass when oxidized by 10% H_2O_2, resulting in a mean leachate pH of 2.73 and mean titratable acidity of 1995 mg $CaCO_3$ l^{-1} (Table 14).

- Galena (PbS) - Galena is not an acid generating sulfide mineral. The mean leachate pH after oxidation by 10% H_2O_2 was 4.07, while the mean titratable acidity was 71 mg $CaCO_3$ l^{-1} (Table 14). The sample gained mass during treatment presumably due to the formation of insoluble metallic oxides. The mean leachate electrical conductivity was 0.06 dS m^{-1}.

- Sphalerite ((Zn, Fe)S) - Sphalerite is an acid generating sulfide mineral, though the stoichiometry of the reaction of sphalerite (which is dominantly zinc) with hydrogen peroxide is unknown. The sphalerite sample lost a mean 24.14% of the original mass resulting in a mean leachate pH of 4.30 (Table 14). The mean sphalerite leachate pH is not significantly different ($p \leq 0.05$) from the non-acid forming minerals barite, gypsum, anhydrite, anglesite, jarosite, chalcocite and galena though the mean sphalerite titratable acidity is significantly different from the same samples. The relatively high sphalerite leachate pH compared to the other acid-forming minerals is unexplained, but may relate to the hydrolysis of zinc occurring during determination of titratable acidity.

- Hardrock pyrite (FeS_2 + impurities) - Pyrite, as established by Equations 20 and 23, is an acid forming sulfide mineral. The inclusion of this sample, which was concentrated from mine waste material, was to provide a frame of reference from an operational mine site. The Hardrock pyrite sample was the least acid generating of the acid producing minerals, generating a mean titratable acidity of 316 mg $CaCO_3$ l^{-1} (Table 14). This sample is identified as Copper Mine Tailings, which was the least acid producing pyrite material identified when treated with 10% H_2O_2.
- Hardrock pyrrhotite ($Fe_{1-x}S$ + impurities) - Pyrrhotite is an acid producing sulfide mineral (Equation 24). The hardrock pyrrhotite sample is a mine environment waste material (Gold Mine Tailings II) used to compare to the "museum grade" pyrrhotite sample (Ward's pyrrhotite). The Hardrock pyrrhotite and Ward's pyrrhotite samples are not significantly different ($p \leq 0.05$) for any of the response variables; mass change, leachate pH, electrical conductivity, sulfur and titratable acidity.
- Coal pyrite (FeS_2 + impurities) - This pyrite sample is the most acid generating sample of all sulfur bearing mineral treatments. Pyrite is an acid forming mineral (Equations 20 and 23), but substantial variation exists in the ease of oxidation of pyrite of different morphologies. The Coal pyrite sample (Coal Cleaning Waste I) is a

massive particle morphology sample which reacts aggressively to oxidation. Upon treatment with 50 ml 10% H_2O_2, the Coal pyrite sample lost a mean 52.90% of the original 1.000 gram mass resulting in a mean leachate pH of 1.51. The Coal pyrite leachate pH is significantly different ($p \leq 0.05$) from all other mineral treatments. The mean titratable acidity was 17660 mg $CaCO_3$ l^{-1}.

Discussion

Delineation of the acid producing potential of sulfur bearing minerals typically is limited to pyrite and marcasite, which are common minerals, and undeniably can generate acidic drainage upon oxidation. Many other sulfur bearing minerals are found in mine environments, though they may or may not be considered acid producing.

The sulfate minerals barite, anhydrite, gypsum, anglesite and jarosite are not acid producing under strongly oxidizing conditions. Additionally, the sulfide minerals chalcocite and galena were found to be nonacid producing, when treated with 10% H_2O_2.

Within the group of minerals considered to be acid producing, a wide range of rates of acid generation are noted between minerals. The minerals found to be acid producing under strongly oxidizing conditions include, pyrite, marcasite, pyrrhotite, arsenopyrite, chalcopyrite and sphalerite.

The stoichiometric dissolution of pyrite or marcasite by oxidation with oxygen and water hydrolysis proceeds in accordance with Equation 26. The

$$FeS_2 + \frac{15}{4}O_2 + \frac{7}{2}H_2O = Fe(OH)_3 + 4H^+ + 2SO_4^{2-} \qquad [26]$$

generation of acidic drainage is a consequence of the oxidation of pyrite, requiring the addition of 31.25 tons $CaCO_3$ per 1000 tons waste to neutralize a material containing 1% sulfur as pyrite. The stoichiometric dissolution of other acid forming minerals (i.e. chalcopyrite) and generation of products is unknown, though simulated weathering of sulfur bearing minerals by 10% H_2O_2 in this experiment has demonstrated that minerals other than pyrite and marcasite can be acid forming. Remediation and reclamation of project areas containing reduced sulfur forms must, therefore, consider the neutralizing requirements of waste materials in the context of the quantity and mineralogy of the reduced sulfur forms. If reduced sulfur forms are present which are not acid forming (e.g. galena or chalcocite), the addition of liming materials to offset potential acidity is not required. When acid forming minerals are present, liming materials are required to prevent the degradation of water quality and impairment of plant performance.

DISSOLUTION OF SULFUR BEARING MINERALS BY H_2O, HCl AND HNO_3: ACID-BASE ACCOUNT METHODOLOGY

Application Of Acid-Base Account Analytical Methodology To Mined Land Reclamation

Acid-base account analytical methods are routinely applied to the analysis of mine waste materials to assess the ability of the material to generate acid upon weathering. Acid-base account (ABA) analytical methods (Sobek et al. 1978) and subsequent modifications (Schafer et al. 1987), serve to identify the sulfur forms in a sample. The ultimate delineation of the acid-producing sulfur fraction in a sample is extremely important in site remediation planning. Millions of dollars are spent each year for liming materials applied to acid producing wastes based on acid-base account analytical results. The effectiveness of acid generating materials on reclamation is dependent on effective neutralization of acid generated by the oxidation of acid producing minerals. Acid-base account is assessed by determining the neutralization potential (NP) and potential acidity (PA) of a sample in accordance with Equation 27.

$$ABA = NP - PA \qquad [27]$$

The units of ABA are tons $CaCO_3$ per 1000 tons waste material, indicating the quantity of liming materials required for neutralization of the potential acidity. The mass of one 0.4 hectare of soil 15 cm deep is approximately 1000 tons, so the units of ABA are tied to site remediation planning. The results from ABA analysis are broken into HCl soluble forms, HNO_3 soluble forms and residual

sulfur forms (Figure 27). More recently (Schafer et al. 1987) has attempted to distinguish acid producing from nonacid producing sulfates through the use of an additional hot water extraction step. The hot water extractable sulfur (e.g. $CaSO_4$) forms are considered to be nonacid forming while the HCl and HNO_3 are considered acid forming. Residual sulfur is commonly considered to be organically bound (CasaGrande 1989) and not acid generating by the Sobek Method though the Schafer Method includes the residual sulfur component as acid producing for calculation of ABA. The sum of all the sulfur forms equates to the total sulfur content (Equation 28).

$$\textbf{Total S} = \textbf{H}_2\textbf{O Extractable S} + \textbf{HCl Extractable S} + \textbf{HNO}_3 \textbf{ Extractable S} + \textbf{Residual S} \quad [28]$$

Calculation of the ABA is presented by two different approaches (Sobek et al. 1978, Schafer et al. 1987). The Sobek Method considers only the nitric acid extractable sulfur component as acid forming (Equation 29).

Sobek Method

$$\textbf{ABA} = \textbf{NP} - 31.25\ (\textbf{HNO}_3 \textbf{ Extractable S}) \quad [29]$$

By comparison, the Schafer Method considers the HNO_3 and HCl extractable sulfur forms, in addition to the residual sulfur, as acid forming (Equation 30).

Schafer Method

$$\textbf{ABA} = \textbf{NP} - [31.25\ (\textbf{HNO}_3 \textbf{ Extractable S} + \textbf{Residual S}) + 23.44\ (\textbf{HCl Extractable S})] \quad [30]$$

For each 1% HNO_3 extractable sulfur, which is not offset by neutralization potential indigenous to a sample, 31.25 tons $CaCO_3$ per 1000 tons waste material is added during reclamation to offset the potential acidity of the material. The

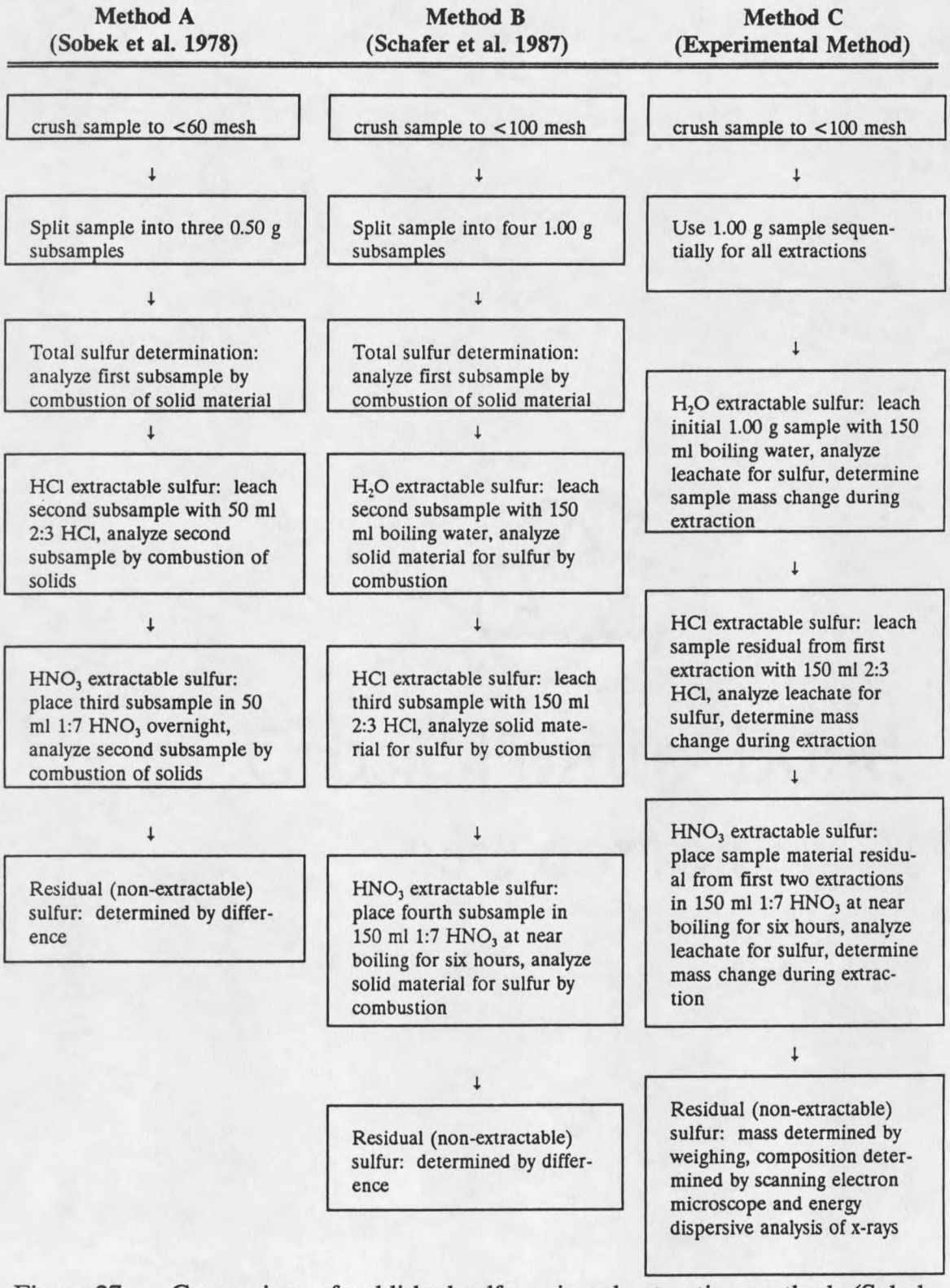

Figure 27. Comparison of published sulfur mineral extraction methods (Sobek et al. 1978 and Schafer et al. 1987) to experimental method.

lime rate to address potential acidity for a project area is subsequently calculated by comparing the neutralization potential to the potential acidity and adding lime to account for any deficit in neutralization potential. The ratio of 31.25 tons $CaCO_3$/1000 tons waste/1% HNO_3 extractable sulfur is derived from the stoichiometric neutralization of acidity generated by the oxidation of FeS_2, where 1 mole FeS_2 generates 4 moles H^+ which is neutralized by 2 moles $CaCO_3$. The Schafer Method considers jarosite as an acid producing sulfate mineral, so 23.44 tons $CaCO_3$/1000 tons waste/1% HCl extractable sulfur are required to ameliorate potential acidity due to jarosite.

The purpose of this experiment is to identify the effectiveness by which minerals, which are expected to yield acid upon weathering, are extracted by laboratory methods designed to identify their presence. Additionally, the extraction of nonacid forming common sulfur containing minerals, by the same extraction methods, are recorded to understand the dissolution of these minerals by ABA extractions.

Methods

Pure mineral samples containing sulfur were obtained from Ward's Scientific Establishment and from operational coal and metal mines. Samples obtained from operational mines were waste materials containing several percent sulfur. This material was subsequently high-graded by water separation methods (shaker table) followed by heavy liquid separation by 1,1,2,2 tetrabromoethane (density =

2.96 g cm^{-3}) (O'Meara et al. 1928). Heavy liquid separation allows for the flotation of silicates (density = 2.65 g cm^{-3}) and their subsequent removal, while the heavier sulfides (pyrite density = 5.01 g cm^{-3}) pass through the liquid. Some impurities will not be removed by this method when light and dense particles are intergrown and not disaggregated.

All samples were crushed to minus 100 mesh (<149 μm) by mortar and pestle and passed through a U.S. Standard Sieve Number 100.

One gram (1.000±0.001 g) samples of each mineral sample were submitted to a sequential extraction by hot water, 2:3 hydrochloric acid and 1:7 nitric acid (Figure 27). A total of 17 mineral samples were used, with three replications of each sample. The treatments were barite, anhydrite, gypsum, anglesite, jarosite, arsenopyrite, Ward's pyrite, chalcocite, Ward's pyrrhotite, chalcopyrite, galena, marcasite, sphalerite, coal barite, hardrock pyrite, hardrock pyrrhotite, and coal pyrite. This experimental method, though not identical to methods established by Sobek et al. (1978) or Schafer et al. (1987), is a close approximation of the extraction methods previously published.

Each 1.000 gram sample was initially placed in a weighed filter paper (Whatman 40, 11 cm) located in a filtration funnel. Deionized water was heated to boiling, 95° C, and poured incrementally through the filter until 150 ml hot water had been added. The hot water was allowed time to drain through the sample by gravity. At the termination of drainage, a leachate sample was collected for sulfur analysis by inductively coupled plasma emission spectroscopy (ICP),

while the filter paper and residual sample were dried in a forced air oven at 40° C for two hours and reweighed.

The filter paper and sample surviving the hot water extraction were replaced in the filter funnel apparatus. Hydrochloric acid solution was prepared for use in extraction in the ratio of 2 parts reagent grade, concentrated HCl, to 3 parts deionized water. A total of 150 ml 2:3 HCl was added to the filtration apparatus and allowed to drain by gravity. Ten milliliters of deionized water were added to the filter paper as a rinsing agent. The resulting leachate was collected and a sample was submitted for sulfur analysis by ICP, while the residual sample and filter paper were dried in a forced air oven at 40° C for two hours and reweighed.

The sample surviving the first two extraction steps was then removed from the filter paper and placed in a weighed 250 ml Erlenmeyer flask. The mass change of the filter paper used for the first two extractions was measured. The HNO_3 extraction solution was prepared in the ratio of 1 part reagent grade, concentrated HNO_3 to 7 parts deionized water. A total of 150 ml 1:7 HNO_3 was added to the flask containing the sample, which was then heated to 75° C and allowed to remain in contact with the sample for six hours. At the termination of six hours, the sample and solution were poured through a weighed 11 cm Whatman 40 filter paper. A rinse of 30 ml deionized water was added to the flask and then poured through the filter paper. The resulting leachate was collected and a sample submitted for sulfur analysis by ICP. The residual sample and filter were

dried at 40° C in a forced air oven for two hours and reweighed. Leachate chemistry results were statistically analyzed using one-way analysis of variance (Snedecor and Cochran 1989).

The residual sample material was retained for chemical analysis by scanning electron microscopy (SEM) and energy dispersive analysis of x-rays (EDAX). Polished aluminum stub mounts were prepared for submission to the SEM by applying a film of colloidal graphite paint to the aluminum stub and sprinkling the sample material onto the paint while wet. A conductive coating of Neutrastat spray was then applied to the surface. Both before extraction and after extraction EDAX records were collected for each sample from an area EDAX scan at 90X magnification.

Mineral Dissolution By ABA Extraction; Tracking Sulfur Forms Present In Mine Wastes

The dissolution response of each mineral sample to treatment with H_2O, HCl and HNO_3 is dependent on the inherent physical properties of each mineral. Mineral dissolution in response to treatment was recorded based on mass loss and leachate sulfur content (Table 15). The relative success of each treatment on mineral dissolution is reflected in the acid-base account (ABA) analysis. When minerals are effectively removed by a treatment, the accrued sulfur component is catalogued as acid forming or nonacid forming, depending on methods identified by Sobek and others (1978), and Schafer and others (1987). Raw data for this experiment are shown in Table 23, Appendix.

Table 15. Summary of sulfur containing mineral response to sequential acid-base account extraction.

Sample Chemical Composition	Mineral Sample Name	H_2O Extraction		HCl Extraction		HNO_3 Extraction		Mean Residual Mass (%)
		Mean* Percent Mass Removed By H_2O Extraction	Mean* Leachate Sulfur (mg l^{-1})	Mean* Percent Mass Removed By HCl Extraction	Mean§ Leachate Sulfur (mg l^{-1})	Mean* Percent Mass Removed By HNO_3 Extraction	Mean* Leachate Sulfur (mg l^{-1})	
$BaSO_4$	Barite	-0.5 D**	1.3 A	-0.8 GH	10 AB	-19.8 EFG	20 A	78.8 HI
$CaSO_4$	Anhydrite	-18.3 B	255 C	-76.1 B	1175 C	-5.8 HI	41 A	-0.2 A
$CaSO_4 \cdot 2H_2O$	Gypsum	-40.6 A	488 D	-56.5 C	612 C	-3.3 I	12 A	-0.4 A
$PbSO_4$	Anglesite	-1.4 D	8.0 A	-44.4 E	427 C	-37.5 D	37 A	16.7 DC
$KFe_3(SO_4)_2(OH)_6$	Jarosite	-0.6 D	2.0 A	-2.5 G	19 AB	-24.6 EF	71 A	72.2 GH
FeAsS	Arsenopyrite	-0.5 D	1.7 A	-1.1 GH	2 A	-69.2 C	414 B	29.3 EF
FeS_2	Ward's Pyrite	-0.5 D	3.3 A	+0.5 GH	1 A	-83.9 AB	2711 CD	16.1 DC
Cu_2S	Chalcocite	-0.3 D	0.7 A	+3.3 H	1 A	-79.9 B	23 A	23.1 DE
$Fe_{(1-x)}S$	Ward's Pyrrhotite	-0.7 D	5.7 A	-80.2 A	114 BC	-12.7 HG	96 A	6.4 AB
$CuFeS_2$	Chalcopyrite	-0.6 D	1.3 A	+0.7 GH	3 AB	-27.1 E	163 AB	73.0 GH
PbS	Galena	-0.4 D	0.3 A	-32.3 F	424 C	-35.9 D	0.7 A	31.4 F
FeS_2	Marcasite	-0.8 D	7.0 A	+0.4 GH	5 AB	-90.4 A	2752 D	9.2 BC
(Zn, Fe)S	Sphalerite	-0.7 D	0.7 A	-2.7 G	11 AB	-12.2 HG	0.7 A	84.4 I
$BaSO_4$ + Impurities	Coal barite	-1.4 D	1.3 A	-3.0 G	25 AB	-26.2 E	62 A	69.3 G
FeS_2 + Impurities	Hardrock pyrite	-0.4 D	0.3 A	-2.7 G	2 A	-68.0 C	2454 C	28.8 EF
$Fe_{(1-x)}S$ + Impurities	Hardrock pyrrhotite	-0.7 D	1.3 A	-52.1 D	76 BC	-16.3 FG	366 AB	30.9 EF
FeS_2 + Impurities	Coal pyrite	-3.0 C	32 B	-0.5 GH	5 AB	-77.0 B	2434 C	19.6 D

* Arithmetic mean of three replications

** Mean values in the same column followed by the same letter are not significantly different ($p \leq 0.05$). ANOVA mean separation tests performed by Newman-Keuls tests of significance.

§ Geometric mean of three replications.

A variety of errors in the application of ABA to calculation of potential acidity are presented in the following results. When acid forming minerals containing sulfur are analyzed and reported present as a sulfur component considered to be nonacid generating, a false negative error occurs. A false negative error results in the underestimation of the potential acidity. A false positive error results when sulfur from a nonacid forming mineral is reported present as a sulfur component considered to be acid forming. Both false negative and false positive errors in ABA calculation are documented in the following results. The specific response of each mineral to the dissolution treatment, or treatments, which induced a prominent effect is discussed mineral by mineral.

- Barite ($BaSO_4$) - Barite is a tremendously insoluble sulfate mineral, which is minimally attacked by boiling H_2O and 2:3 HCl extractions (Table 15). Most of the barite was present as residual material after sequential extraction by boiling H_2O, 2:3 HCl and 1:7 HNO_3. The nitric acid extraction removed a mean 19.8% of the original 1.000 gram mass surviving the first two extractions, while 78.8% of the mass survived all three extractions. The Sobek Method predicts that sulfates will be removed by the HCl extraction, which does not occur in the case of barite, but no error to ABA is incurred. The Schafer Method counts the residual fraction as acid generating, which is inaccurate in the case of barite, since barite is not an acid forming mineral. Since the HNO_3 acid extractable sulfur fraction is consid-

ered acid generating by both Sobek and Schafer, the 19.8% mass removed by HNO_3 and considered acid generating is in error for both methods. Barite can be a common accessory mineral in both coal and hardrock mine environments, so ABA analysis lacking knowledge of the mineralogy may lead to remedial design errors when barite is present.

Anhydrite ($CaSO_4$) - Anhydrite is strongly removed by both boiling H_2O and 2:3 HCl extractions, which is in agreement with the predicted sulfate removal of both Sobek and Schafer methods (Table 15). The solubility of natural anhydrite is 0.1619 grams per 100 ml in hot water (Weast, 1977). In the extraction performed during this experiment (Schafer Method) boiling water was used as the extraction agent instead of hot water and a total volume of 150 ml was applied. Based on anhydrite solubility the calculated maximum potential mass loss per 150 ml is 24.3% while the experimentally observed value was 18.3%. The experimental results suggest that the solubility limit of the solution was approached during the boiling H_2O extraction. In the case of natural samples which do not have sufficient anhydrite present to approach the solubility limit of the extracting solution, the boiling water extraction is very effective at removal of anhydrite (Schafer Method).

The Sobek Method advocates a 2:3 HCl extraction to remove sulfates, which is successful at removal of anhydrite (Table 15). The 2:3 HCl extraction removed a mean 76.1% of the anhydrite sample mass surviving the boiling H_2O extraction, resulting in 1175 mg S^{-1}. Anhydrite is nonacid forming so no error to ABA is initiated by either Sobek (HCl extraction) or Schafer (H_2O extraction) methods. A small amount of sample was carried into the 1:7 HNO_3 extraction where a mean 5.8% of the original mass was taken into solution, but in a natural sample where only a percentage of the entire sample was anhydrite it is anticipated that no sulfur would be contributed to the nitric acid extractable fraction due to prior removal by either H_2O or HCl.

- Gypsum ($CaSO_4 \cdot 2H_2O$) - Gypsum was strongly removed by boiling H_2O and 2:3 HCl as predicted by the Sobek and Schafer Methods, resulting in no error to ABA calculation (Table 15). The dissolution of gypsum was similar to anhydrite, where little sample survived the H_2O and HCl extractions. The solubility of natural gypsum is 0.222 grams per 100 ml in hot water (Weast, 1976). Per 150 ml volume the predicted mass loss is 33.3% while the experimentally observed sample mass loss was 40.6%. The predicted versus experimental finding are not in perfect agreement, but it would appear that the extraction solution was saturated, if not supersaturated, with respect

to gypsum. To calculate the predicted leachate sulfur content generated by dissolution of gypsum, compared to the experimentally observed leachate sulfur, knowledge of the atomic proportion of sulfur is required.

Gypsum has an atomic weight of 172.14 grams/mole. Sulfur represents 18.6% of the atomic weight, or a 1.000 gram sample of gypsum contains 0.186 grams sulfur or 186 milligrams sulfur/gram gypsum. A 0.01 gram gypsum sample would contain 1.86 milligrams sulfur, or a 1% mass loss from an original 1.000 gram sample would equate to a 1.86 milligram sulfur gain in the leachate. Since the extraction solution was 150 ml in volume to convert to a milligram per liter basis a multiplication factor of 6.667 is required. It follows that a 1% sample mass loss during extraction results in a theoretical 12.4 mg l^{-1} sulfur content gain in the leachate. The mean mass loss attributed to the gypsum sample was 40.6%. When multiplied by the expected leachate sulfur content, 12.4 mg l^{-1} , the predicted leachate sulfur content is 504 mg l^{-1} sulfur. The mean experimentally observed leachate sulfur content is 488 mg l^{-1} sulfur, or a 3% relative percent difference between the predicted and observed values. The boiling H_2O extraction is very effective at removal of gypsum.

The 2:3 HCl extraction is also very effective at removal of gypsum, though no derivation of the predicted result is possible, since no published solubility of gypsum in 2:3 HCl was identified. The successful removal of gypsum by both H_2O and HCl will result in no error to ABA unless the solubility limit of the extracting solution is approached, which is unlikely in samples which only contain a few percent sulfur as gypsum.

- Anglesite ($PbSO_4$) - Anglesite is not an acid forming mineral and represents potential error to both Sobek and Schafer Methods of ABA calculation. Anglesite extraction by both 2:3 HCl and 1:7 HNO_3 resulted in mass loss, though a mean 16.7% of the original mass survived all three extractions (Table 15). The 2:3 HCl extraction removed a mean 44.4% of the mass surviving the H_2O extraction, resulting in 427 mg S l^{-1}. The error to the Schafer Method results from counting the HCl extractable sulfur attributed to anglesite as acid generating, which it is not. Since a mean 37.5% of the anglesite mass was removed during 1:7 HNO_3 extraction, the calculation of ABA by both Sobek and Schafer Methods can result in error, due to treatment of the HNO_3 extractable sulfur as acid forming when anglesite contributed to the sulfur component. The mean leachate sulfur content after HNO_3 extraction was 37 mg S l^{-1}, a small sulfur content compared to the 427 mg S l^{-1} resulting from 2:3

HCl extraction. The anomalously low HNO_3 extracted leachate sulfur is unexplained.

- Jarosite ($KFe_3(SO_4)_2(OH)_6$) - Jarosite was not effectively extracted by boiling H_2O, 2:3 HCl or 1:7 HNO_3, resulting in potential error to ABA calculation since a mean 72.2% of the original mineral mass survived all three extractions (Table 15). Jarosite is a common secondary mineral in many mine environments, resulting from incomplete oxidation of pyrite, and the Schafer Method considers it to be acid forming upon elevation of the mine waste pH. Under strongly oxidizing conditions jarosite was determined to be nonacid forming. The Schafer Method predicts that jarosite will be removed by the 2:3 HCl extraction, though only a mean 2.5% of the mass surviving the H_2O extraction was removed during 2:3 HCl extraction.

Many errors to ABA calculation are possible given the ineffectiveness of jarosite dissolution and extraction. The Sobek and Schafer Methods count the HNO_3 extractable sulfur fraction as acid forming in calculation of ABA. Assuming that jarosite is not an acid forming mineral, the mean 24.6% of the sample mass removed by HNO_3 and counted as acid generating is in error. In addition, if it is assumed that jarosite will not be thermodynamically stable upon elevation of pH, and will yield acid, the liming rate required to neutralize the

potential acidity attributed to jarosite would be in error. That is, the lime rate used for calculation of ABA for HNO_3 extractable sulfur is 31.25 tons $CaCO_3$ per 1000 tons waste material (Sobek and Schafer Methods), while the lime rate for neutralization of the potential acidity due to jarosite is 23.44 tons $CaCO_3$ per 1000 tons waste material (Schafer Method).

Since most the jarosite was retained in the residual sulfur fraction and not extracted by ABA methods, the greatest potential error to ABA calculation could result from inaccurate treatment of the residual sulfur fraction. The Schafer Method considers the residual sulfur fraction as acid forming while Sobek does not.

- Arsenopyrite (FeAsS) - Arsenopyrite is an acid forming mineral which is dominantly removed by the 1:7 HNO_3 extraction. A mean 69.2% of the original sample mass was removed by the 1:7 HNO_3 extraction, while 29.3% of the original mass survived all three extractions (Table 15). Since both Sobek and Schafer Methods count the 1:7 HNO_3 extractable fraction as acid producing, no specific error to ABA is initiated, though the stoichiometry of arsenopyrite dissolution and resulting acid generation is unknown. The 31.25 tons $CaCO_3$ per 1000 tons waste material applied per 1% sulfur as pyrite may or may not be adequate to neutralize acidity due to arsenopyrite. The mean 29.3% of the sample retained in the residual sulfur

fraction represents a potential error to the Sobek ABA calculation method because arsenopyrite is an acid forming mineral, yet the Sobek Method counts the residual sulfur fraction as not acid forming.

- Ward's pyrite (FeS_2) - Pyrite is an acid forming mineral, which was dominantly removed by 1:7 HNO_3, as it was anticipated to be removed by the Sobek and Schafer Methods. A mean 83.9% of the pyrite sample mass was extracted by 1:7 HNO_3 (Table 15). Though the HNO_3 extraction is effective at removal of pyrite, a mean 16.1% of the pyrite survived all three extractions and was residual even though HNO_3 was present in excess of the amount of pyrite present, so complete mineral dissolution was theoretically possible. The presence of pyrite in the residual sulfur fraction is not anticipated by ABA analysis and represents a potential error to the Sobek Method of ABA calculation which counts the residual sulfur fraction as nonacid forming.
- Chalcocite (Cu_2S) - Chalcocite was strongly removed by the 1:7 HNO_3 extraction, though chalcocite is not an acid generating mineral. A mean 79.9% of the chalcocite sample mass was removed during the 1:7 HNO_3 extraction though only 23 mg S l^{-1} were measured in the leachate (Table 15). The leachate resulting from 1:7 HNO_3 extraction was notably blue after extraction so the mass loss

data may reflect selective removal of copper while the sulfur is carried forward to the residual fraction. Characterization of the elemental composition of the residual sample material is presented in Section 6.4, indicating that the residual sample material is nearly pure sulfur containing no copper.

The error to ABA resulting from chalcocite dissolution is that sulfur extracted during the 1:7 HNO_3 extraction is considered acid forming by both Sobek and Schafer Methods, though chalcocite is not an acid generating mineral. Further error is introduced by the Schafer Method, since the residual sulfur fraction is considered acid forming, and most of the sulfur resulting from mineral dissolution in the HNO_3 extraction was carried forward to the residual sulfur fraction as pure sulfur, not as the mineral chalcocite.

- Ward's pyrrhotite ($Fe_{1-x}S$) - Pyrrhotite is an acid producing mineral which was dominantly removed by the 2:3 HCl extraction, resulting in liberation of H_2S gas. A mean 80.2% of the sample mass was removed during sample extraction by 2:3 HCl, though only 114 mg S l^{-1} were measured in leachate (Table 15). The smell of H_2S gas was very evident upon treatment of pyrrhotite with HCl.

  The error to ABA calculations are unique to the method of ABA calculation. The Sobek Method considers sulfur forms extracted by 2:3 HCl as nonacid forming, which is in error when pyrrhotite is

present. The error to ABA when pyrrhotite is present may also be repeated when iron monosulfide minerals other than pyrrhotite are present which may be acid forming and HCl soluble (Ribbe 1975, Raiswell 1982). Iron monosulfide minerals such as greigite (Fe_3S_4) and mackinawite ($Fe_{1+x}S$) have been observed in reduced depositional sedimentary environments (Dell 1972). The Schafer Method error to ABA results from counting sulfur extracted during the HCl extraction as jarosite upon calculation of potential acidity, when the neutralization of acid generated by pyrrhotite oxidation is likely 31.25 tons $CaCO_3$ per 1000 tons waste material, and not 23.44 tons $CaCO_3$ per 1000 tons waste material as required for jarosite neutralization.

- Chalcopyrite ($CuFeS_2$) - Chalcopyrite was not effectively removed by any of the three ABA extractions, subsequently most of the sample was retained in the residual sulfur fraction. A mean 73.0% of the original sample mass survived all extractions and was counted as residual sulfur (Table 15). Since chalcopyrite is an acid forming mineral, an error in ABA calculation is induced by the Sobek Method of ABA calculation since the residual sulfur fraction is considered as nonacid generating. The Schafer Method of ABA calculation is not in error when counting the residual sulfur fraction as acid generating in the presence of the mineral chalcopyrite. The mean 27.1%

sample mass removed during the 1:7 HNO_3 extraction step is considered acid generating by both Sobek and Schafer Methods, resulting in no ABA error.

The difficulty in managing sulfur forms in ABA calculation for any mineral is illustrated by chalcopyrite. When the entirety of a mineral sample is not removed during a single extraction, skepticism will exist whether field remediation lime rates based on ABA are accurate or reasonable. Chalcopyrite was only partially extracted by 1:7 HNO_3 during treatment, resulting in sulfur from a single mineral being erroneously considered present in two different sulfur fractions. In the case of chalcopyrite, when the Sobek Method was used to calculate the ABA, significant error would be induced when 27.1% of the sulfur was counted as acid generating and 73.0% of the sulfur was counted as nonacid forming while 100% of the sulfur would be acid forming.

- Galena (PbS) - Galena is not an acid generating mineral and represents a complication to ABA calculation since a significant portion of the mineral was extracted by HCl and HNO_3, and a significant portion of the sample was residual (Table 15). A mean 32.3% of the galena sample was removed by the 2:3 HCl extraction resulting in 424 mg S l^{-1}. No error to ABA calculation is induced by the Sobek Method since the HCl extractable sulfur is counted as

nonacid forming. The Schafer Method of ABA calculation results in error when sulfur due to galena is extracted by 2:3 HCl since the Schafer Method counts the HCl extractable sulfur fraction as acid generating and galena is not acid generating.

Error to ABA calculation result for both Sobek and Schafer Methods when sulfur due to galena is extracted by 1:7 HNO_3 since both methods treat the nitric acid extractable sulfur fraction as acid forming. A mean 35.9% of the sample mass was removed during treatment with 1:7 HNO_3, though only a mean leachate 0.7 mg $S \cdot l^{-1}$ resulted. Some sulfur may have been lost to a gaseous phase when treated with HNO_3 since the leachate sulfur content was low, or sulfur may have been carried partially into the residual fraction while lead was selectively removed by the 1:7 HNO_3 treatment. The residual sulfur fraction contained a mean 31.4% of the original 1.000 gram sample which survived all three extractions. The Sobek Method of ABA calculation would not be in error in the case of galena since galena is nonacid generating and treated as such by the calculation. The Schafer Method of ABA calculation can result in potential error when galena is present since the residual sulfur fraction is treated as acid generating.

- Marcasite (FeS_2) - The removal of marcasite proceeded as expected by both the Sobek and Schafer Method of ABA calculation. A

mean 90.4% of the marcasite sample was removed by the 1:7 HNO_3 extraction resulting in a mean 2752 mg S l^{-1}. Marcasite is an acid forming mineral and was extracted by the HNO_3 extraction as expected, resulting in no error to ABA calculation.

- Sphalerite ((Zn, Fe)S) - The removal of sphalerite by ABA extractions was ineffective, resulting in a mean 84.4% of the original sample surviving all three extractions. Sphalerite is an acid generating mineral so treatment of the residual fraction as nonacid forming (Sobek Method) is in error when sphalerite is present in a sample.
- Coal barite ($BaSO_4$) - The Coal barite sample was not effectively removed by any ABA extraction, consequently most of the sample was residual. A mean 69.3% of the sample was retained as residual material (Table 15). The Coal barite is significantly different ($p \leq 0.05$) from the Barite sample which had a measured mean residual mass of 78.8%. The difference between the pure barite sample (Barite) and natural environment barite sample (Coal barite) is the purity of the sample. The Coal barite contained some pyrite which was extracted by the 1:7 HNO_3 extraction, though the sample was dominantly barite. Error to ABA calculation could be introduced by the Schafer Method of ABA calculation, since the residual fraction is dominantly barite, which is not acid generating, though the residual sulfur fraction is treated as acid forming.

The Coal barite sample demonstrates the field error in ABA calculation resulting from laboratory analysis, since the sample was obtained from an operational mine. Upon request for sample material the mine provided a coal overburden sample near the coal crop line which had a negative ABA. The state regulatory agency had expressed concern that the negative ABA would result in acid generation problems, while the mine staff had no indication that pyrite oxidation was occurring. Upon removal of sulfur containing minerals from the waste material during sample processing, the dominant sulfur mineral in the sample was determined to be barite, which is not acid generating. Error in the prediction of potential acidity by ABA methods in mine environments containing sulfur bearing minerals other than pyrite or marcasite may result in significant error in remedial design.

- Hardrock pyrite (FeS_2 + impurities) - The Hardrock pyrite sample is acid forming and most of the sulfur was extracted by the 1:7 HNO_3 extraction in accordance with ABA calculation. A mean 68.0% of the original sample was extracted by the HNO_3 extraction, which is significantly different ($p \leq 0.05$) than the other two pyrite samples, Ward's pyrite and Coal pyrite, which were more aggressively removed by HNO_3 extraction. The Hardrock pyrite sample (Copper Mine Tailings) was the least reactive sample to oxidation by

10% H_2O_2, so ineffective HNO_3 extraction compared to other FeS_2 samples may be a function of reaction kinetics demonstrated during H_2O_2 weathering.

Since a mean 28.8% of the Hardrock pyrite sample survived all ABA extractions, potential error to ABA calculation is possible depending on treatment of the residual sulfur fraction. The Sobek Method treats the residual fraction as nonacid sulfur forms, which is in error when the residual sulfur fraction contains pyrite as it does in the case of Hardrock pyrite. Since pyrite is the most common sulfide mineral, the ineffectiveness of pyrite extraction by 1:7 HNO_3 may be commonly observed in laboratory analysis of ABA, resulting in a residual sulfur component when none is expected. If the residual sulfur component is characterized as nonacid forming organic sulfur compounds when ABA is applied to samples derived from hardrock mine environments, skepticism pertaining to the validity of the analysis will occur since organic sulfur compounds are relatively uncommon in hardrock mines. The characterization of the residual sulfur fraction as acid generating (Schafer Method) is not in error in the case of the Hardrock pyrite sample.

- Hardrock pyrrhotite ($Fe_{1-x}S$ + impurities) - The Hardrock pyrrhotite sample is acid generating and was primarily removed by the 2:3 HCl extraction. A mean 52.1% of the sample was extracted by the HCl

extraction (Table 15) resulting in liberation of H_2S gas. The sample mass loss of the Hardrock pyrrhotite is significantly different ($p \leq 0.05$) from the Ward's pyrrhotite sample, though the presence of silicate impurities in the Hardrock pyrrhotite contributed to the difference. The mean residual sulfur fraction attributed to the Hardrock pyrite (30.9%) contained silicates identified by SEM/-EDAX.

- Coal pyrite (FeS_2 + impurities) - The Coal pyrite sample was dominantly extracted by the 1:7 HNO_3 treatment, resulting in removal of a mean 77.0% of the original mass (Table 15). The mass removed from the Coal pyrite sample is not significantly different ($p \leq 0.05$) from the Ward's pyrite sample. The mean leachate sulfur content attributed to the Coal pyrite (2434 mg S l^{-1}) is not significantly different ($p \leq 0.05$) from the mean leachate sulfur of the Ward's pyrite (2711 mg S l^{-1}). The calculation of ABA is not notably in error for sulfur extracted by HNO_3, though not all of the sample was extracted by HNO_3.

The Coal pyrite sample which survived all three sample extractions (19.6%) is potentially in error to ABA calculation. Calculation of ABA by the Sobek Method, which considers the residual sulfur fraction as nonacid forming, would result in error.

The Coal pyrite sample also presents potential error to ABA calculation in treatment of the H_2O extractable sulfur fraction (Schafer Method). The sulfur extracted by boiling water is considered non-acid generating, though a mean 3.0% of the Coal pyrite sample was removed by the H_2O extraction. The Coal pyrite sample was submitted to oxidation by deionized water resulting in rapid formation of white salt crusts upon drying which were readily solubilized upon addition of water. The leachate chemistry of the deionized water also quickly changed to acid upon dissolution of the hydrated iron sulfate salts. Leachate acidity is attributed to the presence of iron-sulfate crusts present on the mineral surface as an impurity, which were soluble in hot water. Numerous iron sulfates are known in mine environments including melanterite ($FeSO_4 \cdot 7H_2O$), rozenite ($FeSO_4 \cdot 4H_2O$), and szomolnokite ($FeSO_4 \cdot H_2O$) (Nordstrom 1982), which may demonstrate solubility in water though samples of these materials were not obtained for use in this experiment. The rapid dissolution of hydrated iron sulfate minerals may result in mine environment acidity undetected by ABA analytical methods.

SEM/EDAX Analysis Of Initial And Residual Sample Material

The impact of ABA extraction on mineral chemistry was examined by scanning electron microscopy (SEM) and energy dispersive analysis of x-rays

(EDAX) to assess changes in chemistry during extraction. Samples were prepared to compare mineral elemental concentration before and after ABA extraction. Results of material analysis by SEM/EDAX are presented in Figures 28 through 32 and indicate that some samples were unchanged during ABA extraction while others were chemically altered.

The samples which were unchanged during ABA extraction displayed EDAX spectra after extraction which were nearly identical to the EDAX spectra prior to treatment. The samples barite, jarosite, Ward's pyrite, chalcopyrite, galena, coal barite, and hardrock pyrite were unchanged during ABA extraction. The relative intensity of the EDAX elemental peaks remained in approximately the same ratio.

The samples anglesite, arsenopyrite, chalcocite, Ward's pyrrhotite, marcasite, sphalerite, hardrock pyrrhotite and coal pyrite, changed notably between the before and after extraction EDAX analysis composition. The changes in chemistry are attributed to chemical reactions initiated by the extraction agents, but are not known in specific. Of the sample group chemically altered during the extraction sequence two common scenarios are presented by the EDAX output.

The first chemical alteration scenario is illustrated by anglesite (Figure 29). The lead and sulfur peaks in the initial sample are the dominant peaks in the EDAX spectra. After the extraction sequence the lead and sulfur peaks are still evident, but they are lesser peaks. The post extraction EDAX spectra for angle

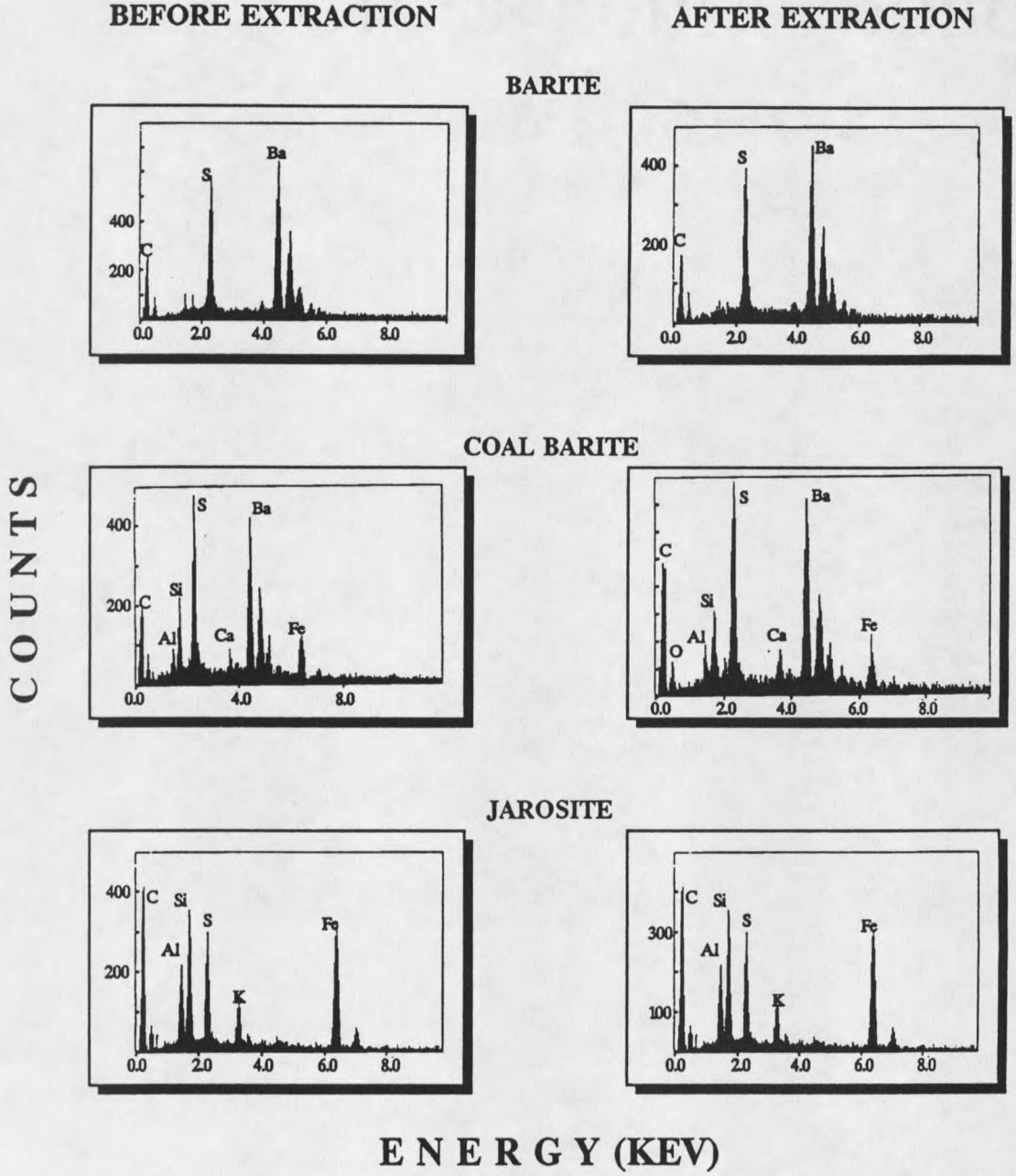

Figure 28. Elemental composition of mineral samples before (left column) and after (right column) ABA extractions as determined by energy dispersive analysis of x-rays (EDAX) for the barite, coal barite, and jarosite samples.

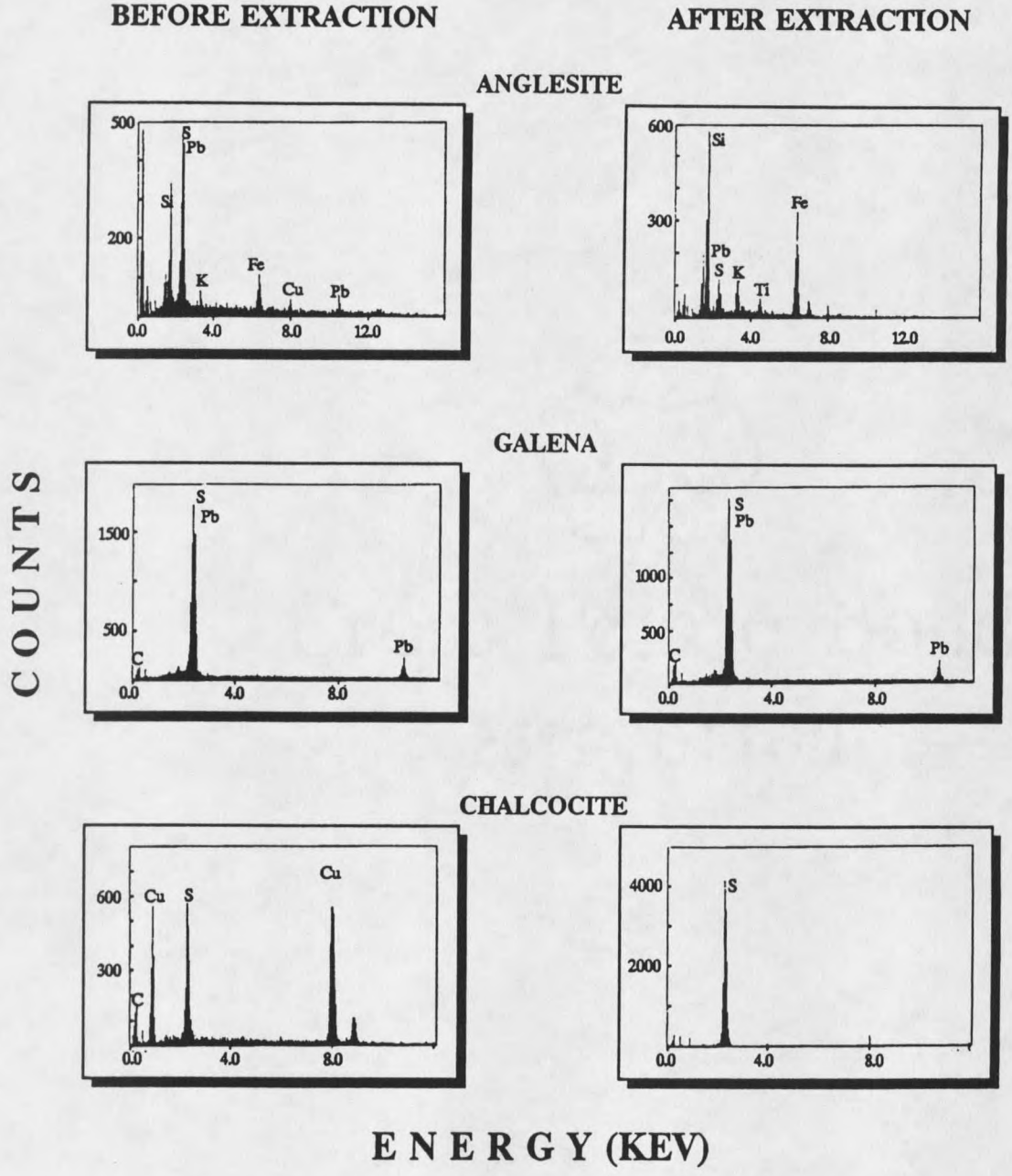

Figure 29. Elemental composition of mineral samples before (left column) and after (right column) ABA extractions as determined by energy dispersive analysis of x-rays (EDAX) for the anglesite, galena, and chalcocite samples.

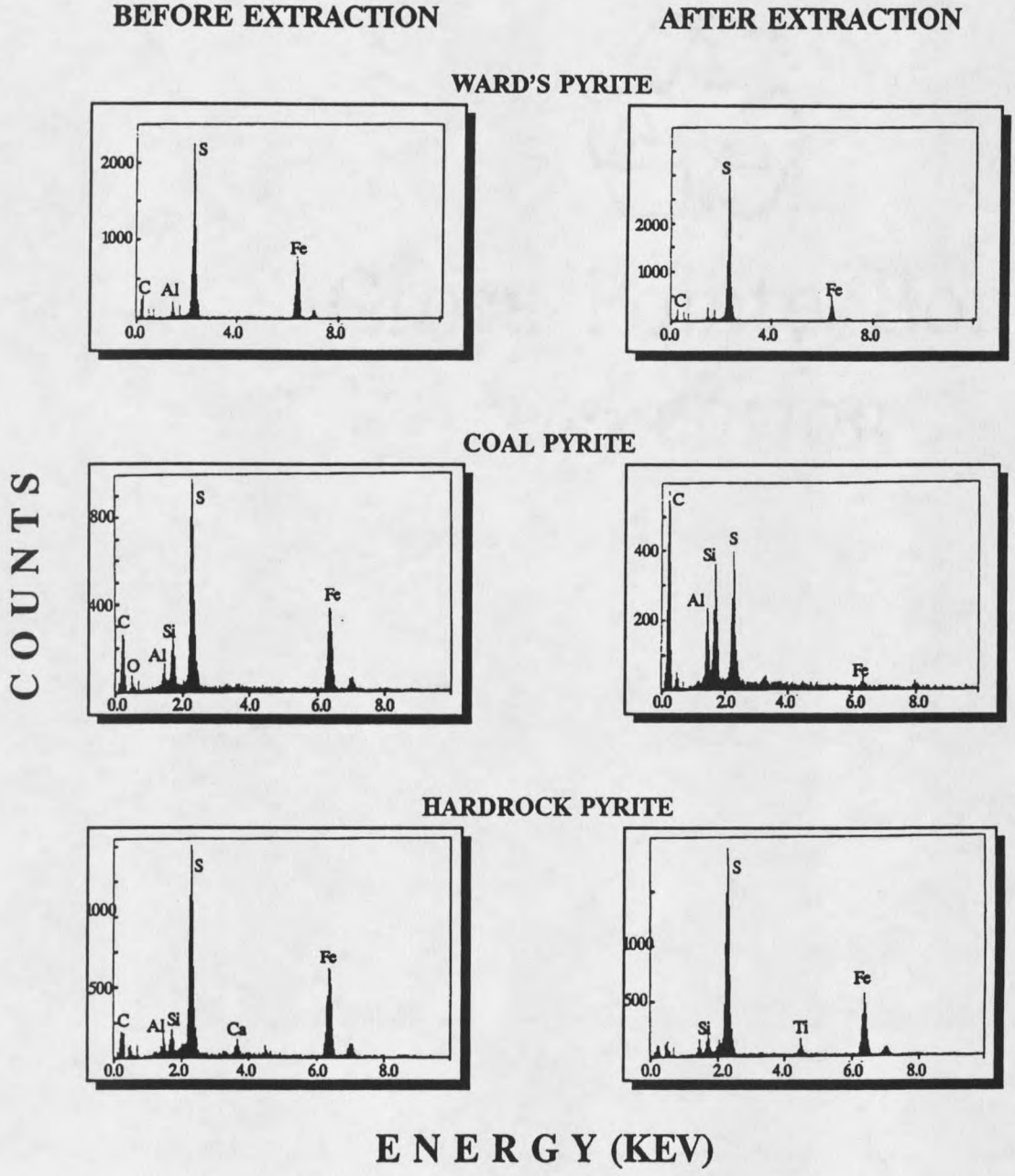

Figure 30. Elemental composition of mineral samples before (left column) and after (right column) ABA extractions as determined by energy dispersive analysis of x-rays (EDAX) for the Ward's pyrite, coal pyrite, and hardrock pyrite samples.

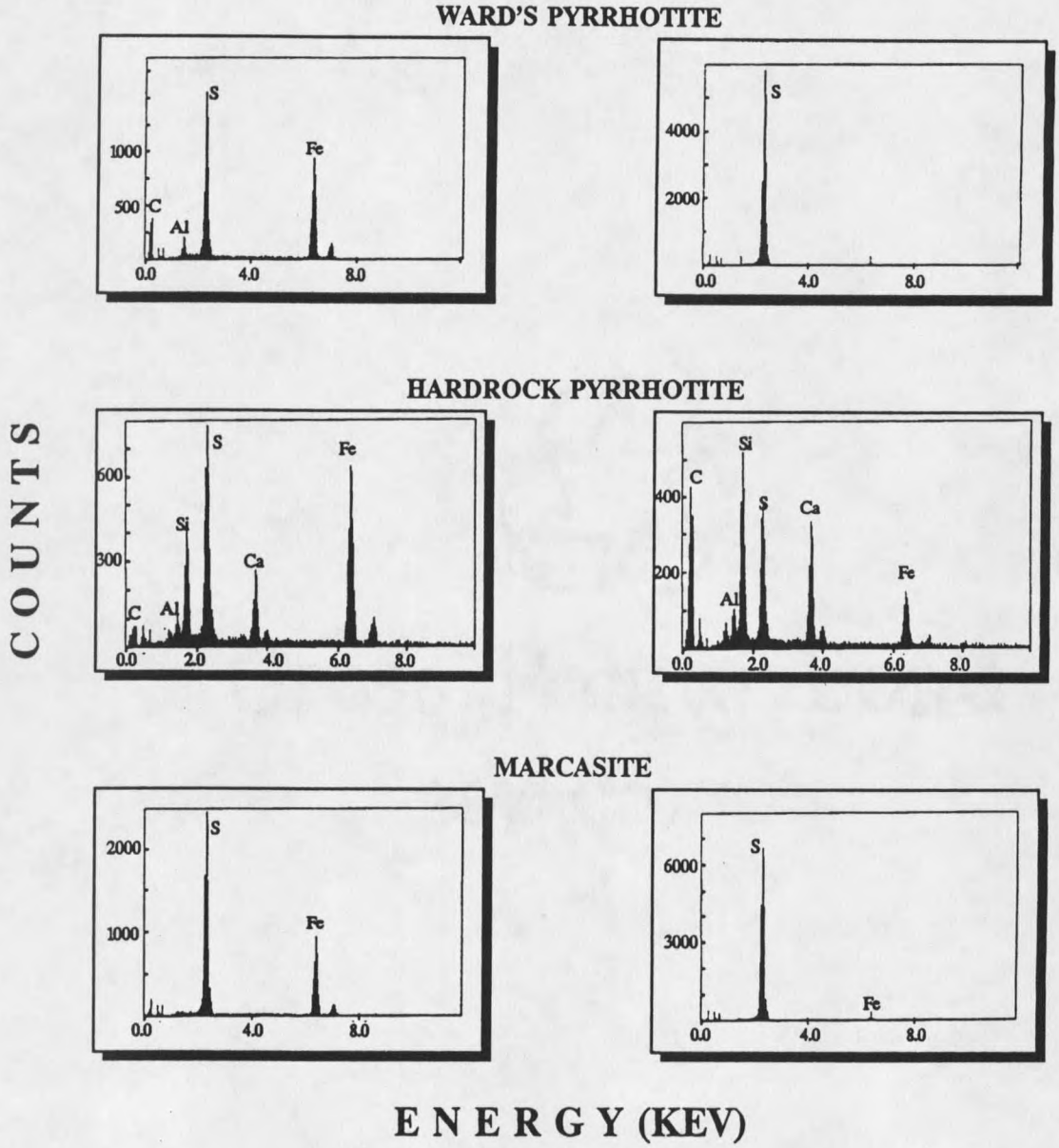

Figure 31. Elemental composition of mineral samples before (left column) and after (right column) ABA extractions as determined by energy dispersive analysis of x-rays (EDAX) for the Ward's pyrrhotite, hardrock pyrrhotite, and marcasite samples.

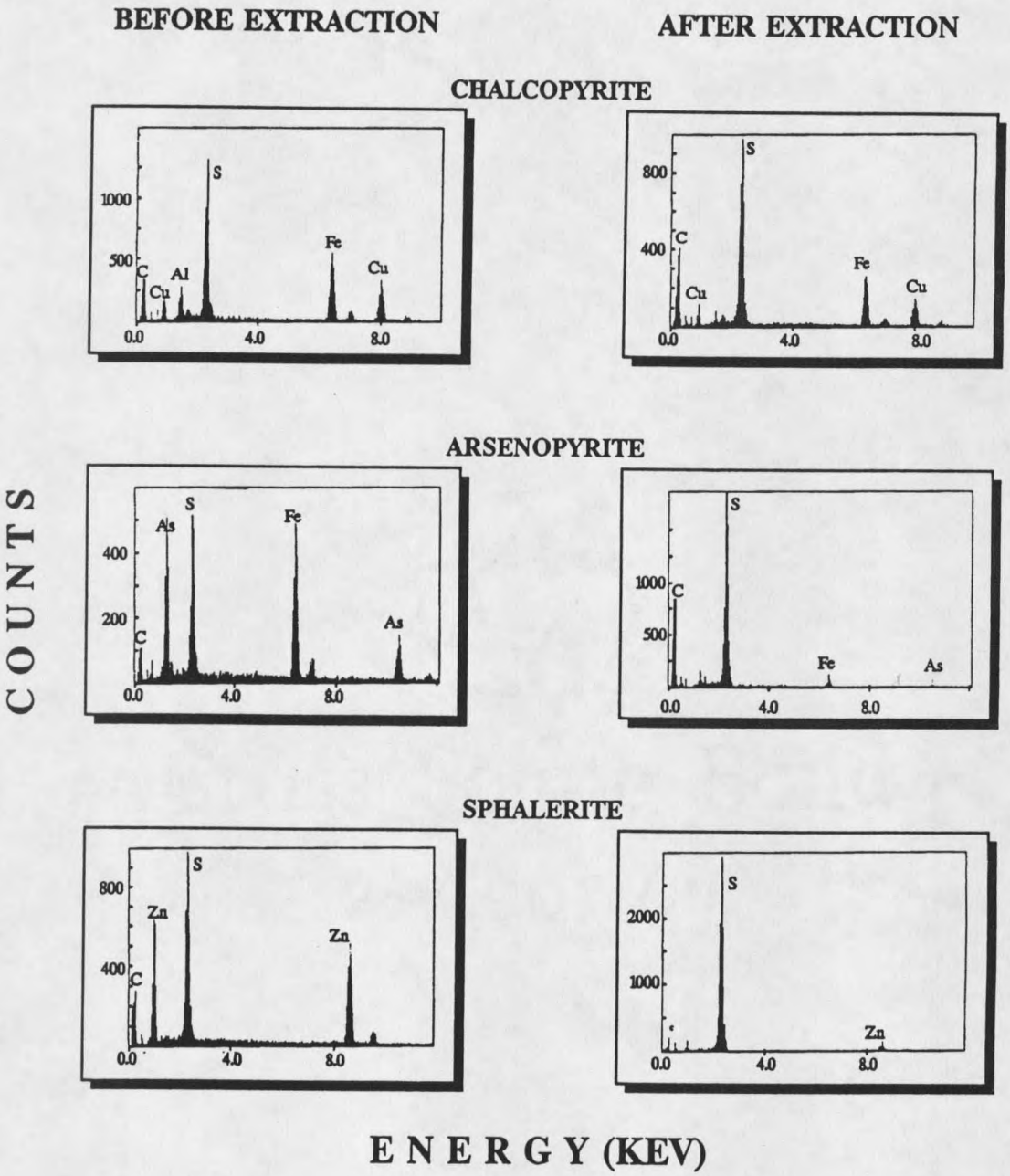

Figure 32. Elemental composition of mineral samples before (left column) and after (right column) ABA extractions as determined by energy dispersive analysis of x-rays (EDAX) for the chalcopyrite, arsenopyrite, and sphalerite samples.

site is dominated by silica and iron, indicating selective removal of lead and sulfur at some point during the extraction. This scenario is also presented by the samples hardrock pyrrhotite (Figure 31) and coal pyrite (Figure 30).

The second chemical alteration scenario is illustrated by the marcasite sample (Figure 31). After the sequential extraction sequence, the EDAX spectra indicates that effectively all of the iron has been removed by the extractions and only sulfur remains. This EDAX evidence is also supported by visual observation of the residual material after extraction which in some cases was a fine yellow powder lacking crystalline structure (i.e. sulfur). Other EDAX spectra characteristic of this scenario include arsenopyrite (Figure 32), chalcocite (Figure 29), Ward's pyrrhotite (Figure 31), and sphalerite (Figure 32). The alteration of the original mineral sample results in the removal of metals by the acid extractions while sulfur is carried into the residual sulfur fraction.

Significant error to ABA calculation is possible when sulfur is carried into the residual sulfur fraction from minerals which are acid generating. In the case of marcasite, a mean 90.4% of the mineral mass was removed by the 1:7 HNO_3 and 9.2% of the mineral mass is carried into the residual fraction (Table 15). Since marcasite is an acid generating mineral, error to ABA is incurred by the Sobek Method of ABA calculation when the residual sulfur fraction is treated as nonacid forming. The error to ABA is further accentuated by the atomic weight differential between iron and sulfur. Since iron is more dense than sulfur and is removed during HNO_3 extraction, the mean 9.2% residual mass of marcasite in

the residual sulfur fraction is entirely attributed to sulfur and not to iron and sulfur. Therefore, the stoichiometric fraction of sulfur from marcasite represented by the 9.2% residual sulfur is greater than if the residual sulfur fraction had been comprised of both iron and sulfur.

Discussion

The ability of acid-base account analytical methods to distinguish acid producing from nonacid producing sulfur forms is very deficient. Potential acidity is calculated differently between the Schafer and Sobek Methods, but errors eminating from both methods were revealed when extraction of both acid and nonacid generating minerals resulted from the same extraction technique.

The general intent of both the Schafer and Sobek Method is to extract nonacid producing minerals which contain sulfur in one step and extract the acid producing sulfur forms in a subsequent step or steps. Management of the residual sulfur fraction is a consequence of incomplete extraction of sulfur forms in a sample. The residual sulfur component is considered nonacid forming by the Sobek Method since it is commonly applied to the analysis of samples derived from coal deposits where organic sulfur compounds are present. The Schafer Method was developed to assess potential acidity in materials contaminated by hardrock mining activities, consequently the residual sulfur fraction was considered acid forming. Neither method (Sobek or Schafer) was entirely accurate or entirely

inaccurate, but results from ABA analysis without supporting characterization of the associated mineralogy invite error.

Potential errors exist in ABA calculation for each extraction, hot water, 2:3 HCl and 1:7 HNO_3, depending on the mineral assemblages present in each sample. The degree to which the errors impact site remediation planning are a consequence of the quantity of the minerals present and chemistry of the minerals present. The effectiveness of ABA calculations will depend on which minerals are extracted from a sample.

Since the laboratory method for ABA calculation does not detail a sequential extraction as was performed in this investigation, the specific error in ABA is only implied by this research finding, though the experimental method is very similar to the Sobek and Schafer Methods (Figure 27). When ABA is performed by either the Schafer or Sobek Methods, sulfur is determined by combustion of the mineral sample before and after extraction, with the residual component determined by difference (Figure 27). No identification of the minerals contributing to the sulfur component is performed.

The hot water extraction step is effective in removing gypsum and anhydrite, provided the extraction solution is present in excess so that the extraction solution does not become saturated with respect to the minerals. The hot water extraction may also remove iron-sulfate minerals, which may be present as oxidized coatings on sulfide minerals, and may contribute to acid generation upon dissolution.

The HCl extraction step does not effectively accomplish the removal of jarosite, though anhydrite, gypsum, pyrrhotite and lead sulfide and lead sulfate compounds are removed by HCl.

The nitric acid extraction step is very effective at removing mass from many minerals, both acid producing and nonacid producing sulfur compounds. Since the nitric acid sulfur forms are frequently considered the primary acid producers, significant error could be introduced by extraction of sulfur from minerals which will not produce acid upon exposure to the atmosphere. For example, a sample containing chalcocite, gypsum, and galena might be considered a strong acid producer based on HNO_3 extractable sulfur results though no acid would ever be generated. Error to the Sobek Method of ABA calculation could also be introduced during the nitric acid extraction step if the mineral marcasite is present and upon dissolution of the mineral if the sulfur is not removed from the sample, but remains as native sulfur and is carried into the residual fraction which is in some cases considered nonacid forming.

The residual sulfur fraction is also the source of potential error for calculation of ABA. When sphalerite and chalcopyrite are present in a sample submitted to analysis by ABA, potential error to ABA calculation by the Sobek Method exists since both minerals are present dominantly in the residual sulfur fraction and both are acid forming, yet not treated as such by the Sobek Method of ABA calculation. Conversely, when barite is present in a sample and analyzed by ABA, most of the mineral will be retained in the residual sulfur fraction. If the Schafer

Method of ABA calculation is used, the sulfur attributable to barite is counted erroneously as acid generating.

The overall result of this investigation is that sulfur fractions identified by ABA analysis do not correctly identify acid producing from nonacid producing sulfur forms, resulting in remedial planning error. Two fundamental errors can result from interpretation of laboratory analytical results. A false positive error is created when sulfur is present in a sample as minerals which are extracted by nitric acid and considered acid forming, yet will not yield acid upon weathering (i.e. chalcocite). Application of neutralizing minerals in the case of a false positive error would be in excess of the actual neutralization requirement. A false negative error is created by considering the hydrochloric acid extractable sulfur as nonacid producing (i.e. Sobek Method) when pyrrhotite or other iron-monosulfides are present which will generate acid upon weathering. A second false negative error is created when the residual sulfur fraction is considered not acid producing (Sobek Method) when it contains acid generating minerals (i.e. chalcopyrite). The false negative errors lead to the underestimation of lime requirement and potentially ineffective neutralization of acidity. Either false negative or false positive errors may lead to ineffective, costly, or disastrous reclamation success depending on the geochemical distribution of sulfur forms present.

The successful application of ABA calculations to the remediation of lands containing sulfur compounds, and especially reduced sulfur compounds, will require knowledge of the specific mineralogy. To consider the nitric acid extract-

able fraction as the only potential acid producing sulfur forms would be an oversimplification of the potentially complex relationship of dissimilar mineral assemblages.

EFFECT OF PYRITE STOICHIOMETRIC VARIATION ON WEATHERABILITY OF ACID PRODUCING MINE WASTES

Impacts Of Pyrite Physical Property Variation On Acid Generation Processes

Pyrite is a common mineral in many geological settings including both sedimentary and igneous environments. Though pyrite is common, appreciable variation in the physical properties of pyrite occur between different geological environments. Physical property variation can include stoichiometry, density, electrical conductivity, crystal form, impurity content, anisotropy, defect density, semiconducting type and presence of fluid or solid inclusions.

In the remediation of land disturbed by mining, the reaction of pyrite with oxygen and water generates acidic conditions (Equation 31).

$$FeS_{2.00} + 3.75\,O_2 + 3.5\,H_2O = Fe(OH)_3 + 2SO_4^{-2} + 4H^+ \qquad [31]$$

In the absence of neutralizing minerals the oxidation of pyrite and generation of acidity can result in negative impacts to water and vegetative resources. The negative impact of pyrite oxidation is variable between mine sites, potentially due to differences in the rate of oxidation of pyrite. The rate of pyrite oxidation has been measured in a laboratory setting, and substantial variation exists. Variance in the rate of oxidation is not easily attributed to any one set of physical properties, but pyrite stoichiometric variation may be directly related to the rate of oxidation.

Stoichiometric variation in crystalline pyrite may occur due to the presence of elements other than iron and sulfur substituting into the crystalline lattice, or by crystalline defect where atomic vacancy in the lattice occurs. The nonstoichiometry of pyrite has been demonstrated (Smith 1942, Rakcheyev 1968, Shuey 1975) to be in the range of $FeS_{1.91}$ to $FeS_{2.11}$, though typically sulfur deficiency is observed. Disagreement exists on whether the observed nonstoichiometry is a consequence of inaccurate analytical technique, or in fact a true observation of crystalline nonhomogeneity.

Pyrite nonstoichiometry may be an important variable in characterization of the weatherability of pyrite from different sources. Massive morphology pyrite, typically formed at low temperature, demonstrates reactivity significantly greater than euhedral pyrite, typically formed at high temperature. Rakcheyev (1968) found that the activation energy measured in the low temperature, and stoichiometrically sulfur deficient, pyrite specimens was lower than the activation energy of the pyrite formed at high temperature. The difference in activation energy, and ease of oxidation of the low temperature pyrites, may be a consequence of the nonstoichiometry.

Deviation in pyrite stoichiometry, in addition to potential influences on the rate of oxidation, may result in inaccurate lime application rates. According to Equation 31, 1 mole $FeS_{2.00}$ when oxidized yields 4 moles H^+ and is neutralized by 2 moles $CaCO_3$. Upgrading this relationship to field scale, 31.25 tons $CaCO_3$ per 1000 tons waste material per 1 % sulfur as pyrite is required to neutralize the

acidity generated. If pyrite is present in a mine waste material that will be submitted to oxidizing conditions that is not stoichiometric, the field lime rate may need adjustment to compensate for nonstoichiometry.

Methods

Seven pyrite samples were selected for analysis of pyrite stoichiometry. The samples, or treatments, are identified as Texas Coal Overburden, Montana Subbituminous Coal, Montana Gold Mine Tailings, Coal Cleaning Waste I, Copper Mine Tailings and Colorado Pyrite. High-graded pyrite was prepared by separation of pyrite from silicates by water supplied shaker table. Upon high-grading, samples were crushed by mortar and pestle to minus 60 mesh (<250 μm). The presence and elemental composition of impurity in the high-graded samples was determined by scanning electron microscopy (SEM) and energy dispersive analysis of x-rays (EDAX).

The high graded samples were subsequently submitted to a two hour rinse with 6 M HCl to remove sulfates from the surfaces of the pyrite particles. Sample material was added to the 6 M HCl rinsing agent in the proportion of 5 grams sample to 100 ml acid. Agitation was provided during the 6 M HCl rinse with a stir bar mixer. Upon completion of two hours of contact between the 6 M HCl and sample, the HCl was filtered from the sample and 300 ml deionized water passed through the sample to remove residual acid. The samples were air dried and stored in a pure nitrogen atmosphere until analysis.

Measurement of Iron and Sulfur By Mineral Destructive Analysis

Laboratory analysis of iron and sulfur was performed on the high-graded samples to determine the percentage of iron and sulfur in each mineral. Three subsamples of each pyrite material (only two for Colorado Pyrite source), and three samples of high purity (99.99+%) ferrous sulfide (FeS) were analyzed for total iron and total sulfur concentrations. Pyrite samples and FeS standards were digested in HNO_3 and H_2O_2 (Method 3050, EPA 1986) and Fe levels were quantified using atomic absorption spectroscopy. Sulfur levels were determined by infrared detection of SO_2 resulting from controlled combustion of each sample. Calibration of each instrument was performed using independent, laboratory supplied FeS standards. Verification of calibration was performed at a 10% frequency during the analytical run using prepared elemental Fe and elemental S standards. Two of the twenty samples were analyzed in duplicate by the laboratory. Results were reported as percent Fe and S.

Accuracy of the quantitative determination of Fe and S was assessed by calculating mean recoveries of Fe and S for the three submitted FeS standards.

Analysis of Iron and Sulfur By Electron Microprobe

The Montana Gold Mine Tailings and Coal Cleaning Waste I samples were selected for quantitative analysis of Fe and S by electron microprobe. Pyrite grains were randomly selected from the mineral samples and cast in an epoxy mold. The epoxy mount was sanded and polished to obtain fresh mineral surfaces. The sample mount was placed in the instrument and backscatter electron

imaging performed to detect compositional zoning if present. A representative location on the mineral grain was identified and subjected to analysis by electron beam. The elemental analysis of the mineral surface was performed in different locations on the individual mineral grain in an area a few micrometers in diameter ($<10\ \mu m^2$). The microprobe analysis was calibrated by collection of counts from a pyrite standard of known chemical composition. The chemical composition of the unknown sample was made by comparison of the count rate of the unknown sample to the standard. All analyses are within 2% relative error.

Pyrite Stoichiometry Determination By Mineral Destructive Analysis

The digestion of pyrite samples for analysis of iron and combustion of pyrite samples for analysis of sulfur yielded the analytical results presented in Table 16. Since the mineral samples were consumed by the analytical methods, the results are considered as a bulk characteristic of the solid mineral, and not a surface coating analysis. Analytical results are presented as the percentage of iron, sulfur, copper and other constituents present as impurities. The elemental composition of the impurities present was identified by EDAX. Most of the impurities are aluminum or silica, though one of the samples had 0.1% copper.

The ratio of iron to sulfur, based on the analytical results presented in Table 16, is presented in Table 17. Results are presented as FeS_x where x is the value in the table, indicating the pyrite stoichiometry based on chemical analysis. Empirical formulae were calculated from the reported percentage composition

Table 16. Measured values of iron, sulfur, and copper in pyrite from different mine environments.

Mine Environment	Replication	Percent				Other Constituents Identified By EDAX*
		Iron	Sulfur	Copper	Other Constituents	
Texas Coal Overburden	1	44.9	50.5	+	4.6	
	2	46.8	52.0	+	1.2	
	3	45.0	52.5	+	2.5	
Coal Cleaning Waste I	1	36.7	40.2	+	23.1	Si, Al
	2	36.4	40.4	+	23.2	Si, Al
	3	36.4	40.7	+	22.9	Si, Al
Montana Gold Mine Tailings	1	46.6	52.0	+	1.4	Si
	2	45.0	50.5	+	4.5	Si
	3	45.6	50.5	+	3.9	Si
Montana Subbituminous Coal	1	43.1	48.5	+	8.4	Si
	2	43.9	48.0	+	8.1	Si
	3	43.8	47.1	+	9.1	Si
Copper Mine Waste Tailings	1	42.3	48.2	0.1	9.5	Cu
	2	40.1	46.5	0.1	13.4	Cu
	3	43.0	50.5	0.1	6.5	Cu
Colorado Pyrite	1	46.7	53.0	+	0.3	
	2	49.1	51.5	+	0.6	
	**	**	**	**	**	

\+ Not determined.
* Energy dispersive analysis of x-rays.
** Not sufficient sample material for analysis.

Table 17. Measured pyrite stoichiometry in different mine environments compared to standard pyrite ($FeS_{2.00}$).

Mine Environment	FeS_x (table value is x)				Standard Deviation
	Replication 1	Replication 2	Replication 3	Mean	
Texas Coal Overburden	1.96	1.94	2.03	1.98	0.05
Montana Subbituminous Coal	1.91	1.93	1.95	1.93*	0.02
Montana Gold Mine Tailings	1.94	1.95	1.93	1.94*	0.01
Coal Cleaning Waste I	1.96	1.90	1.87	1.91	0.05
Copper Mine Tailings	1.98	2.02	2.05	2.02	0.04
Colorado Pyrite	1.98	1.83	--	1.91	0.11

* Mean value is significantly different from standard pyrite composition ($FeS_{2.00}$) at $p \leq 0.05$.

and atomic weights of Fe and S. For example, 40.2% S/32.06 grams per mole = 1.254 moles S; and 36.7% Fe/55.847 grams per mole = 0.657 moles Fe. The molar ratio of Fe to S is 0.657:1.254 or 1:1.91. The simplest empirical formulae is $FeS_{1.91}$.

The accuracy of the determination of iron and sulfur by mineral destructive chemical analysis was assessed by comparison of analytical results to the known composition of FeS standards submitted for analysis. The mean recovery of iron was 99.0 ± 3.7% while the mean recovery of sulfur was 102.7 ± 5.0% at the 95% confidence interval. Since 100% recovery of the FeS standards for both iron and sulfur is contained within the 95% confidence interval, the introduction of analytical bias in the analysis is not anticipated.

The precision, or reproducibility, of analytical results was calculated based on laboratory duplicates and on replicated measurement of pyrite samples

submitted. The relative standard deviation (RSD) calculated from the laboratory duplicate analysis was 2.5% RSD for Fe and 0.7% RSD for S. The RSD calculated from the pyrite replicate samples was 2.7% RSD for Fe and 2.5% RSD for S. The RSD is the coefficient of variation expressed as a percentage, or RSD = 100 (standard deviation/mean). The experimentally calculated RSD is indicative of good analytical precision, though not precise enough to detect small differences in the stoichiometry of pyrite (i.e. $FeS_{1.98}$ versus $FeS_{2.00}$). Statistically significant differences ($p \leq 0.05$) in pyrite stoichiometry (Table 17) were measured for two samples where good reproducibility between replications was attained, though the lack of analytical precision prevented potential identification of differences between other treatments.

The mean pyrite stoichiometry from six mine environments is presented in Table 17. The pyrite stoichiometry of the Montana Subbituminous Coal sample and Montana Gold Mine Tailings samples were both significantly different than the predicted composition FeS_2 and both were sulfur deficient. The Montana Subbituminous Coal mean pyrite stoichiometry was $FeS_{1.93}$ while the Montana Gold Mine Tailings mean pyrite stoichiometry was $FeS_{1.94}$.

The nonstoichiometry of pyrite observed in field samples may result in dissimilar weathering rate characteristics, and may require field management unique to the pyrite source during reclamation.

Electron Microprobe Analysis Of Pyrite Stoichiometry

The stoichiometry of individual pyrite grains was assessed to determine the spatial variability of stoichiometry across mineral grains and to analyze for the presence of impurities. The Montana Gold Mine Tailings sample and Coal Cleaning Waste samples were examined by electron microprobe to assess the elemental composition of Fe, S, Cu, Co, As, Ni and Zn present within individual pyrite grains. The summary of repeated analysis of individual pyrite grains is presented in Table 18.

The pyrite standard used for calibration of the electron microprobe had a measured pyrite stoichiometry of $FeS_{1.99}$ while the mean Montana Gold Mine Tailings sample stoichiometry was $FeS_{1.97}$ and mean Coal Cleaning Waste I sample stoichiometry was $FeS_{1.98}$ (Table 18). The observed mean pyrite stoichiometry values are not significantly different ($p \leq 0.05$) from the pyrite standard. The observed mean pyrite stoichiometries are sulfur deficient relative to the expected chemical composition $FeS_{2.00}$, yet very close to $FeS_{2.00}$. The Montana Gold Mine Tailings pyrite stoichiometry from repeated measurement of three grains ranged from $FeS_{1.91}$ to $FeS_{2.01}$. The Coal Cleaning Waste I sample pyrite stoichiometry from repeated measurement of 4 grains ranged from $FeS_{1.96}$ to $FeS_{2.01}$.

The presence of impurity was detected by electron microprobe in all of the pyrite grains examined (Table 18), though typically at low concentrations. Given these analyses performed by electron microprobe, cobalt was the only element not detected which was a target analyte. In addition to Fe and S, which comprise the

Table 18. Chemical analysis of pyrite by electron microprobe.

Sample Source	Grain Number	Elemental Concentration (%)								Normalized[▲] Elemental Concentrations (%)			
		S	Fe	Cu	Co	As	Ni	Zn	Total	S	Fe	Total	FeSx[•]
Pyrite Standard	--	53.482	46.737	0.043	0.556	0.154	0.003	0.025	101.000	53.365	46.635	100	1.99[+]
	1	51.117	45.589	0.016	0.000	3.626	0.000	0.000	100.348	52.858	47.142	100	1.95
	1	52.653	45.675	0.000	0.000	0.165	0.000	0.000	98.493	53.548	46.452	100	2.01
Montana	1	50.925	45.443	0.028	0.000	2.977	0.000	0.000	99.373	52.844	47.156	100	1.95
Gold	1	50.639	46.088	0.020	0.000	3.538	0.004	0.000	100.289	52.352	47.648	100	1.91
Mine	2	52.723	46.287	0.000	0.000	0.000	0.000	0.000	99.010	53.250	46.750	100	1.98
Tailings	2	53.802	46.859	0.000	0.000	0.000	0.000	0.017	100.678	53.449	46.551	100	2.00
Pyrite	2	53.343	47.221	0.000	0.000	0.059	0.000	0.000	100.623	53.044	46.956	100	1.97
	3	54.063	47.599	0.000	0.000	0.000	0.000	0.000	101.662	53.179	46.821	100	1.98
	3	53.181	46.641	0.025	0.000	0.000	0.000	0.000	99.847	53.276	46.724	100	1.99
	3	53.488	47.088	0.000	0.000	0.051	0.002	0.000	100.629	53.182	46.818	100	1.98
MEAN		52.593	46.449	0.009	0.000	1.042	0.001	0.002		53.102	46.898	100	1.97[+]
	1	53.896	47.388	0.000	0.000	0.000	0.000	0.000	101.284	53.213	46.787	100	1.98
	1	53.634	47.351	0.000	0.000	0.000	0.000	0.000	100.985	53.111	46.889	100	1.97
	1	53.854	47.249	0.000	0.000	0.088	0.015	0.000	101.206	53.266	46.734	100	1.99
Coal	1	54.045	47.507	0.000	0.000	0.011	0.003	0.036	101.602	53.219	46.781	100	1.98
Cleaning	2	53.918	46.730	0.000	0.000	0.125	0.009	0.041	100.828	53.571	46.429	100	2.01
Waste I	3	53.735	47.666	0.000	0.000	0.000	0.013	0.017	101.431	52.993	47.007	100	1.96
Pyrite	3	54.325	47.845	0.061	0.000	0.048	0.004	0.002	102.285	53.171	46.829	100	1.98
	3	53.804	47.468	0.028	0.000	0.092	0.013	0.000	101.405	53.128	46.872	100	1.97
	4	53.318	47.506	0.019	0.000	0.033	0.000	0.011	100.887	52.882	47.118	100	1.96
	4	53.894	47.992	0.016	0.000	0.055	0.006	0.022	101.985	52.896	47.104	100	1.96
MEAN		53.842	47.470	0.012	0.000	0.045	0.006	0.013		53.145	46.855	100	1.98[+]

▲ Normalized iron and sulfur concentrations ignore the presence of impurity in the crystal.

• Pyrite stoichiometry calculated from the normalized iron and sulfur atomic concentrations.

+ Pyrite mean stoichiometry values are not significantly different ($p \leq 0.05$). Mean comparisons by Newman-Keuls.

greatest proportion of all pyrite grains, Cu, As, Ni, and Zn were detected. The only sample which contained greater than one percent impurity was the Montana Gold Mine Tailings sample, Grain 1. The mean arsenic concentration of Grain 1 was 2.577%, and the greatest measured arsenic content was 3.626%. The effect of impurity on mineral dissolution is unknown, but may relate to both the type of impurity and concentration. The presence of impurities such as arsenic within pyrite particles present the additional hazard of being liberated to solution upon oxidation of pyrite, resulting in water quality impairment by acidity and by the presence of toxic metals.

The influence of nonstoichiometry and presence of impurities on weathering of pyrite is not known in specific, but the weathering of pyrite is strongly controlled by imperfections in the crystalline lattice. Imperfections in the crystalline lattice may occur as a consequence of nonstoichiometry, or as a consequence of the presence of impurity. The electron microprobe measured nonstoichiometry of pyrite is not significantly different than $FeS_{2.00}$, but grain to grain, and intergrain variability in pyrite stoichiometry was measured. The presence of elements other than Fe and S is common in pyrite, but concentrations of impurities are typically less than one percent.

Impact Of Pyrite Nonstoichiometry On Field Lime Rate Calculation

One mole pyrite as ($FeS_{2.00}$) is oxidized in the presence of oxygen and water to produce 4 moles acidity as H^+ in accordance with the reaction shown below.

$$FeS_{2.00} + 3.75\, O_2 + 3.5\, H_2O = Fe(OH)_3 + 2\, SO_4^{-2} + 4\, H^+$$

To derive the field lime requirement sufficient to neutralize the acidity produced by this reaction by a sample which contains 1% sulfur as pyrite, the following interpretation is presented.

- A one gram sample containing 1% sulfur as pyrite would contain 0.01 g S.
- (0.01 g S/1 g sample)(1 mole S/32 g S) = 3.1×10^{-4} moles S/1 gram sample.
- (4 moles H^+ yielded/2 moles S oxidized)(3.1×10^{-4} moles S/1 g sample) = 6.25×10^{-4} moles H^+ yielded/1 g sample oxidized.
- (6.25×10^{-4} moles H^+/1 g sample)(454 g/1 pound)(2000 pounds/1 ton)(1000) = 5.676×10^5 moles H^+/1000 tons waste.
- Since the acidity generated by the oxidation of pyrite is neutralized by calcium carbonate, 2 moles H^+ is neutralized by 1 mole $CaCO_3$ in accordance with Equation 32.

$$CaCO_3 + 2\,H^+ = Ca^{2+} + H_2O + CO_2 \qquad [32]$$

- (5.676×10^5 moles H^+/1000 tons waste)(0.5 mole $CaCO_3$/1 mole H^+)(100 g $CaCO_3$/1 mole $CaCO_3$)(0.002203 pounds/1 gram)(0.0005 tons/pound) = 31.25 tons $CaCO_3$ required per 1000 tons waste material to neutralize the acid generated by oxidation of a sample containing one percent pyrite as $FeS_{2.00}$. The oxidation of pyrite which was not stoichiometric would proceed in accordance with Equation 33.

$$FeS_{1.84} + 3.51\,O_2 + 3.34\,H_2O = Fe(OH)_3 + 1.84\,SO_4^{-2} + 3.68\,H^+ \qquad [33]$$

- A one gram sample containing 1% sulfur as nonstoichiometric pyrite would contain 0.01 g S.
- (0.01 g S/1 g sample)(1 mole S/32 g S) = 3.1 x 10^{-4} moles S/1 gram sample.
- (3.68 moles H^+ yielded/1.84 moles S oxidized)(3.1 x 10^{-4} moles S/1 g sample) = 6.25 x 10^{-4} moles H^+ yielded/1 g sample oxidized.

Since the same amount of acidity is yielded per one gram sample containing one percent nonstoichiometric pyrite, the field lime rate calculation result is identical to stoichiometric pyrite, or 31.25 tons $CaCO_3$ per 1000 tons waste material. The field lime rate for nonstoichiometric pyrite is not different from stoichiometric pyrite.

Discussion

Prediction of the acid generation potential of samples containing pyrite derived from mining environments has been accomplished by investigators with limited success (Caruccio et al. 1976). Variation in the rate of acid generation from pyrite is responsible for inaccuracy in estimation of the rate and severity of acid generation. Pyrite forms which oxidize quickly can rapidly degrade environmental quality, while samples which oxidize slowly may have a comparatively minimal impact. Chemical analysis of the abundance of pyrite in a waste sample

does not address the rate of oxidation, only the abundance of sulfur forms present in the sample.

The rate of acid generation has been inferred to be a consequence of the particle size of the pyrite present (Pugh et al. 1984). Where pyrite is present as very small particles the rate of acid generation is inferred to be most rapid since surface area per mass is greatest. This approach is simplistic and neglects the potentially powerful effect of physical properties other than particle size on the rate of oxidation. Particle morphology, whether massive or euhedral, exerts a strong influence on rate of acid generation. Massive pyrite particles of the largest size class (>250 μm) were found to be the most strongly acid generating. Physical properties attributed to pyrite, other than particle size and morphology, may exert a strong influence on the rate of oxidation.

The nonstoichiometry and presence of impurities in pyrite may be an important consideration in characterization of the rate of acid generation. In addition to experimental findings, other authors have demonstrated that pyrite can be nonstoichiometric, but most importantly, Rakcheyev (1968) identified that samples which were nonstoichiometric and sulfur deficient were those formed at low temperature. The low temperature pyrite samples demonstrated the lowest activation energy. Pyrite formed at low temperature includes pyrite from depositional sedimentary environments, characteristic of coal deposits.

The formation of low temperature massive morphology pyrite may result in pyrite crystals comprised of regions of different stoichiometry. Early in the

formation of a pyrite particle, geochemical conditions may have existed such that small euhedral particles of stoichiometric pyrite formed, which were later surrounded by massive nonstoichiometric pyrite. Scanning electron microscope investigation of massive pyrite particles demonstrate that silica and euhedral pyrite can be encapsulated by massive pyrite. The electron microprobe analysis of the Coal Cleaning Waste I sample was performed on one of few well formed crystal surfaces, since analytical results could not be obtained from the rough texture of the massive morphology material comprising the remainder of the crystal. The mean stoichiometry of the small well formed crystal surfaces within the larger massive particles was $FeS_{1.98}$, while chemical analysis of the bulk mineral determined the mean stoichiometry to be $FeS_{1.91}$, suggesting that the early stage, well formed, euhedral pyrite encapsulated by late stage massive pyrite, is closer to the predicted pyrite stoichiometry $FeS_{2.00}$.

The rate of oxidation of pyrite is strongly influenced by the structure of the pyrite crystal lattice. The presence of impurity, or nonstoichiometry of pyrite, exerts a fundamental influence on pyrite oxidation by providing defects in the lattice which are exploited during oxidation. The variability of pyrite stoichiometry at the scale of micrometers on the crystal surface may play an important role in the rate of oxidation, but these small scale differences are not easily detected in bulk samples. Though the *rate* of oxidation may be influenced by nonstoichiometry, the ultimate quantity of acid produced by oxidation of sulfur forms results in the same amount of acid generated per mole of sulfur whether as stoichiomet-

ric pyrite or not. Therefore the presence of lime at 31.25 tons $CaCO_3$ per 1000 tons waste material per 1% sulfur as pyrite will result in sufficient neutralization potential whether the pyrite is present as stoichiometric $FeS_{2.00}$ or not.

Impurities such as arsenic, when incorporated into the pyrite crystal lattice affect the rate of mineral dissolution, but also contribute to the negative impact of pyrite oxidation by contributing toxic metals to solution in addition to iron, sulfate and acidity attributed to pyrite. The evolution of toxic metals upon oxidation of pyrite, assumed to be pure $FeS_{2.00}$ lacking impurity, may be an important consideration in the remediation of sites containing both reduced sulfide minerals and toxic metals. The physical properties of pyrite, therefore, are very important to predicting the environmental impact of exposure of pyrite to oxidizing conditions.

SUMMARY AND CONCLUSIONS

The generation of acid as a consequence of sulfide mineral oxidation, dominantly as pyrite, is a widespread source of environmental quality degradation. Pyrite is a common mineral in both coal and hardrock mining environments, requiring the mitigation of acid generated upon exposure of pyrite to oxidizing conditions as a consequence of mining activity. The neutralization of acid forming minerals is accomplished by laboratory analysis of potential acidity resulting in the addition of liming materials upon remediation of land impacted by acid producing mine wastes. Though analysis of potential acidity is routinely performed on samples containing sulfide minerals, the analytical methods applied fail to address the rate of oxidation of sulfide minerals and distribution of sulfur minerals other than pyrite. Potential errors resulting from inaccurate prediction of acid generation, threaten the success of remedial efforts costing tens of millions of dollars annually.

To address current inadequacies in estimation of acid generation by mine waste materials, research was initiated to better characterize the weathering processes of pyrite and other sulfur bearing minerals. Investigation was initiated to evaluate pyrite physical property variation including particle size and morphology and the ensuing impact on rate of oxidation. Research demonstrating variation in the acid generating properties of sulfur bearing minerals was also performed to establish the impact of minerals other than pyrite on acid generation. Upon characterization of the acid generating behavior of minerals present in mining

environments, the effectiveness of analytical methods routinely applied to determination of potential acidity was assessed through laboratory measurement.

Investigation of acid production processes was accomplished through collection of sulfide materials from operational coal and hardrock mines, and subsequently high-grading the sulfide minerals from waste silicates. The high-graded samples were characterized according to particle morphology and environment of formation, then four size fractions were subjected to aggressive oxidation by 10% H_2O_2. The resulting leachate chemistry was analyzed and related to mineral dissolution behavior documented by scanning electron microscopy. Pure sulfide and sulfate minerals were also subjected to oxidation by 10% H_2O_2 and sequential extraction by hot water, HCl and HNO_3 to determine which common mine environment sulfur bearing minerals, in addition to pyrite, were acid generating and which were included in calculation of potential acidity.

The effect of pyrite physical property variation was documented to exert the dominant control on rate of oxidation compared to pyrite surface area. Massive morphology pyrite particles were found to be significantly ($p \leq 0.05$) more acid generating than the euhedral morphology samples of the same particle size when submitted to the identical treatment. Therefore, the rate of oxidation of massive morphology is greater than the rate of oxidation of euhedral morphology samples. The difference in rate of oxidation is attributed to the physical properties of crystalline pyrite, which varied between mine environments having different geochemical and thermodynamic settings. Pyrite crystals which had the greatest

density of defect in the crystalline lattice resulting from the presence of atomic defects, impurities, inclusions, edges, steps and microcracks had the greatest reactive surface area and consequently the greatest rate of oxidation. Mineral dissolution proceeded by development of etch pits at the locations of crystalline defect. Massive morphology particles had the greatest density of crystalline defect and consequently the greatest rate of oxidation, though pyrite particles of the same particle size and morphology demonstrated significant differences in response to the identical oxidation treatment. The influence of particle size on acid generation was found to be minimal for euhedral morphology samples, while the smallest size fraction of massive morphology samples was found to be the least acid generating compared with the largest size fraction which demonstrated the greatest net acid generation. The *reactive* surface area of pyrite was found to exert an important influence on mineral dissolution. Though large differences in the rate of oxidation were documented, the stoichiometric evolution of leachate products resulting from pyrite oxidation was not different between samples derived from different geological environments. Nonstoichiometry of pyrite and presence of impurity within individual particles was also documented between samples derived from different geological environments. The nonstoichiometry of pyrite was measured to be as great as $FeS_{1.93}$ by mineral destructive analysis, while the presence of impurity was measured to be as high as 2.5% by electron microprobe analysis. The presence of toxic metal impurities, such as arsenic, within the pyrite

crystalline lattice presents the environmental consequence of toxic metal evolution to water in addition to acid evolution upon oxidation of pyrite.

The analysis of samples containing pyrite by acid-base account (ABA) methodology and calculation of potential acidity does not consider the rate of oxidation of pyrite, thereby neglecting an important factor controlling the environmental consequences of pyrite oxidation. Acid-base account also fails to accurately characterize the acid producing and nonacid producing minerals present in a sample. Common sulfur containing minerals were subjected to oxidation by 10% H_2O_2 prior to ABA extraction to determine which were acid generating. The sulfur bearing minerals barite, anhydrite, gypsum, anglesite, jarosite, chalcocite and galena were found to be nonacid forming. The minerals pyrite, marcasite, pyrrhotite, arsenopyrite, chalcopyrite and sphalerite were found to be acid forming. Upon subjecting these same minerals to extraction by hot water, HCl and HNO_3 in accordance with ABA methods, the acid forming and nonacid forming minerals were not accurately distinguished. Due to the inaccurate estimation of potential acidity by ABA extraction, large errors in the calculation of neutralizing mineral requirement are possible, both false negative and false positive. The degree to which ABA analytical ineffectiveness impacts site remediation activities is a consequence of the minerals present, and method of ABA calculation. The method of ABA calculation is based on laboratory measurement and varies between investigators, leading to dissimilar ABA results from the same analytical data.

Therefore, mineralogical characterization of the sulfur bearing minerals in a sample can greatly increase the accuracy of remedial design for treatment of acid producing mine wastes.

Mineralogical identification, particle morphology determination and mineral dissolution behavior can all be assessed by scanning electron microscope (SEM) examination of mineral samples from mining environments. The result of improved geochemical and mineralogical characterization of acid producing mine wastes will be more effective remediation of land and water impacted by mining activity.

REFERENCES CITED

REFERENCES CITED

Arora, H.S., Dixon, J.B. and L.R. Hossner. 1978. Pyrite morphology in lignitic coal and associated strata of East Texas. Soil Sci. 125:151-159.

Beck, J.V. and D.G. Brown. 1968. Direct sulfide oxidation in the solubilization of sulfide ores by *Thiobacillus ferrooxidans.* J. of Bacteriology, 96, pp. 1433.

Berner, R.A. 1970. Sedimentary pyrite formation. Amer. J. of Sci. 268:1-23.

Berner, R.A. 1983. Sedimentary pyrite formation: An update. Geochimica et Cosmochimica Acta, 48:605-615.

Brierley, C.L. 1990. Biohydrometallurgy: Applications in Reclamation, In: Proc. from High Altitude Revegetation Workshop No. 9, Colorado State Univ., Water Resources Research Institute, Keammerer, W.R. and J. Todd (eds.), pp. 138-143.

Caruccio, F.T. 1968. An evaluation of factors affecting acid mine drainage production and the ground water interactions in selected areas of Western Pennsylvania, In: Second Symp. on Coal Mine Drainage Research, Monroeville, PA, pp. 107-152.

Caruccio, F.T. 1970. The quantification of reactive pyrite by grain size, In: Third Symp. on Coal Mine Drainage Research, Monroeville, PA, pp. 123-131.

Caruccio, F.T., Geidel, G. and J.M. Sewell. 1976. The character of drainage as a function of the occurrence of framboidal pyrite and ground water quality in Eastern Kentucky. Sixth Symp. on Coal Mine Drainage Research, Bituminous Coal Research, Inc., 1-16.

Caruccio, F.T., Geidel, G. and A. Pelletier. 1980. The assessment of a stratum's capability to produce acidic drainage. In: Symp. on Surface Mining Hydrology, Sedimentology and Reclamation, Lexington, KY, pp. 437-443.

Casagrande, D.J., Gronli, K. and N. Sutton. 1980. The distribution of sulfur and organic matter in various fractions of peat: Origins of sulfur in coal. Geochimica et Cosmochimica Acta, 44:25-32.

Casagrande, D.J., Finkelman, R.B. and F.T. Caruccio. 1989. The nonparticipa tion of organic sulphur in acid mine drainage generation. Environmental Geochemistry and Health, 11:187-192.

Colmer, A.R. and M.E. Hinkle. 1947. The role of microorganisms in acid mine drainage: A preliminary report. Science, 75:236.

Cravotta, C.A., Brady, K.B.C., Smith, M.W. and R.L. Beam. 1990. Effectiveness of the addition of alkaline materials at surface coal mines in preventing or abating acid mine drainage: Part 1. Geochemical considerations. Proc. of 1990 Mining and Reclamation Conf. and Exhibition, Charleston, WV, pp. 221-225.

Dacey, P.W. and P. Colbourn. 1979. An assessment of methods for the determination of iron pyrites in coal mine spoil. Reclamation Review, 2:113-121.

Dana, D.W. 1944. The System of Mineralogy, Volume I, Elements, Sulfides, Sulfosalts, Oxides, Second Edition. Wiley, NY. 674 p.

Delaney, J.R., Mogk D.W. and M.J. Mottl. 1987. Quartz-cemented breccias from the Mid-Atlantic Ridge: Samples of a high-salinity hydrothermal upflow system. J. of Geophysical Research, 92(B9):9175-9192.

Dell, C.I. 1972. An occurrence of greigite in Lake Superior sediments. Amer. Mineralogist, 57:1303-1304.

Eggleston, C.M., Hochella M.F. and G.A. Parks. 1989. Sample preparation and aging effects on the dissolution rate and surface composition of diopside. Geochimica et Cosmochimica Acta, 53:797-804.

Eggleston, C.M. and M.F. Hochella. 1990. Scanning tunnelling microscopy of sulfide surfaces. Geochimica et Cosmochimica Acta, 54:1511-1517.

Evangelou, V.P., Grove, J.H. and F.D. Rawlings. 1985. Rates of iron sulfide oxidation in coal spoil suspensions. J. of Environ. Qual. 14(1):91-94.

Franson, M.H., Ed. 1989. Standard Methods for the Examination of Water and Wastewater, 17th Edition. Amer. Public Health Assoc., Amer. Water Works Assoc., Water Pollution Control Federation, Washington, DC.

Geidel, G. 1979. Alkaline and acid production potentials of overburden material: The rate of release. Reclamation Review, 2:101-107.

Goldhaber, M.B. 1983. Experimental study of metastable sulfur oxyanion formation during pyrite oxidation at pH 6-9 and 30° C. Amer. J. of Sci. 283:193-217.

Grady, W.C. 1977. Microscopic varieties of pyrite in West Virginia coals. American Institute of Mining, Metallurgical and Petroleum Engineers Transactions, 262, pp. 268.

Haines, L. 1986. The effect of iron disulfide size, type, and morphology on the production of acid mine drainage. M.S. thesis, West Virginia Univ., Morgantown, WV.

Hammack, R.W. 1985. The relationship between the thermal activity of pyrite and the rate of acid generation. In: Proc. of the 1985 National Symp. on Surface Mining, Hydrology, Sedimentology and Reclamation, Univ. of Kentucky, Lexington, KY.

Hochella, M.F., Eggleston, C.M., Elings, V.B., Parks, G.A., Brown, G.E., Wu, C.M. and K. Kjoller. 1989. Mineralogy in two dimensions: Scanning tunneling microscopy of semiconducting minerals with implications for geochemical reactivity. Amer. Mineralogist, 74:1233-1246.

Hochella, M.F. and A.F. White, Eds. 1990. Mineral-Water Interface Geochemis try. Reviews in Mineralogy, Vol. 23. Mineralogical Soc. of Amer., Washington, D.C.

Holdren, G.R. and P.M. Speyer. 1987. Reaction rate-surface area relationships during the early stages of weathering. II. Data on eight additional feldspars. Geochimica et Cosmochimica Acta, 51:2311-2318.

Jaynes, D.B., Rogowski, A.S. and H.B. Pionke. 1984a. Acid mine drainage from reclaimed coal strip mines, 1. Model description. Water Resources Research, 20:233-242.

Jaynes, D.B., Pionke, H.B. and A.S. Rogowski. 1984b. Acid mine drainage from reclaimed coal strip mines, 2. Simulation results of model. Water Resources Research, 20:243-250.

Kullerud, G. and H.S. Yoder. 1959. Pyrite stability relations in the Fe-S system. Economic Geology, 54:534-569.

Lasaga, A.C. and A.E. Blum. 1986. Surface chemistry, etch pits and mineral-water reactions. Geochimica et Cosmochimica Acta, 50:2363-2379.

Leathen, W.W., Braley, S.A. and L.D. McIntyre. 1953. The role of bacteria in the formation of acid from certain sulfuritic constituents associated with bituminous coal. II. Ferrous oxidizing bacteria. Applied Microbiology, 1, pp. 65.

Lindsay, W.L. 1979. Chemical Equilibria is Soils. John Wiley and Sons, Inc., New York, NY, 449 p.

Lowson, R.T. 1982. Aqueous oxidation of pyrite by molecular oxygen. Chemical Reviews, 82(5):461-497.

Mason, B. and L.G. Berry. 1968. Elements of Mineralogy. W.H. Freeman and Co. 244 p.

McKibben, M.A. and H.L. Barnes. 1986. Oxidation of pyrite in low temperature acidic solutions: Rate laws and surface textures. Geochimica et Cosmochimica Acta, 50: 1509-1520.

Miller, R.G. 1981. Simultaneous statistical Inference, New York: Springer-Verlag.

Nicholson, R.V., Gillham, R.W. and E.J. Reardon. 1988. Pyrite oxidation in carbonate-buffered solutions: 1. Experimental kinetics. Geochimica et Cosmochimica Acta, 52: 1077-1085.

Nordstrom, D.K. 1982. Aqueous pyrite oxidation and the consequent formation of secondary iron minerals, In: Acid sulfate weathering, SSSA Special Publ. Number 10, Soil Sci. Soc. of Amer., Madison, WI, pp. 37-56.

O'Meara, R.G. and J.B. Clemmer. 1928. Methods of preparing and cleaning some common heavy liquids used in ore testing. U.S. Bur. of Mines Publ. 2897, 6 p.

O'Shay, T, Hossner, L.R. and J.B. Dixon. 1990. A modified hydrogen peroxide oxidation method for determination of potential acidity in pyritic overburden. J. of Environ. Qual. 19:778-782.

Powell, A.R. 1920. Determination of sulfur forms in coal. The Journal of Industrial and Engineering Chemisty, 887-890.

Pugh, C.E., Hossner, L.R. and J.B. Dixon. 1981. Pyrite and marcasite surface area as influenced by morphology and particle diameter. Soil Sci. Soc. of Amer. J. 45:979-982.

Pugh, C.E., Hossner, L.R. and J.B. Dixon. 1984. Oxidation rate of iron sulfides as affected by surface area, morphology, oxygen concentration, and autotrophic bacteria. Soil Sci. 137(5):305-314.

Raiswell, R. and J. Plant. 1980. The incorporation of trace elements into pyrite during diagenesis of black shales, Yorkshire, England. Economic Geology, 75:684-699.

Raiswell, R. 1982. Pyrite texture, isotopic composition and the availability of iron. Amer. J. of Sci. 282:1244-1263.

Rakcheyev, A.D. and L.V. Chernyshev. 1968. Activation energy and chemical composition of pyrite as a function of its mode of synthesis. Doklady Akademii Nauk SSSR, 183(5):1184-1187.

Ribbe, P.H., Ed. 1975. Sulfide Mineralogy, Volume 1. Mineralogical Soc. of Amer., Washington, DC.

SAS Institute, Inc. 1985. SAS® User's Guide: Statistics, Version 5 Edition, Cary, NC: SAS Institute, Inc. 956 p.

Schafer and Associates and Reclamation Research. 1987. Laboratory analytical protocol for the Streambank Tailings and Revegetation Study, Silver Bow Creek RI/FS, EPA Region VIII, Doc. No. SBC-STARS-LAP-F-RI-121187.

Schafer and Associates and Reclamation Research. 1989. Streambank Tailings and Revegetation Studies, STARS PHASE II: Field-scale treatability study, Silver Bow Creek RI/FS, EPA Region VIII, Doc. No. SBC-STARS-PhaseII-D-RO-020189.

Schuman, G., F.T. Caruccio and W.S. Bradham. 1991. An assessment of factors affecting pyrite reactivity. U.S. Bur. of Mines Contract J0398006, NTIS PB92-140227.

Shuey, R.T. 1975. Semiconducting Ore Minerals, Elsevier, New York, NY. 415 p.

Singer, P.C. and W. Stumm. 1970. Acidic mine drainage: The rate determining step. Science, 167, pp. 1121.

Smith, F.G. 1942. Variation in the properties of pyrite. Amer. Mineralogist; 27:1-19.

Smittenberg, J., Harmsen, G.W., Quispel, A. and D. Otzen. 1951. Rapid methods for determining different types of sulphur compounds in soil. Plant and Soil III, 4:353-361.

Snedecor, C.W. and W.G. Cochran. 1989. Statistical Methods, 8th Edition. Iowa State Press, Ames, IA.

Sobek, A.A., Schuller, W.A., Freeman, J.R. and R.M. Smith. 1978. Field and laboratory methods applicable to overburdens and minesoils. Cincinnati, OH. U.S. Environmental Protection Agency Environmental Protection Technology, EPA-600/2-78-054, 203 p.

Stanton, R.L. 1957. Studies of polished surfaces of pyrite and some implications. Canadian Mineralogy, 6:87-118.

Weast, R.C. (ed.). 1976. Handbook of Chemistry and Physics, 5th Edition. CRC Press, Cleveland, OH.

Wiersma, C.L. and J.D. Rimstidt. 1984. Rates of reaction of pyrite and marcasite with ferric iron at pH 2. Geochimica et Cosmochimica Acta, 48:85-92.

Williams, E.G., Rose, A.W., Parizek, R.R. and S.A. Waters. 1982. Factors controlling the generation of acid mine drainage. Final Report on Research Grant No. G5105086, Pennsylvania Mining and Mineral Resources Research Institute, Pennsylvania State Univ., 265 p.

Zhabina, N.N. and I.I. Volkov. 1978. A method of determination of various sulfur compounds in sea sediments and rocks. In: Environmental Biogeochemistry and Geomicrobiology, Ann Arbor Science, W.E. Krumbein (ed.), Ann Arbor, MI, 735-746.

APPENDIX

Experimental Data

Table 19. Raw data for hydrogen peroxide weathering of pyrite.

Sample Name	Particle Size (μm)	Mass Loss (%)	EC (dS m^{-1})	Acidity to pH (mg $CaCO_3$ l^{-1})	Sulfate (mg l^{-1})	Iron (mg l^{-1})	pH	Reaction Time (days)
Texas Coal Overburden	>250	-65.08	34.68	23183	24003	6084	1.56	0.647
Texas Coal Overburden	>250	-68.88	34.36	22421	23676	5952	1.57	0.901
Texas Coal Overburden	>250	-68.06	34.52	23999	23241	6036	1.58	0.897
Texas Coal Overburden	106-250	-68.55	35.02	22924	23723	6080	1.6	0.933
Texas Coal Overburden	106-250	-68.42	35.67	23471	24550	6406	1.62	0.908
Texas Coal Overburden	106-250	-71.01	35.67	25331	24109	6273	1.62	0.892
Texas Coal Overburden	38-106	-66.05	33.23	22312	22159	5760	1.68	0.915
Texas Coal Overburden	38-106	-63.86	32.74	21550	21756	5688	1.67	0.937
Texas Coal Overburden	38-106	-64.4	33.07	23292	22417	5784	1.68	0.887
Texas Coal Overburden	<38	-39.87	21.77	14204	12810	3300	1.62	0.385
Texas Coal Overburden	<38	-39.06	22.74	14040	12731	3312	1.63	0.533
Texas Coal Overburden	<38	-39.1	22.25	14367	12512	3288	1.63	0.533
Copper Mine Tailings	>250	.	1.57	544	503	122	2.81	0.649
Copper Mine Tailings	>250	-2.05	1.44	517	485	116	2.81	0.645
Copper Mine Tailings	>250	-2.1	1.55	544	500	122	2.82	0.641
Copper Mine Tailings	106-250	-2.77	2.14	762	701	182	2.67	0.618
Copper Mine Tailings	106-250	-3.02	2.12	707	698	180	2.63	0.69
Copper Mine Tailings	106-250	-2.27	2.06	816	672	176	2.69	0.607
Copper Mine Tailings	38-106	-2.53	1.93	707	658	163	2.72	0.126
Copper Mine Tailings	38-106	-2.34	2.09	707	712	173	2.74	0.108
Copper Mine Tailings	38-106	-2.22	1.97	653	647	158	2.75	0.11
Copper Mine Tailings	<38	-4.26	3.63	1181	1156	248	2.54	0.001
Copper Mine Tailings	<38	-4.58	3.68	1238	1245	277	2.55	0.001
Copper Mine Tailings	<38	-4.52	3.16	1125	1171	279	2.61	0.001
Nevada Gold Ore	>250	-79.38	61.43	28834	27600	8430	2.07	1.197
Nevada Gold Ore	>250	-71.84	60.12	27345	25972	8018	2.1	1.083
Nevada Gold Ore	>250	-72.49	59.88	28699	25346	7713	1.89	1.119
Nevada Gold Ore	106-250	-30.7	29.65	12334	12743	3700	2	0.949
Nevada Gold Ore	106-250	-33.49	30.75	13283	12537	3628	1.98	0.951
Nevada Gold Ore	106-250	-34.45	29.35	13283	13477	3850	1.97	0.804
Nevada Gold Ore	38-106	-30.87	24.49	9725	9644	2796	1.88	0.937
Nevada Gold Ore	38-106	-19.95	25.19	9725	9100	2608	1.9	0.913
Nevada Gold Ore	38-106	-24.63	24.68	10171	9106	2689	1.85	0.899
Nevada Gold Ore	<38	-5.3	.	9038	5726	253	1.71	0.643
Nevada Gold Ore	<38	-5.53	33.42	8954	5447	231	1.71	0.647
Nevada Gold Ore	<38	-10.11	36.43	9799	5905	276	1.7	0.644

Table 19. Continued.

Sample Name	Particle Size (μm)	Mass Loss (%)	EC (dS m^{-1})	Acidity to pH (mg $CaCO_3$ l^{-1})	Sulfate (mg l^{-1})	Iron (mg l^{-1})	pH	Reaction Time (days)
MT Gold Mine Tailings	106-250	-11.98	8.7	4268	3987	1237	2.1	1.53
MT Gold Mine Tailings	106-250	-11.87	8.26	4212	3932	1226	2.07	1.53
MT Gold Mine Tailings	106-250	-12.82	8.34	4437	4005	1253	1.89	1.529
MT Gold Mine Tailings	38-106	-14.15	9.4	4863	4512	1422	1.88	0.576
MT Gold Mine Tailings	38-106	-13.74	9.17	4752	4376	1376	1.94	0.576
MT Gold Mine Tailings	38-106	-13.74	9.32	4863	4563	1417	1.86	0.675
MT Gold Mine Tailings	<38	-8.95	6.22	2929	2955	833	2.04	0.169
MT Gold Mine Tailings	<38	-7.49	5.21	2376	2463	694	2.09	0.153
MT Gold Mine Tailings	<38	-8.03	5.53	2542	2614	746	2.06	0.115
Moly Mine Tailings	>250	-10.29	6.6	3371	3383	1009	2.21	0.456
Moly Mine Tailings	>250	-10.69	6.96	3537	3606	1064	1.99	0.457
Moly Mine Tailings	>250	-10.71	6.91	3592	3534	961	2.11	0.457
Moly Mine Tailings	106-250	-9.83	6.46	3316	3221	966	2.11	0.345
Moly Mine Tailings	106-250	-9.9	6.32	3260	3221	979	2.12	0.344
Moly Mine Tailings	106-250	-10.01	6.43	3316	3236	947	2.1	0.344
Moly Mine Tailings	38-106	-9.91	6.46	3260	3164	955	2.08	0.227
Moly Mine Tailings	38-106	-9.03	5.98	3012	2848	900	2.09	0.228
Moly Mine Tailings	38-106	-9.44	6.05	3758	2977	925	2.08	0.227
Moly Mine Tailings	<38	-14.7	9.17	5167	4613	1471	1.89	0.003
Moly Mine Tailings	<38	-14.21	8.69	4669	4372	1405	1.89	0.005
Moly Mine Tailings	<38	-15.03	9.13	5029	4764	1504	1.86	0.005
Coal Cleaning Waste I	>250	-58.37	28.44	20695	19056	5748	1.59	0.905
Coal Cleaning Waste I	>250	-60.48	28.92	20446	19135	5772	1.54	0.952
Coal Cleaning Waste I	>250	-59.36	29.52	20170	18901	5760	1.49	0.899
Coal Cleaning Waste I	106-250	-58.13	29.88	19286	17876	5532	1.46	0.705
Coal Cleaning Waste I	106-250	-60.18	28.08	19037	17538	4992	1.47	0.575
Coal Cleaning Waste I	106-250	-60.49	30.12	20833	18880	5808	1.43	0.689
Coal Cleaning Waste I	38-106	-59.21	29.07	19767	17763	5458	1.44	0.452
Coal Cleaning Waste I	38-106	-58.6	28.94	19399	18145	5556	1.48	0.475
Coal Cleaning Waste I	38-106	-58.77	28.21	18778	17796	5458	1.47	0.476
Coal Cleaning Waste I	<38	-33.41	18.44	10724	9827	3077	1.63	0.237
Coal Cleaning Waste I	<38	-33.48	18.8	10892	9761	3059	1.62	0.238
Coal Cleaning Waste I	<38	-33.39	18.8	10836	10201	3123	1.62	0.238
Coal Cleaning Waste II	>250	-48.98	27.01	19015	18687	5356	1.46	1.114
Coal Cleaning Waste II	>250	-49.28	27.69	17778	18105	5088	1.5	1.143
Coal Cleaning Waste II	>250	-50.69	27.52	17807	17821	5113	1.53	1.142
Coal Cleaning Waste II	106-250	-53.36	28.19	18253	18743	5387	1.54	1.144

Table 19. Continued.

Sample Name	Particle Size (μm)	Mass Loss (%)	EC (dS m^{-1})	Acidity to pH (mg $CaCO_3$ l^{-1})	Sulfate (mg l^{-1})	Iron (mg l^{-1})	pH	Reaction Time (days)
Coal Cleaning Waste II	106-250	-53.23	29.02	19101	19458	5564	1.46	1.146
Coal Cleaning Waste II	106-250	-54.06	28.69	18896	19641	5514	1.43	1.148
Coal Cleaning Waste II	38-106	-48.31	26.59	17204	15591	4585	1.47	1.238
Coal Cleaning Waste II	38-106	-48.62	26.75	17371	16772	7423	1.54	1.237
Coal Cleaning Waste II	38-106	-48.5	27.06	17874	16764	4961	1.5	1.301
Coal Cleaning Waste II	<38	-35.99	22.04	12489	12149	3576	1.58	0.949
Coal Cleaning Waste II	<38	-36.29	21.26	12737	12562	3708	1.57	0.948
Coal Cleaning Waste II	<38	-35.74	20.94	12820	12286	3576	1.55	0.947
Metal Mine Tailings	106-250	-21.8	14.05	7736	7852	2258	1.74	1.36
Metal Mine Tailings	106-250	-20.35	13.52	7294	7292	2122	1.78	1.358
Metal Mine Tailings	106-250	-20.61	13.61	7488	7683	2183	1.74	1.357
Metal Mine Tailings	38-106	-17.44	12.48	6631	6641	1936	1.72	0.785
Metal Mine Tailings	38-106	-18.18	12.72	6797	6601	1993	1.7	0.781
Metal Mine Tailings	38-106	-17.72	12.31	7957	6256	1880	1.67	0.767
Metal Mine Tailings	<38	-11.2	7.93	3675	3534	1064	1.9	1.085
Metal Mine Tailings	<38	-9.85	7.61	3481	3347	1025	1.93	1.089
Metal Mine Tailings	<38	-10.54	8.02	3730	3750	1090	1.78	1.085
WY Coal Overburden	>250	-42.19	19.09	11644	10168	3256	1.67	0.835
WY Coal Overburden	>250	-41.57	18.3	13201	10847	3486	1.59	0.834
WY Coal Overburden	>250	-42.74	20.43	12970	10667	3353	1.63	0.833
WY Coal Overburden	106-250	-41.63	22.79	13793	12359	3942	1.62	0.541
WY Coal Overburden	106-250	-40.15	23.36	13310	12112	3855	1.58	0.54
WY Coal Overburden	106-250	-40.07	22.59	12989	11785	3792	1.61	0.539
WY Coal Overburden	38-106	-36.32	20.92	11801	10737	3371	1.62	0.591
Underground Coal Waste	>250	-66.96	38.33	22147	21907	6332	1.62	1.197
Underground Coal Waste	>250	-64	36.99	22901	22794	6598	1.63	1.196
Underground Coal Waste	>250	-68.8	36.51	22398	22754	6392	1.61	1.196
Underground Coal Waste	106-250	-65.54	37.63	21747	22189	6364	1.63	1.197
Underground Coal Waste	106-250	-65.25	37.25	21834	22835	6528	1.64	1.192
Underground Coal Waste	106-250	-65.79	38.01	22474	22484	6402	1.61	1.191
Underground Coal Waste	38-106	-67.35	40.27	23046	23842	6839	1.6	1.196
Underground Coal Waste	38-106	-69.96	40.78	23635	24310	6775	1.57	1.195
Underground Coal Waste	38-106	-69.13	40.4	24018	24164	6865	1.59	1.195
Underground Coal Waste	<38	-33.87	18.25	11388	11356	3321	1.69	0.305
Underground Coal Waste	<38	-33.55	18.01	11473	11249	3363	1.83	0.304
Underground Coal Waste	<38	-32.03	18.13	11359	11323	3411	1.8	0.304
Gold Mine Tailings II	106-250	-8.05	4.03	1588	1995	683	2.41	0.776

Table 19. Continued.

Sample Name	Particle Size (μm)	Mass Loss (%)	EC ($dS\ m^{-1}$)	Acidity to pH ($mg\ CaCO_3\ l^{-1}$)	Sulfate ($mg\ l^{-1}$)	Iron ($mg\ l^{-1}$)	pH	Reaction Time (days)
Gold Mine Tailings II	106-250	-7.3	3.62	1538	1846	614	2.45	0.775
Gold Mine Tailings II	106-250	-7.59	3.77	1786	1937	625	2.35	0.775
Gold Mine Tailings II	38-106	-9.78	3.38	2355	2462	1038	2.28	0.478
Gold Mine Tailings II	38-106	-9.44	3.47	2393	2408	1008	2.21	0.478
Gold Mine Tailings II	38-106	-9.51	3.57	2393	2355	960	2.34	0.477
Gold Mine Tailings II	<38	-5.34	4.3	2069	2351	772	2.39	0.718
Gold Mine Tailings II	<38	-4.79	4.32	1902	2387	729	2.41	0.717
Gold Mine Tailings II	<38	-5.47	4.47	1957	2482	802	2.39	0.717
Gold Mine Tailings I	106-250	-3.68	2.65	1137	1133	312	2.62	0.652
Gold Mine Tailings I	106-250	-3.43	2.94	1300	1142	316	2.45	0.652
Gold Mine Tailings I	106-250	-3.8	2.71	1170	1154	316	2.52	0.651
Gold Mine Tailings I	38-106	-3.99	3.26	1492	1417	413	2.42	0.02
Gold Mine Tailings I	38-106	-3.63	3.13	1382	1377	396	2.44	0.02
Gold Mine Tailings I	<38	-3.98	3.05	1348	1345	362	2.53	0.005
Gold Mine Tailings I	<38	-4.63	2.88	1236	1272	343	2.55	0.004
Gold Mine Tailings I	<38	-4.13	2.99	1264	1319	354	2.55	0.003
Gold Mine Ore	>250	-8.36	6.39	2861	2884	820	1.97	1.393
Gold Mine Ore	>250	-7.84	6.13	2750	2642	790	1.96	1.391
Gold Mine Ore	>250	-9.01	7.06	3250	3000	911	1.94	1.391
Gold Mine Ore	106-250	-10.19	7.65	3435	3351	961	2.03	0.914
Gold Mine Ore	106-250	-9.86	7.4	3184	3213	969	2.04	0.911
Gold Mine Ore	106-250	-10.51	8.02	3686	3438	1036	2.03	0.911
Gold Mine Ore	38-106	-9.05	6.95	3150	2981	929	2.03	0.63
Gold Mine Ore	38-106	-9.32	6.8	3205	3146	937	2.03	0.629
Gold Mine Ore	38-106	-9.45	7.03	3205	3150	955	2.02	0.629
Gold Mine Ore	<38	-10.83	7.94	4072	3764	1154	2.08	0.006
Gold Mine Ore	<38	-11.77	7.87	4156	3745	1132	2.05	0.006
Gold Mine Ore	<38	-10.78	8.15	4212	3881	1201	1.95	0.006
Control	>250	-1.35	0.19	28	<1	<1	3.87	20.736
Control	>250	-0.84	0.06	39	<1	<1	3.87	20.736
Control	>250	-0.71	0.06	39	<1	<1	3.99	20.735
Control	106-250	-1.36	0.06	28	<1	<1	3.87	20.734
Control	106-250	-0.93	0.07	28	<1	<1	3.76	20.733
Control	106-250	-0.28	0.08	28	7	<1	3.73	20.733
Control	38-106	-1.24	0.06	28	<1	<1	3.86	20.732
Control	38-106	-1.1	0.06	28	7	<1	3.85	20.731
Control	38-106	-0.96	0.06	28	<1	<1	3.87	20.731

Table 19. Continued.

Sample Name	Particle Size (μm)	Mass Loss (%)	EC (dS m^{-1})	Acidity to pH (mg $CaCO_3$ l^{-1})	Sulfate (mg l^{-1})	Iron (mg l^{-1})	pH	Reaction Time (days)
Control	<38	-1.39	0.25	44	65	7	3.37	8.796
Control	<38	-1.12	0.17	44	40	2	3.64	13.646
Control	<38	-1.1	0.23	44	58	5	3.47	11.691

Table 20. Raw data for stoichiometric balance of leachate parameters resulting from pyrite oxidation.

Treatment	Size Fraction (μm)	Rep	Moles Acidity	Moles Sulfate	Moles Iron
CONTROL	>250	1	0.43	0.00	0.00
CONTROL	106-250	2	0.39	0.01	0.00
CONTROL	38-106	3	0.31	0.01	0.00
CONTROL	<38	4	0.44	0.28	0.04
COPPER MINE TAILINGS	>250	1	3.11	1.50	0.63
COPPER MINE TAILINGS	106-250	2	3.41	1.61	0.72
COPPER MINE TAILINGS	38-106	3	3.52	1.79	0.75
COPPER MINE TAILINGS	<38	4	3.20	1.68	0.65
METAL MINE TAILINGS	>250	1			
METAL MINE TAILINGS	106-250	2	4.32	2.28	1.13
METAL MINE TAILINGS	38-106	3	4.83	2.29	1.17
METAL MINE TAILINGS	<38	4	4.15	2.11	1.09
MT GOLD MINE TAILINGS	>250	1			
MT GOLD MINE TAILINGS	106-250	2	4.25	2.04	1.09
MT GOLD MINE TAILINGS	38-106	3	4.19	2.03	1.09
MT GOLD MINE TAILINGS	<38	4	3.86	2.06	1.00
GOLD MINE TAILINGS I	>250	1			
GOLD MINE TAILINGS I	106-250	2	3.98	1.97	0.93
GOLD MINE TAILINGS I	38-106	3	4.54	2.30	1.14
GOLD MINE TAILINGS I	<38	4	3.64	1.94	0.90
GOLD MINE TAILINGS II	>250	1			
GOLD MINE TAILINGS II	106-250	2	2.58	1.58	0.90
GOLD MINE TAILINGS II	38-106	3	2.99	1.58	1.13
GOLD MINE TAILINGS II	<38	4	4.58	2.90	1.59
GOLD MINE ORE	>250	1	4.24	2.12	1.08
GOLD MINE ORE	106-250	2	4.06	2.05	1.05
GOLD MINE ORE	38-106	3	4.14	2.09	1.09
GOLD MINE ORE	<38	4	4.49	2.14	1.13
MOLY MINE TAILINGS	>250	1	3.99	2.08	1.03
MOLY MINE TAILINGS	106-250	2	4.01	2.04	1.05
MOLY MINE TAILINGS	38-106	3	4.26	1.99	1.06
MOLY MINE TAILINGS	<38	4	4.08	1.96	1.07
WY COAL OVERBURDEN	>250	1	3.60	1.57	0.86
WY COAL OVERBURDEN	106-250	2	3.96	1.87	1.03
WY COAL OVERBURDEN	38-106	3	3.91	1.85	1.00
WY COAL OVERBURDEN	<38	4			
TX COAL OVERBURDEN	>250	1	4.15	2.20	0.96
TX COAL OVERBURDEN	106-250	2	4.15	2.18	0.97
TX COAL OVERBURDEN	38-106	3	4.16	2.14	0.96
TX COAL OVERBURDEN	<38	4	6.41	2.02	0.90
NV GOLD ORE	>250	1	4.57	2.21	1.17
NV GOLD ORE	106-250	2	4.75	2.46	1.22
NV GOLD ORE	38-106	3	4.73	2.31	1.16
NV GOLD ORE	<38	4	15.99	5.11	0.39
COAL CLEANING WASTE I	>250	1	4.15	2.01	1.05
COAL CLEANING WASTE I	106-250	2	3.99	1.90	0.99
COAL CLEANING WASTE I	38-106	3	3.95	1.91	1.01
COAL CLEANING WASTE I	<38	4	6.33	1.86	1.00

Table 20. Continued.

Treatment	Size Fraction (μm)	Rep	Moles Acidity	Moles Sulfate	Moles Iron
COAL CLEANING WASTE II	>250	1	4.42	2.30	1.13
COAL CLEANING WASTE II	106-250	2	4.22	2.26	1.11
COAL CLEANING WASTE II	38-106	3	4.34	2.12	1.26
COAL CLEANING WASTE II	<38	4	4.24	2.15	1.08
UNDERGROUND COAL WASTE	>250	1	4.07	2.12	1.04
UNDERGROUND COAL WASTE	106-250	2	4.05	2.15	1.06
UNDERGROUND COAL WASTE	38-106	3	4.13	2.20	1.07
UNDERGROUND COAL WASTE	<38	4	2.00	2.14	1.09

Table 21. Raw data for leachate chemistry resulting from oxidation of pyrite by deionized water.

Mineral Name	Size Fraction (microns)	Mass Change (%)	pH	EC (dS m^{-1})	Titratable Acidity to pH 7 mg $CaCO_3$ l^{-1}	SO_4 mg l^{-1}	Fe mg l^{-1}
GOLD MINE ORE	<149	-0.08	4.18	0.13	14	30	1
GOLD MINE ORE	<149	0.04	4.19	0.09	14	27	2
GOLD MINE ORE	<149	0.06	4.22	0.09	10	30	1
COAL CLEANING WASTE I	<149	-7.63	2.69	2.87	1121	1786	834
COAL CLEANING WASTE I	<149	-7.78	2.68	3.12	1093	1903	884
COAL CLEANING WASTE I	<149	-7.96	2.59	3.06	988	1876	869
COAL CLEANING WASTE II	<149	-0.61	3.28	0.48	181	201	78
COAL CLEANING WASTE II	<149	-0.54	3.36	0.43	162	177	73
COAL CLEANING WASTE II	<149	-0.51	3.35	0.45	171	186	75
COPPER MINE TAILINGS	<149	-0.02	4.77	0.09	10	24	0
COPPER MINE TAILINGS	<149	-0.01	4.48	0.08	5	27	0
COPPER MINE TAILINGS	<149	0.00	5.05	0.08	10	24	0

Table 22. Raw data for hydrogen peroxide weathering on common sulfur bearing minerals.

Replication	Mineral I.D.	Mass Change (%)	pH	S mg l^{-1}	EC dS m^{-1}	Acidity to pH 7 mg $CaCO_3$ l^{-1}
1	BARITE	-0.49	3.83	2	0.00	23
	ANHYDRITE	-12.10	6.93	580	0.18	11
	GYPSUM	-13.73	4.27	596	0.18	40
	ANGLESITE	-0.67	4.78	13	0.00	23
	JAROSITE	-5.69	4.14	7	0.00	29
	ARSENOPYRITE	6.30	1.57	1356	18.60	4716
	WARD'S PYRITE	-40.46	1.65	3520	17.64	10749
	CHALCOCITE	3.29	4.98	29	0.25	80
	WARD'S PYRRHOTITE	-2.64	2.72	334	2.02	905
	CHALCOPYRITE	-6.80	2.69	997	4.03	2537
	GALENA	12.71	4.08	37	0.00	74
	MARCASITE	-12.09	2.06	1254	8.33	3921
	SPHALERITE	-31.85	4.57	2556	0.67	7011
	HARDROCK PYRITE	-2	2.88	118	1.20	336
	HARDROCK PYRRHOTITE	-5.19	2.59	508	3.17	1391
	COAL PYRITE	-60.67	1.46	6230	29.04	19825
2	BARITE	-0.87	4.05	2	0.00	46
	ANHYDRITE	-12.84	7.05	576	2.58	0
	GYPSUM	-14.32	4.17	568	2.65	57
	ANGLESITE	-1.29	4.47	14	0.16	34
	JAROSITE	-0.87	4.11	5	0.05	46
	ARSENOPYRITE	3.13	1.79	1656	22.44	5319
	WARD'S PYRITE	-12.99	2	1363	8.64	4278
	CHALCOCITE	1.48	4.32	36	0.40	137
	WARD'S PYRRHOTITE	-1.47	2.7	350	2.30	1117
	CHALCOPYRITE	-4.51	2.81	644	3.31	1756
	GALENA	8.36	3.91	30	0.16	68
	MARCASITE	-46.44	1.76	2497	14.89	8527
	SPHALERITE	-20.11	4.02	1356	5.17	3784
	HARDROCK PYRITE	-1.34	2.97	94	1.08	274
	HARDROCK PYRRHOTITE	-5.29	2.64	509	2.78	6882
	COAL PYRITE	-46.57	1.65	5028	25.28	16150
3	BARITE	-0.89	4.32	2	0.01	46
	ANHYDRITE	-14.02	7.06	574	2.77	0
	GYPSUM	-15.18	4.21	541	2.80	46
	ANGLESITE	-1.87	4.5	16	0.01	46
	JAROSITE	-1.75	4.11	6	0.01	34
	ARSENOPYRITE	4.69	1.69	862	14.06	3290
	WARD'S PYRITE	-25.37	1.8	2731	15.10	8692
	CHALCOCITE	4.29	4.23	49	0.36	194
	WARD'S PYRRHOTITE	-1.86	2.7	450	2.52	1254
	CHALCOPYRITE	-5.37	2.7	601	3.24	1824
	GALENA	7.19	4.23	31	0.14	68
	MARCASITE	-45.56	1.69	2386	15.40	8226
	SPHALERITE	-18.21	4.37	1207	5.11	3674
	HARDROCK PYRITE	-1.17	2.92	104	1.18	342
	HARDROCK PYRRHOTITE	-5.66	2.59	559	3.00	1756
	COAL PYRITE	-49.54	1.45	4880	27.01	16946

Table 23. Raw data for ABA experimentation.

Replication	Mineral Name	Original Sample Mass (grams)	% Mass Removed By Water Extraction	% Mass Removed By HCl Extraction	% Mass Gained By Filter Paper	% Mass Removed By HNO_3 Extraction	Percent Residual	Water Leachate Sulfur ($mg\ l^{-1}$)	HCl Dilution Corrected Leachate Sulfur ($mg\ l^{-1}$)	HNO_3 Dilution Corrected Leachate Sulfur ($mg\ l^{-1}$)
	BARITE	1.0015	-0.42	-0.79	14.34	-20.44	78.35	2	11	19
	ANHYDRITE	0.9994	-16.23	-79.43	1.95	-4.88	-0.54	245	1212	48
	GYPSUM	1.0006	-38.43	-57.00	1.31	-5.43	-0.85	485	641	37
	ANGLESITE	0.9996	-1.36	-38.32	8.02	-42.01	18.32	8	435	53
	JAROSITE	0.9999	-0.53	-2.15	12.70	-22.95	74.37	3	19	70
	ARSENOPYRITE	1.001	-0.48	-0.99	4.40	-65.18	33.35	3	3	373
	WARD'S PYRITE	1.0006	-0.45	0.67	7.57	-86.55	13.67	3	0	2766
	CHALCOCITE	1.0008	-0.31	2.56	13.49	-79.21	23.04	1	0	17
1	WARD'S PYRRHOTITE	1	-1.23	-80.73	5.57	-10.69	7.35	8	2366	50
	CHALCOPYRITE	1.0004	-0.80	0.68	5.19	-19.89	79.99	2	4	155
	GALENA	1.0015	-0.49	-28.26	5.52	-36.32	34.94	0	1527	0
	MARCASITE	0.9992	-0.91	0.50	4.96	-89.81	9.78	8	3	2750
	SPHALERITE	1.0008	-1.14	-2.69	8.21	-11.62	84.55	1	0	1
	COAL BARITE	1.0015	-0.83	-4.10	10.24	-18.33	76.73	2	124	106
	HARDROCK PYRITE	1.0005	-0.44	-2.71	1.34	-68.29	28.57	0	1	2447
	HARDROCK PYRRHOTITE	1.0003	-0.68	-53.25	2.33	-17.00	29.06	2	1251	419
	COAL PYRITE	0.999	-3.01	-0.10	5.38	-77.46	19.43	28	5	2383

Table 23. Continued.

Replication	Mineral Name	Original Sample Mass (grams)	% Mass Removed By Water Extraction	% Mass Removed By HCl Extraction	% Mass Gained By Filter Paper	% Mass Removed By HNO_3 Extraction	Percent Residual	Water Leachate Sulfur (mg l^{-1})	HCl Dilution Corrected Leachate Sulfur (mg l^{-1})	HNO_3 Dilution Corrected Leachate Sulfur (mg l^{-1})
	BARITE	1.0004	-0.83	-0.68	12.02	-16.99	81.50	0	9	18
	ANHYDRITE	1.0018	-20.19	-75.87	2.41	-3.59	0.34	258	1092	1
	GYPSUM	0.9994	-40.81	-57.85	0.72	-1.13	0.20	486	628	0
	ANGLESITE	0.9996	-1.72	-43.82	9.51	-35.10	19.36	7	378	28
	JAROSITE	1.0012	-0.87	-2.13	16.44	-27.84	69.17	0	18	70
	ARSENOPYRITE	0.9988	-0.73	-0.72	7.77	-62.95	35.60	0	0	390
	WARD'S PYRITE	1	-0.73	0.76	7.33	-74.06	25.97	2	0	2269
	CHALCOCITE	1.0001	-0.25	2.77	17.06	-77.69	24.83	0	0	28
2	WARD'S PYRRHOTITE	1.0023	-0.56	-80.06	3.49	-12.77	6.61	4	295	112
	CHALCOPYRITE	1.0002	-0.79	0.63	6.80	-30.14	69.70	0	10	106
	GALENA	1.0003	-0.57	-32.99	6.71	-35.25	31.19	0	201	1
	MARCASITE	1.0005	-0.95	0.50	5.00	-89.64	9.92	6	4	3020
	SPHALERITE	1.0005	-0.59	-3.08	9.06	-13.78	82.55	0	11	1
	COAL BARITE	0.3473	-2.51	-3.48	14.74	-29.08	64.93	0	23	34
	HARDROCK PYRITE	1.0017	-0.55	-3.09	1.70	-65.86	30.50	0	4	2465
	HARDROCK PYRRHOTITE	0.9994	-1.00	-50.73	3.91	-15.88	32.39	0	355	355
	COAL PYRITE	0.9991	-2.89	-0.75	6.32	-76.26	20.10	32	18	2747

Table 23. Continued.

Replication	Mineral Name	Original Sample Mass (grams)	% Mass Removed By Water Extraction	% Mass Removed By HCl Extraction	% Mass Gained By Filter Paper	% Mass Removed By HNO_3 Extraction	Percent Residual	Water Leachate Sulfur (mg l^{-1})	HCl Dilution Corrected Leachate Sulfur (mg l^{-1})	HNO_3 Dilution Corrected Leachate Sulfur (mg l^{-1})
	BARITE	0.9996	-0.26	-1.08	17.27	-22.02	76.64	2	11	25
	ANHYDRITE	1.0005	-18.37	-73.12	3.28	-8.93	-0.42	262	1234	74
	GYPSUM	1.0011	-42.55	-54.56	2.69	-3.45	-0.56	492	560	0
	ANGLESITE	0.999	-1.05	-51.15	16.51	-35.38	12.42	9	469	29
	JAROSITE	1.0007	-0.53	-3.23	12.64	-23.14	73.10	3	20	72
	ARSENOPYRITE	1.0008	-0.25	-1.47	8.31	-79.46	18.82	2	1	480
	WARD'S PYRITE	0.9992	-0.37	0.07	7.83	-90.99	8.71	5	0	3098
	CHALCOCITE	1.0007	-0.22	4.53	21.52	-82.74	21.56	1	0	24
3	WARD'S PYRRHOTITE	1.001	-0.29	-79.83	6.85	-14.53	5.35	5	2	125
	CHALCOPYRITE	1.001	-0.25	0.89	10.09	-31.34	69.30	2	0	227
	GALENA	0.9998	-0.23	-35.59	9.88	-36.03	28.16	1	253	1
	MARCASITE	1.001	-0.63	0.18	6.47	-91.76	7.79	7	9	2486
	SPHALERITE	1	-0.34	-2.33	8.82	-11.31	86.02	1	0	0
	COAL BARITE	0.3279	-0.91	-1.56	14.82	-31.14	66.39	2	5	49
	HARDROCK PYRITE	1.0005	-0.22	-2.45	3.03	-69.92	27.42	1	0	2450
	HARDROCK PYRRHOTITE	1.0005	-0.47	-52.35	3.55	-15.99	31.18	2	0	323
	COAL PYRITE	1.0002	-2.98	-0.57	7.57	-77.29	19.16	37	0	2172